



**781**  
**2023**

# Berichte

zur Polar- und Meeresforschung

Reports on Polar and Marine Research

**The Expedition PS137  
of the Research Vessel POLARSTERN  
to the Arctic Ocean in 2023**

Edited by

Vera Schlindwein

with contributions of the participants

Die Berichte zur Polar- und Meeresforschung werden vom Alfred-Wegener-Institut, Helmholtz-Zentrum für Polar- und Meeresforschung (AWI) in Bremerhaven, Deutschland, in Fortsetzung der vormaligen Berichte zur Polarforschung herausgegeben. Sie erscheinen in unregelmäßiger Abfolge.

Die Berichte zur Polar- und Meeresforschung enthalten Darstellungen und Ergebnisse der vom AWI selbst oder mit seiner Unterstützung durchgeführten Forschungsarbeiten in den Polargebieten und in den Meeren.

Die Publikationen umfassen Expeditionsberichte der vom AWI betriebenen Schiffe, Flugzeuge und Stationen, Forschungsergebnisse (inkl. Dissertationen) des Instituts und des Archivs für deutsche Polarforschung, sowie Abstracts und Proceedings von nationalen und internationalen Tagungen und Workshops des AWI.

Die Beiträge geben nicht notwendigerweise die Auffassung des AWI wider.

Herausgeber  
Dr. Horst Bornemann

Redaktionelle Bearbeitung und Layout  
Susan Amir Sawadkuhi

Alfred-Wegener-Institut  
Helmholtz-Zentrum für Polar- und Meeresforschung  
Am Handelshafen 12  
27570 Bremerhaven  
Germany

[www.awi.de](http://www.awi.de)  
[www.awi.de/reports](http://www.awi.de/reports)

Der Erstautor bzw. herausgebende Autor eines Bandes der Berichte zur Polar- und Meeresforschung versichert, dass er über alle Rechte am Werk verfügt und überträgt sämtliche Rechte auch im Namen seiner Koautoren an das AWI. Ein einfaches Nutzungsrecht verbleibt, wenn nicht anders angegeben, beim Autor (bei den Autoren). Das AWI beansprucht die Publikation der eingereichten Manuskripte über sein Repositorium ePIC (electronic Publication Information Center, s. Innenseite am Rückdeckel) mit optionalem print-on-demand.

The Reports on Polar and Marine Research are issued by the Alfred Wegener Institute, Helmholtz Centre for Polar and Marine Research (AWI) in Bremerhaven, Germany, succeeding the former Reports on Polar Research. They are published at irregular intervals.

The Reports on Polar and Marine Research contain presentations and results of research activities in polar regions and in the seas either carried out by the AWI or with its support.

Publications comprise expedition reports of the ships, aircrafts, and stations operated by the AWI, research results (incl. dissertations) of the Institute and the Archiv für deutsche Polarforschung, as well as abstracts and proceedings of national and international conferences and workshops of the AWI.

The papers contained in the Reports do not necessarily reflect the opinion of the AWI.

Editor  
Dr. Horst Bornemann

Editorial editing and layout  
Susan Amir Sawadkuhi

Alfred-Wegener-Institut  
Helmholtz-Zentrum für Polar- und Meeresforschung  
Am Handelshafen 12  
27570 Bremerhaven  
Germany

[www.awi.de](http://www.awi.de)  
[www.awi.de/en/reports](http://www.awi.de/en/reports)

The first or editing author of an issue of Reports on Polar and Marine Research ensures that he possesses all rights of the opus, and transfers all rights to the AWI, including those associated with the co-authors. The non-exclusive right of use (einfaches Nutzungsrecht) remains with the author unless stated otherwise. The AWI reserves the right to publish the submitted articles in its repository ePIC (electronic Publication Information Center, see inside page of verso) with the option to "print-on-demand".

*Treffen von Polarstern und Kronprins Haakon nach erfolgreicher gemeinsamer Arbeit  
am Aurora Hydrothermalfeld.  
(Foto: Christian Rohleder, DWD)*

*Meeting of Polarstern und Kronprins Haakon after successful completion of joint operations  
at Aurora Vent Field.  
(Photo: Christian Rohleder, DWD)*

# **The Expedition PS137 of the Research Vessel POLARSTERN to the Arctic Ocean in 2023**

---

**Edited by**

**Vera Schlindwein  
with contributions of the participants**

**Please cite or link this publication using the identifiers**

**<https://hdl.handle.net/10013/epic.cf05aa62-b266-43db-ab1b-e921624eb4d7>**

**[https://doi.org/10.57738/BzPM\\_0781\\_2023](https://doi.org/10.57738/BzPM_0781_2023)**

**ISSN 1866-3192**

**PS137 – ALOIS**

**21 June 2023 – 31 July 2023**

**Tromsø – Tromsø**

**Chief scientist  
Vera Schlindwein**

**Coordinator  
Ingo Schewe**

## **Contents**

<b>1.</b>	<b>Überblick und Expeditionsverlauf</b>	<b>2</b>
	<b>Summary and Itinerary</b>	<b>6</b>
	<b>Weather Conditions during PS137</b>	<b>9</b>
	<b>Ice Conditions during PS137</b>	<b>12</b>
<b>2.</b>	<b>Geophysical Survey Programme</b>	<b>16</b>
<b>3.</b>	<b>Nereid under Ice Hybrid AUV-ROV Operations</b>	<b>27</b>
<b>4.</b>	<b>Hydroacoustics</b>	<b>37</b>
<b>5.</b>	<b>Habitat Mapping</b>	<b>46</b>
<b>6.</b>	<b>Heatflow</b>	<b>55</b>
<b>7.</b>	<b>Geology and Petrology</b>	<b>60</b>
<b>8.</b>	<b>Physical Oceanography and Biogeochemistry of Hydrothermal Plumes</b>	<b>65</b>
<b>9.</b>	<b>Hydrothermal Plume Microbiology</b>	<b>72</b>
<b>10.</b>	<b>Physical Oceanography and Ocean-Sea Ice Coupling in the Marginal Ice Zone</b>	<b>80</b>
<b>11.</b>	<b>Sea Ice</b>	<b>93</b>
	<b>APPENDIX</b>	<b>106</b>
<b>A.1</b>	<b>Teilnehmende Institute / Participating Institutes</b>	<b>107</b>
<b>A.2</b>	<b>Fahrtteilnehmer:innen / Cruise Participants</b>	<b>109</b>
<b>A.3</b>	<b>Schiffsbesatzung / Ship's Crew</b>	<b>111</b>
<b>A.4</b>	<b>Stationsliste / Station List PS137</b>	<b>113</b>

# 1. ÜBERBLICK UND EXPEDITIONSVERLAUF

Vera Schlindwein

DE.AWI

ALOIS (Arctic Lithosphere-Ocean Interaction Study) ist ein wegweisendes interdisziplinäres Experiment, das die Entstehung neuer Lithosphäre am arktischen Gakkel-Rücken und die damit verbundene hydrothermale Zirkulation erforscht. Vor 20 Jahren entdeckte die AMORE Expedition, dass sich die ultralangsame Ozeanbodenspreizung am Gakkel-Rücken nicht mit gängigen Modellen erklären lässt und mit ungewöhnlich starker hydrothermaler Aktivität einhergeht. Trotz dieser bahnbrechenden Erkenntnisse fanden wegen der schwierigen Eisbedingungen kaum weitere Experimente statt. Uns standen nun speziell für Meereis konzipierte Tiefseetauchroboter und Ozeanbodenseismometer zur Verfügung, mit denen wir Aurora (Abb. 1.1), eines der wenigen bislang entdeckten Hydrothermalfelder an ultralangsamem Rücken überhaupt und das einzige im Arktischen Ozean, kartieren und geophysikalisch, biogeochemisch und mikrobiologisch beproben konnten. Ein Jahr lang konnten wir dessen Seismizität und hydrothermalen Plume beobachten, ermöglicht durch die logistische Kombination mit der Expedition ATWAICE (PS131). Entlang des Gakkel Rücken wollten wir außerdem die Herkunft weiterer hydrothermaler Anomalien klären und die Quellen am Meeresboden suchen. Bei 3°E am Gakkel Rücken trennt eine markante Grenze seit Entstehung des Eurasischen Beckens Bereiche unterschiedlicher Lithosphärenentwicklung. Geplant war, zusammen mit der norwegischen GoNorth Kampagne an Bord des Forschungsschiffes *Kronprins Haakon* mit seismischen und geologischen Profilen und Gesteinsproben die Lithosphärenstruktur und Herkunft der Schmelzen beidseits der Grenze zu klären.

ALOIS trägt zu AWIs Programmforschung bei und setzt die erfolgreiche Kooperation mit dem Exzellenzcluster MARUM und WHOI fort. Als zweiter Fahrtabschnitt der Expedition ATWAICE (PS131) im Sommer 2022 hatten wir zudem die Aufgabe, ozeanographische Verankerungen entlang des Yermak Plateaus zu bergen, die auf einem Profil durch die Eisrandzone das Einfließen warmen atlantischen Wassers unter das Meereis erfassen sollten. Zugleich bot ALOIS die Möglichkeit, erneut Helikopter- und eisbasierte Messungen von Schmelztümpelverteilungen auf dem Meereis in Fortsetzung der ATWAICE Kampagne zu unternehmen. Damit integriert die Expedition zentrale Ziele des Helmholtz-Forschungsprogramms „Changing Earth – Sustaining our Future“ mit einer Verbindung zu den Themen “Ocean and Cryosphere in Climate.

*Polarstern* verließ Tromsø am Abend des 21. Juni bei sehr guten Wetterbedingungen um nach einem kurzen logistischen Hafenanlauf in Longyearbyen am 24. Juni 2023 das Forschungsprogramm der Expedition PS137 beginnen zu können, zunächst mit einer Kalibrierung des Hydrosweep Systems.

## 25. – 28. Juni 2023, Yermak Plateau

Auf dem Weg zum Yermak Plateau (Abb. 1.1) zur Bergung der ersten Verankerung der ATWAICE Expedition trafen wir bereits sehr früh auf dichtes Meereis, so dass die Verankerungsarbeiten eine Herausforderung darstellten. Mit Warten auf Bereiche mit offenem Wasser an der richtigen Lokation, Eisbrechen und geschickten Schiffsmanövern konnten 6 von 7 Verankerungen erfolgreich geborgen werden. Eine Verankerung lag unter einer massiven Eisscholle von circa 16 km Durchmesser und hätte mehrtägiges Warten erfordert bis die Eisdrift die Lokation

freigegeben hätte. Zwischen den Verankerungsarbeiten fanden CTDs, teilweise mit Tests der *In-situ* Pumpen statt, sowie zwei schiffsbasierte und eine Helikopter-basierte Eisstation.

### 29. Juni – 1. Juli 2023, Lena Trog

Am 29. Juni 2023 begannen wir unseren Weg Richtung Aurora mit schwerer Eisfahrt, jedoch immer wieder größeren Flächen offenen Wassers. In einer dieser Flächen wurde das Nereid Under Ice Vehicle (NUI) das erste Mal zu Wasser gelassen und einem erfolgreichen Systemtest unterzogen. Am 30. Juni erreichten wir große Bereiche offenen Wassers im Lena Trog (Abb. 1.1) südlich vom Aurora Hydrothermalfeld, das zu dem Zeitpunkt von einer sehr großflächigen, vermutlich 3-jährigen Eisscholle blockiert wurde, so dass wir Gesteinsprobennahme und Wärmestrommessungen im kaum beprobten nördlichen Lena Trog unternahmen und mit dem Fächerecholot unkartiertes Terrain vermessen konnten.

### 2. – 13. Juli 2023, Aurora

Nach schwerer Eisfahrt erreichten wir das Aurora Hydrothermalfeld am 2. Juli und konnten am frühen Morgen des 3. Juli die dortige Verankerung abbergen. Ein erster Tauchgang des NUI musste wegen technischer Schwierigkeiten abgebrochen werden, die darauffolgende CTD aufgrund eines Defekts am Bugstrahler, was zu einem knapp 12-stündigen Forschungsausfall führte. In den folgenden Tagen unternahmen wir je nach Eissituation Versuche per Eisdrift das Hydrothermalfeld zu erreichen und dabei mit CTD und *In-situ* Pumpen mikrobiologische Proben und physikalische Messdaten zu gewinnen oder bei geeigneter Eissituation Ozeanbodenseismometer zu bergen. Parallel wurden mit dem Helikopter weitere Eisstationen durchgeführt und Magnetiksurveys geflogen. Insgesamt erschwerte die massive Eisbedeckung im Messgebiet und die fehlende Möglichkeit, mit dem Bugstrahler die Steuerbordseite des Schiffs eisfrei zu halten, das Arbeiten sehr. Bis zum 13. Juli gelang es uns dennoch, 6 von 8 Seismometern zu bergen. Ein Gerät konnte sich von seinem Anker nicht befreien. Außerdem konnten Proben aus dem hydrothermalen Plume mit der CTD gewonnen, bei zwei NUI Tauchgängen das Hydrothermalfeld erreicht, neue schwarze Raucher gefunden und Gesteinsproben genommen werden. Unmittelbar neben den schwarzen Rauchern fanden sich auch Austritte klarer, gut 130°C heißer Fluide, die beprobt wurden.

### 13. – 19. Juli 2023, Western Volcanic Zone

Am 9. Juli 2023 erreichte uns die Nachricht, dass die *Kronprins Haakon* für Reparaturarbeiten nach Tromsø zurückkehren musste. Dies bedeutete, dass die geplanten gemeinsamen Arbeiten an der 3°E Grenze, die ein zweites Schiff erfordern (Seismik und Dredgen), nicht mehr durchgeführt werden konnten. Die schweren Eisbedingungen und die eingeschränkten Arbeitsmöglichkeiten durch den fehlenden Bugstrahler veranlassten uns, die 3°E Grenze als Ziel aufzugeben und lediglich bis 1°45'W (Abb. 1.1) zu fahren auf der Suche nach neuen Hydrothermalquellen. Diesen Weg begannen wir am 13. Juli und steuerten zunächst einen hohen Berg der östlichen Riftflanke des Gakkelerücken an, um OFOBS Kameraaufnahmen des Meeresboden zu machen und die Habitatbedingungen zu kartieren. Danach setzten wir unsere Fahrt entlang der westlichen Riftflanke fort, um dort am 15. und 16. Juli Wärmestrommessungen entlang eines Profils in Spreizungsrichtung zu unternehmen. Die nachfolgenden verbleibenden 16 Meilen Luftlinie zur Position des hydrothermalen Plumes bei 1°45'W gestalteten sich bei 100 % Eisbedeckung als sehr schwierig. Die Eisbedingungen waren geprägt von dickem, mehrjährigem Eis mit hoher Sedimentfracht und wenig offenen Stellen, die nicht in Fahrtrichtung orientiert waren. Nach 14 Stunden, die wir mit dem Brechen einer Scholle verbracht hatten, wurde klar, dass die Lokation des vermuteten Plumes nicht mehr erreicht werden konnte, bevor eine ausgedehnte Scholle mit dichtem Eis das Arbeiten dort unmöglich machte. Daher fuhren wir eine weitere Wärmestrommessung und eine CTD an

der westlichen Flanke des Riffvals, bevor wir in unserer eigenen Fahrspur den Rückweg zum Aurora Hydrothermalfeld antraten.

#### **20. – 24. Juli 2023, Aurora und nördlicher Lena Trog**

Am 20. Juli erreichten wir kurz vor der *Kronprins Haakon* das Aurora Hydrothermalfeld und begannen dort mit gemeinsamen Arbeiten. Ein sehr erfolgreicher Tauchgang mit NUI lieferte eine bathymetrische Karte des Hydrothermalfelds, Fluidproben von heissem, schwarzem Rauch und Koordinaten für Gesteinsproben, die an den nachfolgenden Tagen durch das größere ROV der *Kronprins Haakon* genommen wurden. In der Zwischenzeit gelang uns, eines der verbleibenden Ozeanbodenseismometer zu bergen. Danach unternahmen wir bei variabler Eisdrift mehrere Versuche, den Plume mit der CTD und den *In situ* Pumpen für biologische Probennahme zu durchqueren. In der Zwischenzeit konnte die *Kronprins Haakon* mit ihrem ROV das letzte verbliebene Seismometer mit defektem Auslöser bergen und danach noch weitere Gesteinsproben von neu entdeckten Schloten nehmen. Am Abend des 22. Juli gewannen wir noch ein umfangreiches Wärmestromprofil am nördlichen Ende des Lena Trog im Übergang zur Aurora Region, während die *Kronprins Haakon* mit letzten Arbeiten am Hydrothermalfeld beschäftigt war. Im Konvoi ging es dann am 23. Juli entlang eines CTD Profils der *Kronprins Haakon* durch das dichte Meereis nach Süden. Bevor sich unsere Wege am 24. Juli trennten, übernahmen wir noch das geborgene Ozeanbodenseismometer von der *Kronprins Haakon* und eine Eisboje, die aufgrund der Verspätung der *Kronprins Haakon* nicht ausgebracht werden konnte und bei PS138 weiter nördlich abgesetzt werden soll. Zudem gab es für Wissenschaft und Besatzung die Möglichkeit, das jeweils andere Schiff zu besichtigen, Absprachen über Proben zu treffen und sich auszutauschen.

#### **25. – 27. Juli 2023, Lucky B**

Am 25. Juli erreichten wir eine "Lucky B" genannte Stelle im Lena Trog, von der hydrothermale Anomalien und Funde von Sulfiden von früheren Expeditionen bekannt waren. NUI erstellte bei einem Tauchgang eine bathymetrische Karte und ortete die hydrothermale Anomalie, die im Anschluss während zwei CTDs beprobt wurde. Mit zwei OFOBS Profilen konnten die Habitatbedingungen auf dem Gipfel und am Boden des Hangs, der die stärkste hydrothermale Anomalie zeigte, untersucht werden. Die *Kronprins Haakon* arbeitete in der Nähe an einer vulkanischen Struktur und unternahm Wärmestrommessungen, bevor sie ebenfalls ausgestattet mit Koordinaten unserer CTD und NUI Messungen ROV Tauchgänge an der Lucky B-Lokation unternahm. Nach Forschungsende am 27. Juli 2023 um 01:00 traten wir durch loses Meereis die Rückreise nach Tromsø an.

#### **28. Juli 2023, Jøtul**

Auf dem Weg brachten wir am Knipovich Rücken rund um das neu entdeckte Jøtul Hydrothermalfeld noch 7 Ozeanbodenseismometer aus, die in 14 Monaten von der *Maria S. Merian* wieder geborgen werden sollen.

Am 31. Juli 2023 erreichte *Polarstern* wohlbehalten Tromsø.

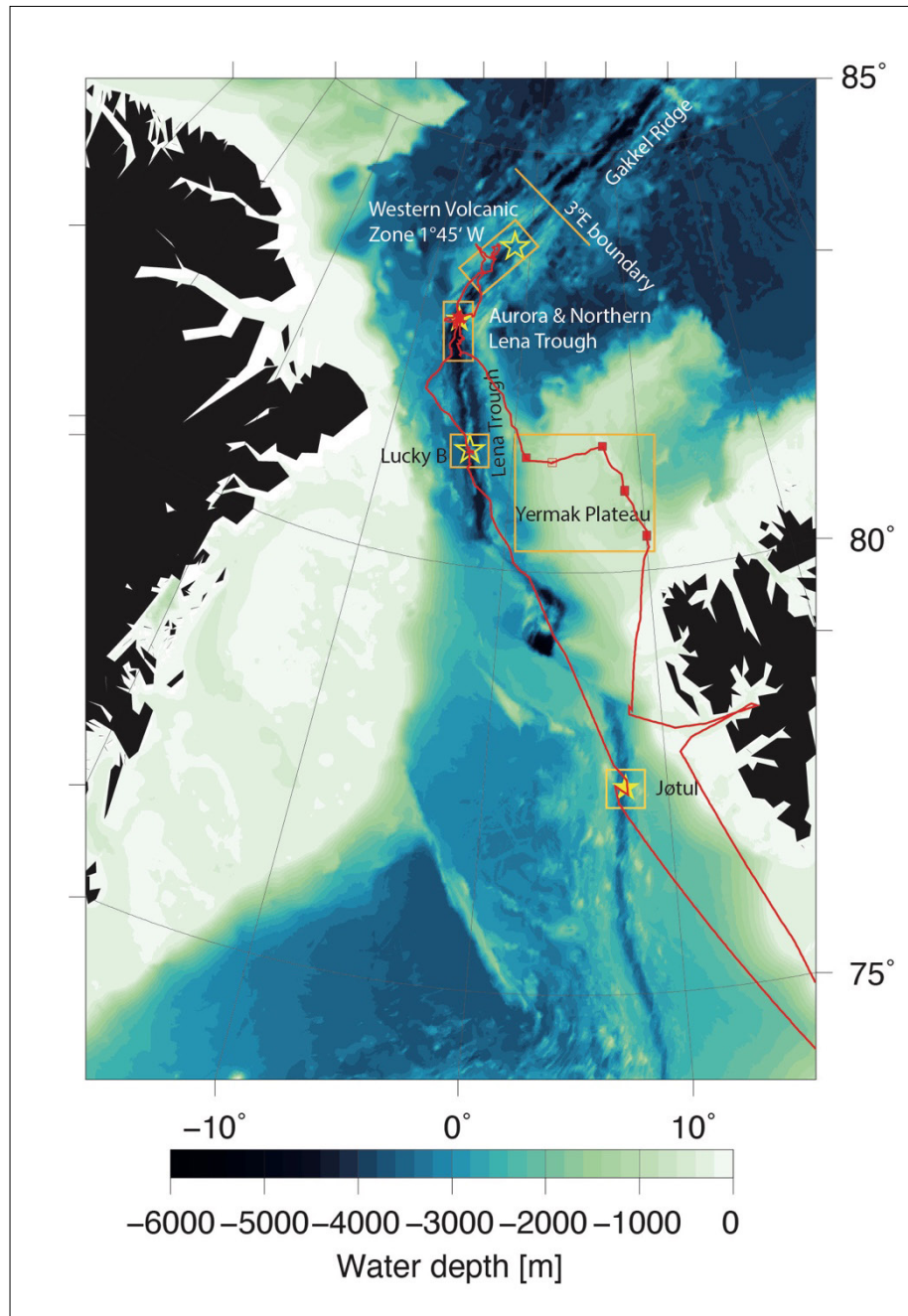


Abb. 1.1: Karte der Fahrtroute und der Untersuchungsgebiete;  
gelbe Sterne: bekannte (offen: vermutete) Hydrothermalquellen;  
rote Quadrate: geborgene Verankerungen (offenes Quadrat: keine Bergung);  
Bathymetrie: IBCAO ver4. Siehe <https://doi.pangaea.de/10.1594/PANGAEA.963315> für eine  
Darstellung des Master tracks in Verbindung mit der Stationsliste für PS137

Fig. 1.1: Map of the cruise track and the working areas;  
yellow stars: known (open: presumed) hydrothermal vents;  
red squares: recovered moorings, (open square: no recovery);  
Bathymetry IBCAO ver4. See <https://doi.pangaea.de/10.1594/PANGAEA.963315> to display the master  
track in conjunction with the station list for PS137.

## SUMMARY AND ITINERARY

ALOIS (Arctic Lithosphere-Ocean Interaction Study) is a pioneering interdisciplinary experiment investigating the formation of new lithosphere at the Arctic Gakkel Ridge and its associated hydrothermal circulation. Twenty years ago, the AMORE expedition discovered that ultraslow seafloor spreading at the Gakkel Ridge cannot be explained by common models and is accompanied by unusually strong hydrothermal activity. Despite these groundbreaking discoveries, hardly any further experiments took place because of the difficult ice conditions. We now have deep-sea diving robots and ocean-bottom seismometers (OBS) specially designed for sea ice at our disposal which enable us to map Aurora, one of the few hydrothermal vent fields ever discovered on ultraslow spreading ridges and the only one in the Arctic Ocean, and sample it geophysically, biogeochemically and microbiologically. For one year we observed its seismicity and the dynamics of its hydrothermal plume, made possible by the logistical combination with the expedition ATWAICE (PS131) in summer 2022. Along the Gakkel Ridge, we also wanted to clarify the origin of other hydrothermal anomalies in the water column and search for their sources on the seafloor. At 3°E on Gakkel Ridge, a prominent boundary has separated areas of different lithospheric development since the formation of the Eurasian Basin. The plan was to clarify the source of melts and the different lithospheric structure to each side of the boundary by acquiring seismic and geological profiles together with the Norwegian GoNorth campaign on board the research vessel *Kronprins Haakon*.

ALOIS contributes to AWI's programme research and continues the successful cooperation with the Cluster of Excellence MARUM and WHOI. As second cruise leg of the successful ATWAICE expedition (PS131) in 2022, our task was to recover oceanographic moorings along the Yermak Plateau, which should record the inflow of warm Atlantic water under the sea ice on a profile through the marginal ice zone. At the same time, ALOIS offered the opportunity to again undertake helicopter and ice-based measurements of melt pond distributions on the sea ice in continuation of the ATWAICE campaign. Thus, the expedition integrates central goals of the Helmholtz research programme "Changing Earth – Sustaining our Future" with a link to the topics "Ocean and Cryosphere in Climate".

*Polarstern* left Tromsø on the evening of 21 June 2023 in very good weather conditions and, after a short logistical port call in Longyearbyen, started the research programme of expedition PS137 on 24 June 2023, with a calibration of the Hydrosweep system.

### **25 – 28 June 2023, Yermak Plateau**

On the way to the Yermak Plateau to recover the first mooring of the ATWAICE expedition, we encountered dense sea ice very early on, making the mooring work a challenge. With waiting for areas of open water at the right location, breaking ice and careful ship maneuvering, 6 out of 7 moorings were successfully recovered. One mooring was under a massive ice floe approximately 10 miles in diameter and would have required several days of waiting for ice drift to clear the location. CTDs, some with tests of the *in-situ* pumps, took place between the mooring work, as well as two ship-based and one helicopter-based ice station.

### 29 June – 1 July 2023, Lena Trough

On 29 June 2023 we started our way towards Aurora with travelling through dense sea ice, but intermittently also larger areas of open water. In one of these areas, the Nereid Under Ice Vehicle (NUI) was launched for the first time and subjected to a successful system test. On 30 June 2023 we reached large areas of open water in the Lena Trough south of the Aurora Vent Field, which was at the time blocked by a very large, presumably 3-year-old ice floe. Therefore, we undertook rock sampling and heat flow measurements in the sparsely sampled northern Lena Trough and covered uncharted terrain with multibeam profiling.

### 2 – 13 July 2023, Aurora

After travel in severe sea-ice conditions, we reached the Aurora Vent Field on 2 July 2023 and could, in the early morning of 3 July 2023, recover the mooring there. A first dive of the NUI had to be aborted due to technical problems, the subsequent CTD due to a defect in the bow thruster, which led to a break in research activities of almost 12 hours. In the following days, depending on the ice situation, we attempted to reach the hydrothermal field by ice drift and obtained water samples and physical data with the CTD and the *in-situ* pumps or, if the ice situation was suitable, we recovered ocean bottom seismometers. At the same time, ice stations were carried out with the helicopter and magnetic surveys were flown. Overall, the massive ice cover in the survey area and the inability to keep the ship's starboard side ice-free without a bow thruster made work very difficult. Despite these difficulties, we still managed to recover 6 of 8 seismometers until 13 July 2023. One ocean bottom seismometer could not free itself from its anchor weight. In addition, samples could be obtained from the hydrothermal plume with the CTD and two NUI dives reached the hydrothermal field, found new black smokers and took rock samples. Next to the black smokers, we sampled a discharge area of clear fluids with a temperature of more than 130°C.

### 13 – 19 July 2023, Western Volcanic Zone

On 9 July 2023, we learned that the *Kronprins Haakon* had to return to Tromsø for repair work. This meant that the planned joint activities at the 3°E boundary, which require a second vessel (seismic profiling and dredge operations), could no longer be carried out. The dense sea ice and the limited maneuvering capabilities due to the missing bow thruster lead us to abandon the 3°E boundary as a research target and only sail along the Western Volcanic Zone to 1°45'W in search of new hydrothermal vents. We started this journey on 13 July 2023 and first headed for a high mountain on the eastern rift flank of Gakkel Ridge to take OFOBS video observations of the seafloor and map habitat conditions. Then we continued our journey along the western flank of the rift valley. On 15 and 16 July 2023 we took heat flow measurements along a profile in spreading direction. The subsequent remaining 16 nmi to the position of the presumed hydrothermal plume at 1°45'W turned out to be very difficult with 100 % ice cover. The ice conditions were characterized by thick, multi-year ice with a high sediment load and few open areas that were not oriented in our direction of travel. After 14 hours spent breaking a single ice floe, it became clear that the location of the suspected plume could not be reached before a large floe of dense ice approaching from north made work there impossible. Therefore, we conducted another heat flow and a CTD station on the western part of the rift valley before heading back to the Aurora hydrothermal field following our own track.

### 20 – 26 July 2023, Aurora and northern Lena Trough

On 20 July 2023 we reached the Aurora hydrothermal field shortly before the *Kronprins Haakon* arrived and started working together there. A very successful dive with NUI provided a bathymetric map of the hydrothermal field, fluid samples of hot black smoke and coordinates

---

for rock samples taken by *Kronprins Haakon's* larger ROV on the following days. In the meantime, we managed to recover one of the remaining ocean bottom seismometers. We then made several attempts to hit the hydrothermal plume with the CTD and *in-situ* pumps for biological sampling, which was partly compromised by unpredictably variable ice drift. Meanwhile, *Kronprins Haakon's* ROV was able to recover the last remaining seismometer with a defective releaser and then take further rock samples from the newly discovered vents. On the evening of 22 July 2023, we acquired another extensive heat flow profile at the northern end of the Lena Trough at the transition to the Aurora region while *Kronprins Haakon* was busy with final work on the hydrothermal field. On 23 July 2023, we left southwards through the dense sea ice as a convoy of two ships along a CTD profile of *Kronprins Haakon*. Before our ways separated on 24 July 2023, we lifted the recovered ocean bottom seismometer and an ice buoy from *Kronprins Haakon* to *Polarstern*. The ice buoy could not be deployed due to the delay of *Kronprins Haakon* and will now to be deployed further north during the subsequent cruise PS138. In addition, the science parties and crews of both vessels had the opportunity to inspect the other ship, discuss further collaboration and to exchange ideas.

### **25 – 27 July 2023, Lucky B**

On 25 July 2023, we reached a location in Lena Trough called "Lucky B", from which hydrothermal anomalies and dredge hauls with large amounts of sulphides were known from previous expeditions. NUI completed a dive there, yielding a bathymetric map and a good overview of the location of the hydrothermal anomaly, which was subsequently sampled during two CTDs. Two OFOBS profiles were used to study the habitat conditions at the top and bottom of the slope showing the strongest hydrothermal anomaly. *Kronprins Haakon* was working nearby on a volcanic structure and taking heat flow measurements before conducting ROV dives at the Lucky B location, informed with coordinates from our CTD and NUI measurements. After the end of our research on 27 July 2023 at 01:00, we started our return journey to Tromsø through loose sea ice.

### **28 July 2023, Jøtul**

On the way to Tromsø, we deployed 7 ocean bottom seismometers at Knipovich Ridge around the newly discovered Jøtul hydrothermal vent field. The instruments will be recovered in 14 months during a cruise of *Maria S. Merian*.

*Polarstern* reached Tromsø safely on 31 July 2023.

## WEATHER CONDITIONS DURING PS137

Patrick Suter

DE.DWD

### **Tromsø – Svalbard**

On the evening of 21 June 2023 *Polarstern* departed from Tromsø and set out for the expedition PS137 to the Arctic. With a high-pressure system over the Barents Sea, calm conditions prevailed. Apart from a fresh easterly current near the coast, weak winds and wave heights below 1 m dominated. While moving northwards, the air slowly cooled and condensed, causing fog to form from the evening of 22 June. A short stopover in Longyearbyen followed on the morning of 24 June. In the meantime, a high-pressure ridge had extended from the Greenland Sea to the north of Fram Strait, which meant that a southwesterly current prevailed in Fram Strait. The winds reached 5 Bft in the fjord near Longyearbyen due to channelling effects. At the same time, the low stratus cloud cover in the fjord temporarily cleared and, despite widespread high-level clouds, there was also a little sunshine

### **Fram Strait – Aurora Vent Field**

In the afternoon of 24 June, the first scientific measurements were carried out just west of Svalbard in light winds. On 25 June *Polarstern* moved northwards into the marginal ice zone. With a prevailing high-pressure ridge, the southwesterly wind temporarily increased to 5 to 6 Bft by the evening and the sky was overcast with stratiform clouds. With the arrival of the ice, waves and swell vanished. Then the journey continued north into the sea ice. By 27 June, a high-pressure system had formed northwest of Svalbard, which then moved slowly eastwards. With weak northerly winds, fog repeatedly occurred. On 28 June and again on 30 June, two surface lows formed over the northeast of Greenland. These then moved slowly eastwards north of *Polarstern*. The southerly flow in the downstream area of them reached up to 5 Bft. With the simultaneous inflow of drier air, there were repeated sunny and cloudless phases during these days, whereby the transitions to fog were very sharp. On the rear side of the lows, fog reappeared again in both cases with northwesterly winds.

### **Research area Aurora (between 82°30'N – 84°N and 07°30'W – 03°30'W)**

In the meantime, *Polarstern* had reached the research area Aurora on 30 June after a journey through thick multi-year sea ice. On 2 July, the second of the lows described above moved southwards towards Svalbard. This led to a calm high-pressure phase with weak to moderate winds from the southeast to the south until 6 July. The high-pressure zone extended from northeast of Svalbard to north of Greenland. While supercooled fog prevailed throughout 2 and 3 July, drier and slightly milder air flowed in from the southeast in the morning of 4 July. As a result, the sun was shining from a cloudless sky with gentle plus temperatures until the early morning of 8 July. At the same time, the weather situation began to change on 7 July. A high-pressure zone, supported by a blocking and quasi-stationary high in the middle and upper troposphere, which until then was most of the time dominant over the research area, took a farewell to the south.

On 7 July, a surface low had formed over northeast Greenland. The southerly current increased to 6 Bft from the afternoon onwards. With the southerly winds, large areas of stratus cloud had formed over Fram Strait, which flooded the research area in the form of dense fog from the morning of 8 July. The low slowly moved north of *Polarstern* towards the east. The current weakened and turned to the northwest by the evening. The cloud ceiling lifted slightly by 9 July, but fog patches repeatedly led to reduced visibility and sometimes freezing drizzle.

By 10 July, a ridge of high pressure over Greenland had spread northeastwards into the research area and remained stationary until 13 July. This led to calm and mostly light-wind conditions. Repeated phases of fog and quite sunny weather conditions alternated, accompanied by changing mid- and high-level cloudiness.

From 14 July, the weather was dominated by a large low-pressure complex over the Kara Sea. With weak to moderate winds from northerly directions, frontal systems with a lot of moisture repeatedly reached the research area until 18 July. The period of bad weather was introduced by warm air advection and a textbook-like frontal process with approaching high- and mid-level clouds and a slowly descending cloud bases on 14 July. Afterwards, dense fog with intermittent and partly supercooled precipitation often set the pace. Only on 17 July, an intermediate ridge of high pressure led to a slight improvement in the weather in the form of mostly good visibility and a break-up of the low stratus clouds. At the same time, *Polarstern* continued to move its way north-northeast through dense multi-year sea ice and reached the northernmost point of the expedition near 83°51'N 03°30'W on the evening of 17 July.

On the evening of 18 July, *Polarstern* headed back south and reached the main research area of Aurora near 82°54'N 06°20'W again by 21 July. The low-pressure zone over the Kara Sea had weakened by 19 July and its influence on the weather diminished. Meanwhile, the vertical extent of the fog had decreased by 19 July and it became shallower. Visibility remained below 1 km almost throughout, but the sun shone through the thin layer of fog all day.

Until 24 July, two very similar weather situations occurred in direct succession: Starting from a high on the coast of East Greenland, a ridge initially extended northwards into the research area. The ridge shifted slightly eastwards and a surface low developed twice over the northeast of Greenland during this period. Between the surface low and the ridge, the current turned south and increased to 4 to 5 Bft. The two surface lows detached themselves from northeast Greenland and moved eastwards with southwestward extending trough during the night of 22 July and the second low until the evening of 24 July. The current turned west to northwest with a slight decrease due to the eastward shift of the trough. While sunshine prevailed continuously on the 20 and until the late afternoon of the 21 July, there was a transition on the 22 July with most of the time very low stratus, but only intermittent phases of fog. On 23 and 24 July dense fog prevailed without interruption.

During this period, the scientific work was accompanied by the Norwegian research vessel *Kronprins Haakon*, which was also on expedition in the Aurora area. The ships exchanged information and data and supported each other in recovering measuring instruments and samples. From 23 July, *Polarstern* left Aurora and headed south through dense sea ice to Lucky B.

### **Lucky B (around 81°20'N 03°30'W)**

The weather during the transit and at Lucky B was mainly determined by a large low-pressure area near the North Pole, which repeatedly steered frontal systems from the north into the research area. A first frontal system reached *Polarstern* only in a weakened form until 25 July, as a weak high-pressure area acted against it from the south. On 26 July, a warm front followed, which brought dense, mid- and high clouds, occasionally low stratus, fog phases and a few

raindrops. By the evening, an active cold front arrived from the north. This brought moderate rain, which led to poor visibility. After a brief improvement in the weather directly behind the cold front and increasing northwesterly to northerly winds, foggy air flowed in until the morning of 27 July. At the same time, the transit back to Tromsø began that night.

#### **Transit over eastern Fram Strait to Tromsø**

On 27 July, a moderate northerly current blew between a high over the western Fram Strait and a low-pressure zone over Svalbard and east of it. After initially foggy air, near the ground drier and slightly unstable air in the lower troposphere flowed in. By the afternoon, the weather became alternately cloudy and sunny with some moderate snow showers. On 28 July, the transit back led over the eastern Fram Strait, where seven so-called OBS were deployed in the evening. At the same time, the pressure gradient increased somewhat, resulting in a fresh northerly flow. When leaving the ice, the sea reached 1.5 m with swell from northeast to north. The aforementioned high moved towards Svalbard by 29 July. Thus the wind weakened and calm conditions prevailed with often dense low-level clouds and occasional drizzle. In the course of 30 July, *Polarstern* approached a low-pressure complex over Scandinavia and the southern Barents Sea as it steamed through the Norwegian Sea. As a result, the northeasterly current increased to 5 Bft and the waves to around 1.5 metres. In the fjords near Tromsø, the wind dropped. When the ship approached the coast, visibility deteriorated and it was misty, respectively foggy during the night. In the morning *Polarstern* arrived in Tromsø accompanied by sunshine and few low stratus, bringing expedition PS137 to an end.

In summary, it can be said that the general weather pattern from past summer expeditions in the Arctic was similar on this trip. The pressure distribution was often determined by weak pressure systems and repeatedly by local effects. The average sea-level pressure was 1016.4 hPa. As usual, the weather was largely characterised by the constantly cold boundary layer, respectively a surface inversion and accordingly often by fog. Fog was registered on 30 of 41 days. The average temperature in the research area was  $-0.3^{\circ}\text{C}$ , with an absolute maximum of just over  $2^{\circ}\text{C}$  and a minimum of  $-3.7^{\circ}\text{C}$ . The highest measured 10-minute mean wind speed was 27.4 kt (6 to 7 Bft), with a maximum 3-second gust of 32.5 kt (7 Bft).

# ICE CONDITIONS DURING PS137

H. Jakob Bünger

DE.DRIFT NOISE

## 25 June – 02 July 2023

*Polarstern* reached the sea-ice edge at approximately 80.0°N, 09.8°E on 25 June 2023. Moorings Y1 and Y2 were located in the marginal ice zone, just north of the edge of > 90 % sea-ice concentration (SIC). After recovery of the two moorings *Polarstern* transited through > 90 % SIC to moorings Y3, Y4 and Y5, Y6 (Fig. 1.2, left). The area was dominated by medium-sized, big and vast multi-year ice (MYI) floes. Especially the big and vast floes showed considerable ridges, while flatter areas were covered with frozen melt ponds. The considerable size of the floes ensured that there were open water areas available to navigate through or for mooring recovery.

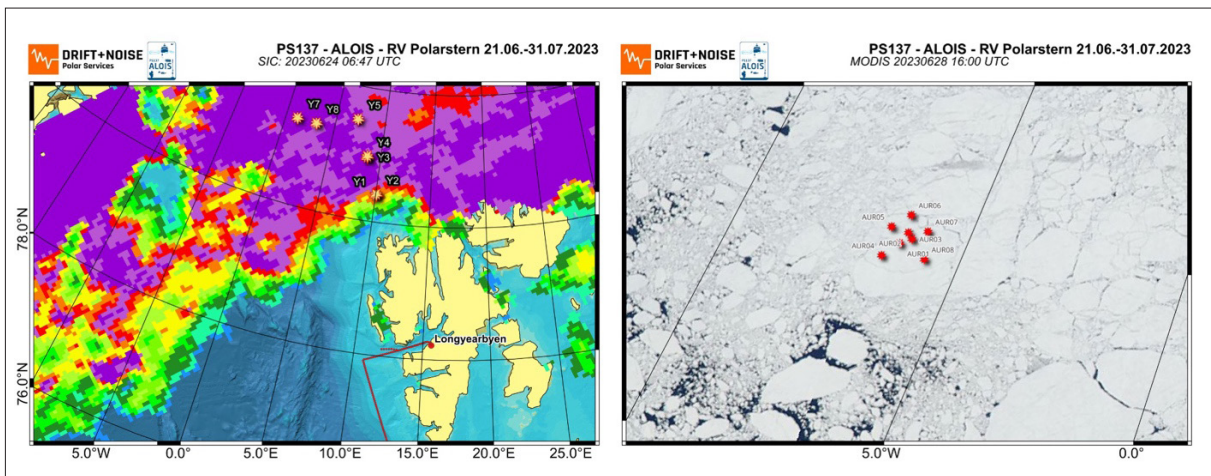


Fig. 1.2: Left: 24 June 2023 (06:47 UTC) AMSR-2 sea-ice concentration provided by the Japan Aerospace Exploration Agency (JAXA) and processed (according to Spreen et al., 2008). Right: 28 June 2023 Moderate Resolution Imaging Spectroradiometer (MODIS) optical satellite image (provided by NASA World View) of the Aurora Vent Field research area.

The transit between moorings Y5/Y6 and Y8 led through a field of more compressed ice with fewer open water areas. Upon reaching the Y8 location a giant floe (approximately 12 nmi diameter) was located over the mooring and prevented the recovery. Following the recovery of mooring Y7 the focus switched to the Aurora Vent Field (between 82.5 and 84°N and 7.5 and 3.5°W). The transit from the Y7 location to Aurora was characterized by an area with lower SIC and vast open water areas around giant MYI floes. However, approaching Aurora *Polarstern* entered an area of heavily compressed MYI (Fig. 1.2, right). Although the giant floes showed long cracks, pressure on the entire system prevented the broken pieces from moving freely and opening up leads. Areas with smaller floes showed considerable compression zones and ridge formation which slowed *Polarstern* down significantly. According to backtracking analysis (Krumpfen et al., 2019), the ice field originated from the shallow shelves in the Eastern Laptev

Sea and was about three years old when it passed over the vent field. In order to support the ice and drift analysis two drift buoys (P281 and P282) were deployed to the northwest and northeast of the Aurora Vent Field on 01 July 2023.

### 03 July – 09 July 2023

Between 3 and 9 July 2023 the Aurora Vent Field region remained covered with a compressed sea ice field consisting of mainly big, vast and giant floes. Given the calm weather conditions with high pressure influence and weak southerly winds over the research area the general southward drift was slowed down and dominated by inertial oscillation. During this oscillation ice drift speeds decreased to average values around 0.06 knots around midnight and noon of each day. Maximum average drift speeds of around 0.2 knots were reached at around 6 am and 6 pm each day. Every drift speed decrease was accompanied by a change in drift direction to the east. With increasing drift speeds in the morning and evening drift direction changed back to southerly directions resulting in an overall south easterly drift until 6 July 2023 (Fig. 1.3, left).

Following the change in weather conditions and increase in wind speeds on 6 July 2023 the sea-ice drift changed from an overall southeasterly drift towards an eastward drift. The easterly drift reached maximum average speeds of up to 0.35 knots and persisted until the evening of 8 July 2023 when winds weakened and started coming from the northwest. With the weather and drift shift the frozen ponds really started to melt and ice floe surfaces started to change considerably, showing large open melt ponds on the flat surfaces between ridges.

A third AWI drift buoy (P283) was deployed northwest of the Aurora Vent Field on 9 July 2023.

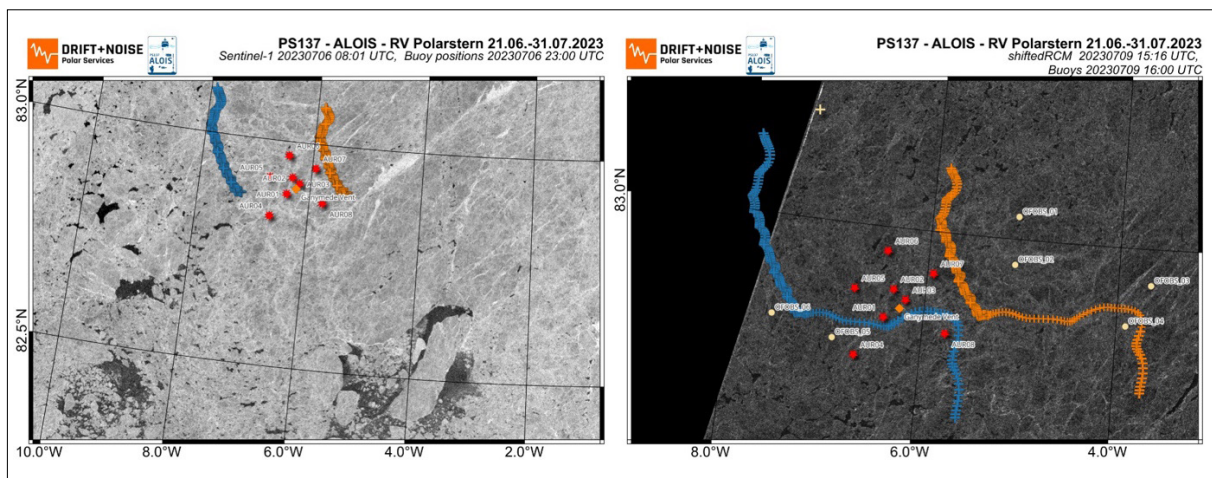


Fig. 1.3: Left: 6 July 2023 (08:01 UTC) Sentinel-1 radar satellite image (ESA) and AWI drift buoy positions (until 6 July 23:00 UTC). Right: 9 July 2023 (07:08 UTC) RADARSAT Constellation Mission (RCM, provided by the Canadian Space Agency) radar image shifted to the 9 July (15:16 UTC) position and AWI drift buoy positions until 9 July, 16:00 UTC.

### 10 July – 16 July 2023

After the change from easterly to southerly sea-ice drift on 08/09 July, southerly drift persisted until 16 July. All three buoys were recovered on 13 July and P281 was redeployed just south of the Plume Site research area at approximately 83.8°N, 1.7°W. On 12 July 2023, *Polarstern* started the transit from the Aurora Vent Field towards the Plume Site. While the weather shift and change in drift direction and speed had loosened up the ice around the Aurora Vent Field

a little bit, more compressed and sediment-laden MYI was dominant over the Plume Site and along the transit path.

### 17 July – 23 July 2023

Heavy ice conditions slowed down *Polarstern* on its way to the Plume Site research area. Vast, sediment-laden, and heavily-ridged ice floes (Fig. 1.4, left) provided few open water areas between them, however, given the overall pressure on the system contact points between floes showed thick and fresh ridges and *Polarstern* was slowed down between open water areas and made little progress.

Predicted sea-ice drift directions and satellite radar imagery projected very little change in the heavy and compressed ice system and due to time constraints and overall difficulties moving through the ice it was decided to turn back towards Aurora on 18 July 2023 (Fig. 1.4, right).

Progress back to Aurora was a little easier, because *Polarstern* was able to use its old track for the majority of the way, however, conditions remained challenging because of the continuously high pressure on the system.

Back at the Aurora Vent Field the P282 drift buoy was redeployed to the north of the area and the overall slow eastward drift (maximum average values of approximately 0.2 knots) and availability of open water areas allowed for additional deep-sea operations and instrument recoveries. Drift changed direction towards the southeast and increased to maximum average values of 0.3 knots on 21/22 July 2023 (Fig. 1.5, left). *Polarstern* left the Aurora Vent Field towards the South on 23 July 2023.

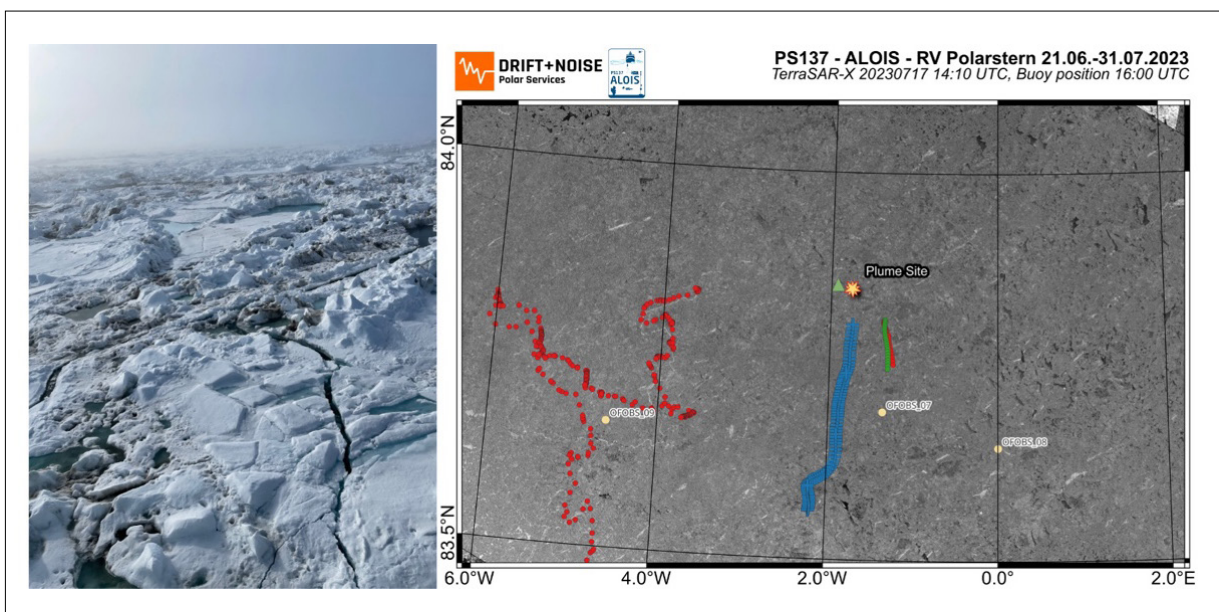


Fig. 1.4: Left: Heavily ridged and sediment-laden sea-ice floes observed during the transit from the Aurora Vent Field to the Plume Site research area on 19 July 2023 (Photo: H. J. Bünger).  
Right: 17 July 2023 (14:10 UTC) TerraSAR-X radar image (provided by the German Aerospace Agency, DLR) of the Plume Site area and P281 drift buoy trajectory (14 July until 17 July 2023, 16:00 UTC).

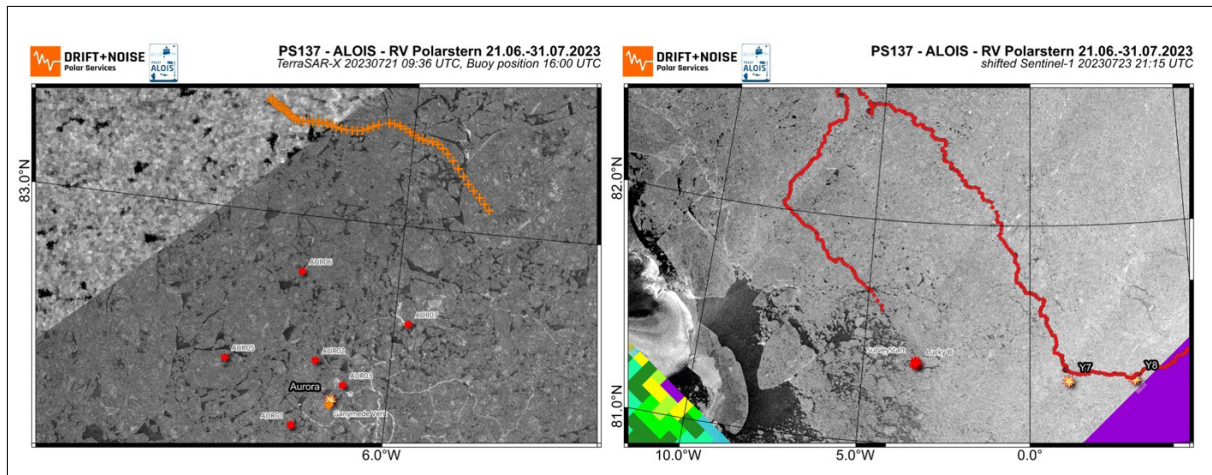


Fig. 1.5: Left: 21 July 2023 (09:36 UTC) TerraSAR-X radar satellite image (provided by DLR) of the ice conditions over the Aurora Vent Field and P282 drift buoy trajectory (20 July until 21 July, 16:00 UTC). Right: 21 July (08:25 UTC) Sentinel-1 radar image (provided by ESA) of the area between the Aurora Vent Field and the Lucky B Site shifted into 23 July (21:15 UTC) position.

## 24 July – 28 July 2023

Although ice conditions remained challenging, with thick MYI ice floes being most dominant, the southward transit was favoured by decreasing ice pressure. Avoiding giant ice floes that moved in from the northwest, *Polarstern* reached an area with lower SIC (50-70 %) and was able to reach the Lucky B research area (at approximately 81.3°N and 3.5°W) in the evening of 24 July 2023. With very little pressure and freely moving ice floes around the Lucky B site, enough open water areas were available for station work. The ice drift remained constant at around 0.3 knots in southerly directions for the remainder of station work. Leaving the Lucky B site on 27 July, *Polarstern* crossed an area of higher SIC (up to 90 %) but with no considerable difficulties for the navigation. The sea-ice edge was passed in the early hours of 28 July 2023 at 78.8°N, 4.9°E.

## References

- Krumpen T, Belter HJ, Boetius A et al. (2019) Arctic warming interrupts the Transpolar Drift and affects long-range transport of sea ice and ice-rafted matter. *Scientific Reports* 9:5459. <https://doi.org/10.1038/s41598-019-41456-y>
- Spreen G, Kaleschke L, Heygster G (2008) Sea ice remote sensing using AMSR-E 89-GHz channels. *Journal of Geophysical Research: Oceans* 113(C2). <https://doi.org/10.1029/2005JC003384>

## 2. GEOPHYSICAL SURVEY PROGRAMME

Mechita Schmidt-Aursch<sup>1</sup>, Henning Kirk<sup>1</sup>, Norbert  
Lensch<sup>1</sup>, Matthias Pilot<sup>1</sup>, Chiara Tobisch<sup>1</sup>, Annika  
Hellbrück<sup>1</sup>, Viktoria Thamm<sup>1</sup>, Vera Schlindwein<sup>1,2</sup>

<sup>1</sup>DE.AWI

<sup>2</sup>DE.UNI Bremen

**Grant-No. AWI\_PS137\_02**

### Objectives

The key objective of the geophysical programme is to understand active seafloor spreading processes at ultraslow spreading ridges better. Gakkel Ridge belongs to the slowest spreading mid-ocean ridges of the global system of diverging plate boundaries. Here, the production of melt filling the gap between the Eurasian and the American plate can hardly keep pace with the separation speed of the two continents. Instead of an elevated mid-ocean ridge with constant magma production resulting in an oceanic crust of about 8 km thickness, slow and especially ultraslow spreading ridges have irregular magma production in space and time such that a deep rift valley may form. In addition, the oceanic crust may be locally overthickened, thin or even absent exposing the Earth's mantle to the seafloor. The hydrothermal circulation of seawater through the newly formed ocean floor contributes to its cooling and an efficient exchange of energy and matter between the lithosphere and the ocean forming also the basis for deep-sea life around hydrothermal vent sites. Compared to the limited supply of melt, hydrothermalism at ultraslow spreading ridges appears to be abundant (Edmonds et al., 2003).

Microearthquakes accompany these spreading processes. They delineate active fault structures serving as pathways for hydrothermal fluids, show magma movement or cracking and tremor produced by hydrothermal circulation (e.g. Meier and Schlindwein, 2018, 2021). In addition, earthquake waves passing through the subsurface can be used to image the crustal structure and reveal areas of melt (Meier et al., 2022). We will further measure anomalies in the Earth's magnetic field caused by local geology. Magmatic rocks become permanently magnetized as the rocks cool, freezing in the prevailing magnetic field. In areas, where magma production is missing, magnetic anomalies are strongly subdued such that even away from the present plate boundary when the seafloor gets older and is sediment-covered, we can get an idea of its origin and physical properties. With a combination of active and passive seismic and magnetic and gravity field measurements, we aimed to explore the spatially strongly varying crustal structure of the ultraslow Gakkel ridge, targeting especially the 3°E boundary, where magmatic and amagmatic spreading occur in close vicinity, and to explore the style and geological functioning of hydrothermal circulation at Aurora vent field. On our way back to Tromsø, we visited the newly discovered Jøtul vent field and deployed seismometers there. This vent field has a different geological setting compared to Aurora vent field such that we can broaden our understanding of hydrothermal circulation by a comprehensive study of vent fields with different geology.

### Work at sea

#### *Passive seismology*

During PS137 we recovered 8 ocean bottom seismometers (OBS) that had been deployed during PS131 in an area of approximately 15 km x 15 km around the Aurora vent field (Fig. 2.1a). We closely monitored the ice conditions and drift such that when there was an area of open water which would drift over the position of an OBS, we were in position early enough to acoustically release the OBS in time for it to surface in an area of open water. Each OBS was equipped with a Posidonia transponder which we used to locate the OBS on the seafloor and track it on the way up after it was released. The OBSs rise with a speed of approximately 1.0 - 1.1 m/s so there was enough time after the release to clear the expected surface area of ice if needed.

We started with OBSs AUR07 and AUR08, which surfaced in the area of open water *Polarstern* was waiting in. Recovery was then done by hooking the OBSs to the ships winch from the zodiac boat and lifting them on deck over the starboard side by the crane. Similarly, the recovery of AUR05 was also very smooth with the OBS being recovered with a hook attaching the rope to the crane directly from the starboard side. The other OBS recoveries did not go as smoothly with AUR01, AUR02 and AUR04 getting stuck beneath ice floes. Due to the attached Posidonia transponder hanging ~180 m below the OBS we were able to constantly locate the OBS. For all three OBSs the first approach was to carefully break the ice so that it could free itself. For AUR01 this approach took 1.5 h until it surfaced on the water from where it was then recovered directly from the starboard side of the ship. However, the releaser was damaged during ice breaking. A similar approach was not successful for AUR04 and we later deployed the rescue ROV of the NUI team to attach a line to the OBS and pull it out from underneath the ice floe. We tried a similar approach with AUR02 which got stuck in a cavern on the bottom of an ice floe such that it was not visible for the rescue ROV. Further attempts with a custom made recovery grapnel were not successful as the ship could not manoeuvre well enough due to ice conditions. Finally, using the full power of *Polarstern* to break the ice floe was successful, but damaged frame, releaser and potentially the seismometer. We visited AUR06 two times without receiving a Posidonia signal. Additionally ice conditions were not favourable for a recovery during the second visit. On a last attempt we received a reliable location from the Posidonia system and the timing was such that the OBS surfaced in open water, even though it had drifted by about 200 m during the rise to the surface (Fig. 2.2). The recovery of AUR03 was done by the Aegir6000 ROV of the *Kronprins Haakon* which was in the same research area at the time. The ROV was able to pick up the OBS from the seafloor and bring it on deck of the *Kronprins Haakon*. Apparently the anchor weight was still attached and the releaser had not worked properly, even though the deck unit had received an acoustic answer acknowledging the release command. The OBS was then handed over to *Polarstern* by the crane of *Kronprins Haakon*.

Once on board we synchronized the OBS clocks and stopped recording. Leveling of AUR02 (Trillium Compact, SN: 003295) has not worked properly (Fig. 2.4b), the other 7 seismometers leveled as planned. Skew values for the OBSs ranged between -18.0 s to 12.3 s (Tab. 2.2).

The raw data was downloaded and copied as backup. Each station recorded between 48 – 51 GB of data (Tab. 2.1). The data was then converted to miniseed format and probabilistic power spectral density plots (PPSDs) were calculated for all channels. For quality control the data was inspected on random days throughout the deployment. Further analysis requires the correction of the clock drift between the stations.

We further deployed a network of 7 OBSs in an area of around 15 km x 15 km around the Jøtul vent field (Fig. 2.1b). OBSs were deployed in free-fall mode and record ground motion at a sampling rate of 100 Hz (Tab. 2.2). Recovery is planned during a *Maria S. Merian* cruise in September 2024. Recording parameters are summarized in Table 2.3.

#### *Airborne magnetic survey*

Parallel to the ship-based work, we acquired magnetic data with a PicoEnvirotec airborne system. We used an optical magnetometer mounted into a so-called bird, which was towed on a 30 m long rope beneath the helicopter to prevent any disturbances from the aircraft. Two computers in the helicopter recorded the total magnetic field and auxiliary data from the onboard GPS and radar altimeter systems. Technical problems with the power supply of the magnetometer system prevented survey flights at the beginning of the cruise. After solving these problems, difficult weather conditions, especially fog, did not allow many measurements. Nevertheless, during five days we could perform ten flights with a maximum duration of two hours each (Fig. 2.3, Tab. 2.4). The mean flight velocity was 80 kn (148 km/h), the mean flight level was 300 ft (91 m). In total, 1,391 nmi (2,573 km) of line data could be recorded.

Around the Aurora vent field and in the northern Lena Trough we acquired 15 west-east trending lines of 40 nmi (74 km) each. The line spacing was 2 nmi (3.7 km), so an area of in total 40 x 28 nmi (74 x 52 km) could be mapped. This covered the entire vent field, the central valley and the adjacent rift flanks. At the transition from the northern Lena Trough into the western Gakkel Ridge, we were able to conduct three flights recording six northwest-southeast trending lines of approx. 70 nmi (130 km) length each. With a line spacing of 2 nmi (3.7 km), an area of 70 nm x 10 nmi (130 km x 185 km) was surveyed. This covered not only the Gakkel Ridge, but also adjoining parts of the Nansen and Amundsen basins. The heavy sea-ice conditions and humid weather with insufficient visibilities prevented any helicopter-based magnetic measurements in the central or eastern Western Volcanic Zone (WVZ) of Gakkel Ridge.

The overall data quality is very good. Clear positive and negative seafloor spreading anomalies are visible, which should allow a precise dating of the western Gakkel Ridge and the northern Lena Trough. Amplitude variations of the positive anomaly in the central valley will help to understand the transition between magmatic and amagmatic spreading in this area.

#### *Gravity data*

Continuous gravity data was acquired during the cruise with the permanently installed Bodenseewerke KSS32 gravimeter. Harbour measurements were performed at the beginning and at the end of the cruise in Tromsø at the Nordnorsk Kunstmuseum (former Police station). Due to a technical problem of the instrument, data is only available after 26 June 2023.

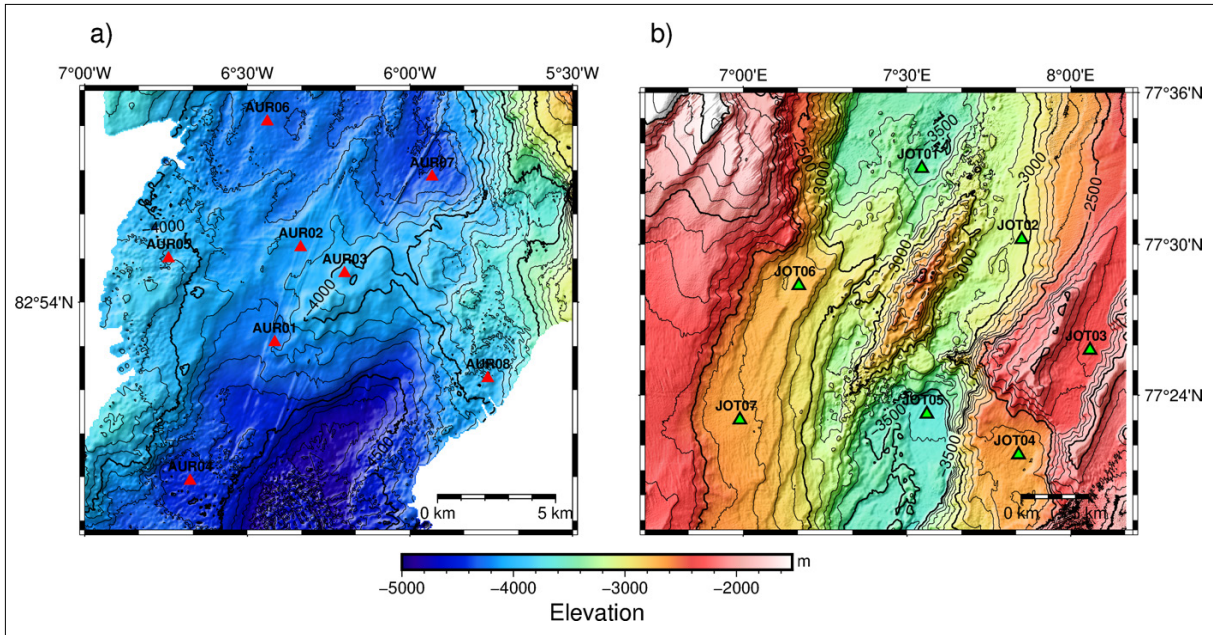


Fig. 2.1: a) Position on the seafloor of the 8 recovered OBS stations (red triangles) around Aurora vent field b) Deployment positions of the 7 OBS stations (green triangles) around Jøtul vent field

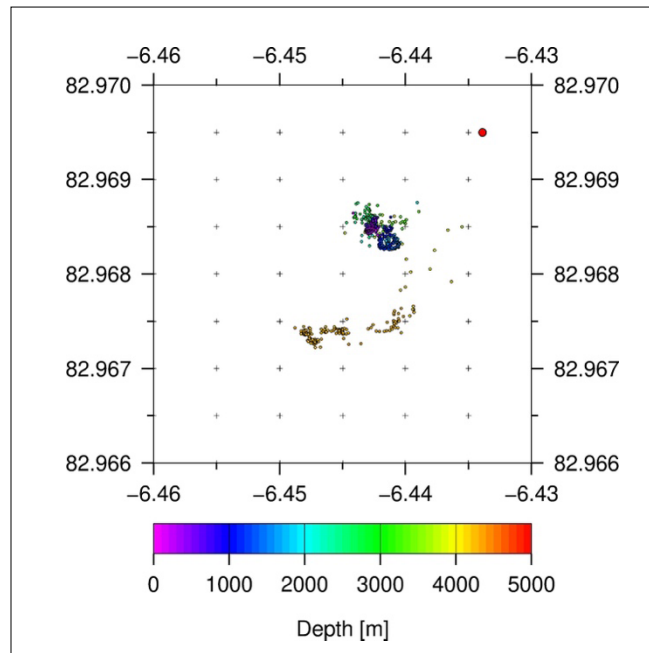


Fig. 2.2: Tracked Posidonia location of OBS AUR06 after release; red dot indicates the initial deployment position.

**Tab. 2.1:** Summary of OBS deployment and recovery near Aurora vent site.

Station	Deployment			Recovery			Data	
	Date Time [UTC]	Position Latitude Longitude	Depth [m]	Date Time [UTC]	Position Latitude Longitude	Depth [m]	Amount [GB]	Recorded days
AUR01	25.07.2022 09:53	82° 52.979' N 06° 25.383' W	4215	07.07.2023 15:35	82° 53.067' N 06° 20.384' W	4235	48.5	348
AUR02	25.07.2022 00:05	82° 55.131' N 06° 20.667' W	4155	10.07.2023 04:12	82° 53.232' N 06° 20.652' W	4160	48.9	351
AUR03	24.07.2022 23:25	82° 54.589' N 06° 12.218' W	3988	22.07.2023 11:48	82° 54.152' N 06° 08.226' W	3990	50.8	363
AUR04	24.07.2022 16:48	82° 50.100' N 06° 40.500' W	4408	09.07.2023 08:59	82° 47.842' N 06° 35.087' W	4588	48.8	350
AUR05	25.07.2022 17:19	82° 55.072' N 06° 44.413' W	3900	12.07.2023 03:14	82° 55.015' N 06° 44.387' W	3893	49.1	353
AUR06	25.07.2022 19:50	82° 58.167' N 06° 26.032' W	4250	21.07.2023 16:35	82° 58.109' N 06° 26.301' W	4244	50.4	362
AUR07	25.07.2022 22:14	82° 56.753' N 05° 55.852' W	4354	04.07.2023 21:08	82° 56.817' N 05° 56.761' W	4386	48.0	345
AUR08	24.07.2022 19:44	82° 52.112' N 05° 45.272' W	3917	06.07.2023 16:03	82° 52.368' N 05° 45.064' W	3903	48.4	347

**Tab. 2.2:** Parameters and position on the seafloor of the of OBS network around Aurora vent site.

Station	Position on seafloor			Recording		
	Latitude	Longitude	Depth [m]	Start Time [UTC]	Stop Time [UTC]	Skew [ $\mu$ s]
AUR01	82° 53.088' N	06° 24.948' W	4262	25.07.2022 00:39:10	27.07.2023 16:35:12	12278612
AUR02	82° 55.248' N	06° 20.166' W	4183	24.07.2022 21:21:38	10.07.2023 $\mu$ 04:44:28	-9265124
AUR03	82° 54.660' N	06° 12.054' W	4029	24.07.2022 20:40:46	23.07.2023 11:41:40	-7258220
AUR04	82° 49.908' N	06° 40.548 ' W	4511	24.07.2022 13:33:51	09.07.2023 09:10:17	-10915025
AUR05	82° 54.996' N	06° 44.550' W	3968	25.07.2022 16:34:02	12.07.2023 03:46:00	1124089
AUR06	82° 58.098' N	06° 26.322' W	4223	25.07.2022 18:59:59	21.07.2023 16:57:26	5250678
AUR07	82° 56.850' N	05° 55.914' W	4434	25.07.2022 20:53:05	04.07.2023 21:47:47	-13399243
AUR08	82° 52.266' N	05° 45.648' W	3941	24.07.2022 16:37:28	06.07.2023 16:34:09	-17996628

**Tab. 2.3:** Programming settings and deployment positions of OBS network near Jøtul vent site.

Station	Programming		Deployment			
	Recording start time [UTC]	Autorelease time [UTC]	Date Time [UTC]	Position at surface		
				Latitude	Longitude	Depth [m]
JOT01	28.07.2023 15:20:51	19.06.2025 13:00	28.07.2023 16:04	77° 33.013' N	07° 32.704' E	3477
JOT02	28.07.2023 15:52:43	20.06.2025 01:00	28.07.2023 16:53	77° 30.201' N	07° 51.036' E	3055
JOT03	28.07.2023 16:15:55	19.06.2025 07:00	28.07.2023 17:37	77° 25.800' N	08° 03.530' E	2312
JOT04	28.07.2023 17:03:46	20.06.2025 07:00	28.07.2023 18:17	77° 21.621' N	07° 50.448' E	2663
JOT05	28.07.2023 17:49	20.06.2025 13:00	28.07.2023 18:55	77° 23.249' N	07° 33.633' E	3620
JOT06	28.07.2023 18:28:27	20.06.2025 19:00	28.07.2023 19:50	77° 28.373' N	07° 10.174' E	2759
JOT07	28.07.2023 19:10:02	19.06.2025 19:00	28.07.2023 00:00	77° 23.014' N	06° 59.366' E	2662

**Tab. 2.4:** Recording parameters of OBS network near Jøtul vent site.

Station	Recording Start Time [UTC]	Sample Rate [Hz]	Gain	Seismometer	Hydro-phone	Recorder	Temperature sensor
			[HXYZ]	Type	Inverted (I)	SN	SN
JOT01	25.07.2022 15:20:51	100	4 1 1 1	Trillium Compact	H	61607087	1854377
JOT02	25.07.2022 15:53:43	100	4 1 1 1	Trillium Compact	H	61607298	1854371
JOT03	25.07.2022 16:15:33	100	4 1 1 1	Trillium Compact	H	61607210	1854370
JOT04	28.07.2022 17:03:46	100	2 1 1 1	Trillium Compact	H	61607102	-
JOT05	28.07.2022 17:49:00	100	2 1 1 1	Trillium Compact	H	61607070	1854207
JOT06	28.07.2022 18:28:27	100	2 1 1 1	Trillium Compact	H	61607190	1854406
JOT07	28.07.2023 19:09:30	100	on on on on	Trillium Compact	H	6d7	-

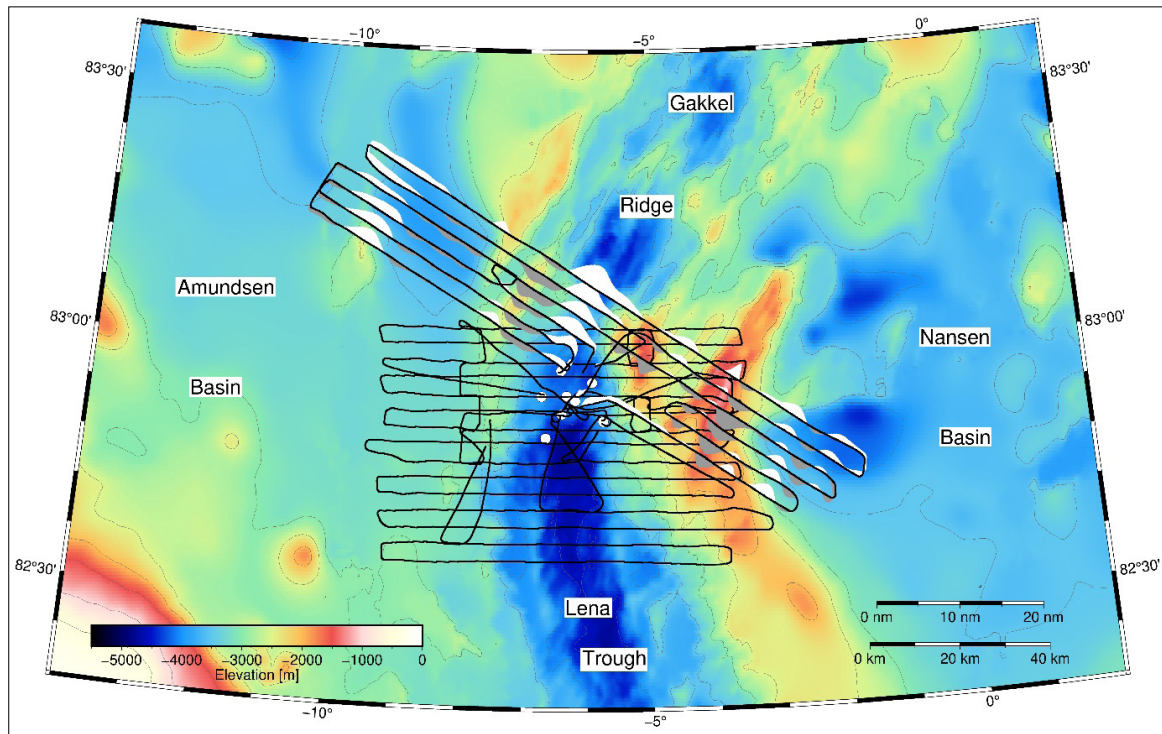


Fig. 2.3: Position of aeromagnetic survey lines. White dots represent the position of the OBS. A data example is shown for the northernmost profiles.

Tab. 2.5: List of aeromagnetic survey lines as seen in Fig. 2.3.

Date	Time [UTC]		Fiducial		Heading [deg]	Length [nmi]	Binary file	Area
	Start	End	Start	End				
6 July 2023	09:29:08	11:16:57	0	6469	90 / 270	146	B3070609.P28	Lena Trough
6 July 2023	12:52:49	14:35:30	0	6161	90 / 270	137	B3070612.P52	Lena Trough
7 July 2023	07:40:57	09:14:03	0	5586	90 / 270	128	B3070707.P40	Lena Trough
7 July 2023	11:08:59	12:48:34	0	5975	90 / 270	138	B3070711.P08	Lena Trough
10 July 2023	12:02:48	13:33:04	0	5416	90 / 270	127	B3071012.P02	Lena Trough
10 July 2023	14:30:34	16:18:58	0	6504	90 / 270	151	B3071014.P30	Lena Trough
12 July 2023	07:20:45	08:46:38	0	5153	90 / 270	118	B3071207.P20	Lena Trough
21 July 2023	07:54:51	09:39:02	0	6251	125 / 305	144	B3072107.P54	Gakkel Ridge
21 July 2023	10:40:05	12:40:06	0	7201	125 / 305	165	B3072110.P39	Gakkel Ridge
21 July 2023	13:34:51	15:17:57	0	6186	125 / 305	137	B3072113.P34	Gakkel Ridge

### **Preliminary results**

#### *OBS data*

The data quality of the seismic records is good, with the PPSDs of all OBSs apart from AUR02 showing low noise levels close the lower end of the Peterson Low Noise Model (Peterson 1993, Fig. 2.4). The secondary microseismic peak near 5 s period is clearly visible for all stations. AUR02, despite occasionally showing clear phase arrivals, overall had a low sensitivity and a poorly pronounced secondary microseismic peak. The correction of the clock drift cannot be done during the cruise, thus, only a first look on the raw data was done during the cruise. An example of a recorded local earthquake with clear phase onsets can be seen in Figure 2.5. Subsequent processing after the time correction will include systematic event detection and phase picking to compile an earthquake catalogue for the Aurora region.

#### *Magnetic data*

During the cruise, only a very limited data processing could be performed as necessary external information (daily variations) from onshore observatories in Greenland and Svalbard was not available. Figure 2.3 shows an example of IGRF-corrected data for the northernmost lines. Spreading anomalies are clearly visible.

#### *Gravity data*

No data processing could be done during the cruise due to the missing harbour measurement at the end of the cruise. Thus, we can not report any results here.

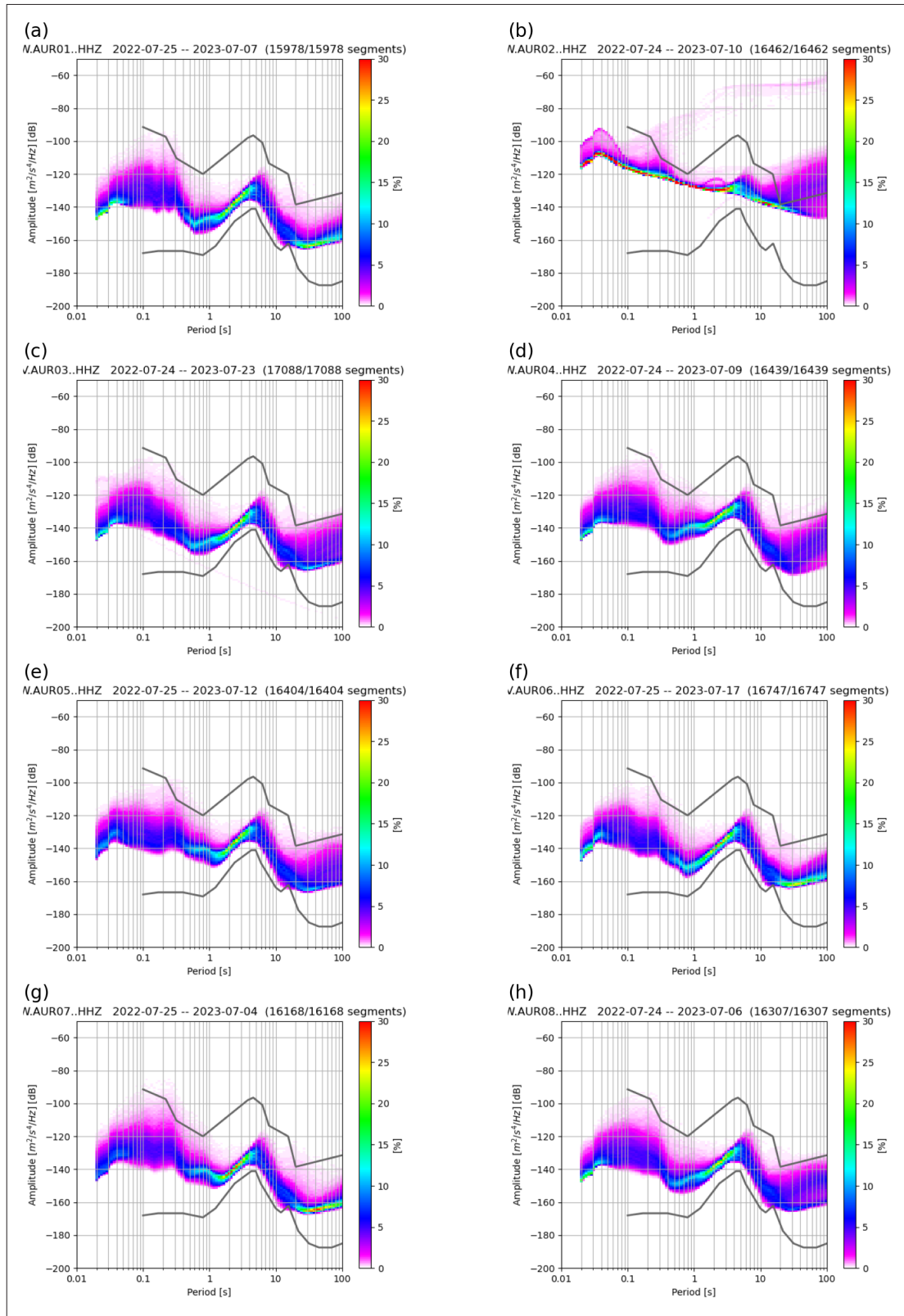


Fig. 2.4: PPSDs of the vertical component (HZ) from each of the 8 OBS stations (a-h). Grey lines represent Peterson Low Noise Model (Peterson 1993)

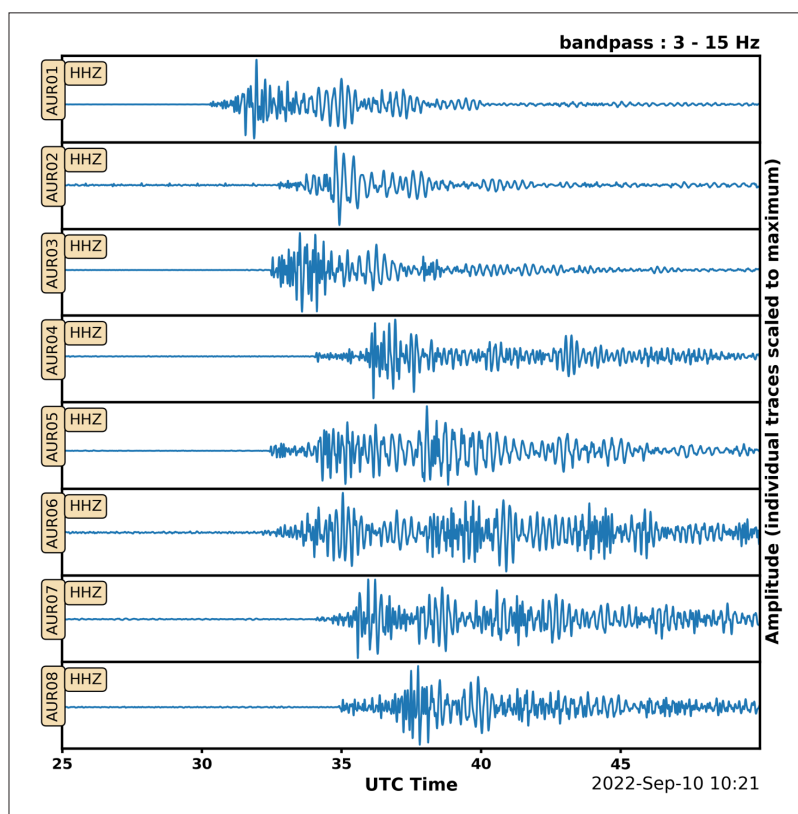


Fig. 2.5: Continuous seismic data showing a local event on the vertical component of all 8 stations from 10 September 2022. A bandpass filter (3 – 15 Hz) is applied to the data and the amplitudes are scaled to the maximum of the individual traces.

### Data management

Magnetic and gravity data will be archived, published and disseminated according to international standards by the World Data Center PANGAEA Data Publisher for Earth & Environmental Science (<https://www.pangaea.de>). By default, the CC-BY license will be applied.

Raw seismological data will be archived and published in PANGAEA. Time-corrected miniseed archives of the seismological data will be submitted to GEOFON from where they are accessible with seismological data base query tools.

This expedition was supported by the Helmholtz Research Programme “Changing Earth – Sustaining our Future” Topic 2, Subtopic 3.

In all publications based on this expedition, the **Grant No. AWI\_PS137\_02** will be quoted and the following publication will be cited:

Alfred-Wegener-Institut Helmholtz-Zentrum für Polar- und Meeresforschung (2017) Polar Research and Supply Vessel POLARSTERN Operated by the Alfred-Wegener-Institute. Journal of large-scale research facilities, 3, A119. <http://dx.doi.org/10.17815/jlsrf-3-163>.

For OBS data Alfred-Wegener-Institut Helmholtz-Zentrum für Polar- und Meeresforschung et al. (2017). DEPAS (Deutscher Geräte-Pool für amphibische Seismologie): German Instrument Pool for Amphibian Seismology. Journal of largescale research facilities, 3, A122. <http://dx.doi.org/10.17815/jlsrf-3-165> will be cited

## References

- Edmonds HN, Michael PJ, Baker ET, Connelly DP, Snow JE, Langmuir CH, Dick HJB, Mu R, German CR, Graham DW (2003) Discovery of abundant hydrothermal venting on the ultraslow-spreading Gakkel ridge in the Arctic Ocean. *Nature* 421. <https://doi.org/10.1038/nature01351>
- Kanzow T (2023) The Expedition PS131 of the Research Vessel Polarstern to the Fram Strait in 2022. *Reports on Polar and Marine Research* 770. [https://doi.org/10.57738/BzPM\\_0770\\_2023](https://doi.org/10.57738/BzPM_0770_2023)
- Meier M, Schlindwein V (2018) First In Situ Seismic Record of Spreading Events at the Ultraslow Spreading Southwest Indian Ridge. *Geophysical Research Letters* 45. <https://doi.org/10.1029/2018GL079928>
- Meier M, Schlindwein V, Scholz J-R, Geils J, Schmidt-Aursch Mc, Krüger F, Czuba W, Janik T (2021) Segment-scale seismicity of the ultraslow spreading Knipovich Ridge. *Geochemistry Geophysics Geosystems* 22. <https://doi.org/10.1029/2020GC009375>
- Meier M, Schlindwein V, Schmid F (2022) Magmatic activity and dynamics of melt supply of volcanic centers of ultraslow spreading ridges: hints from local earthquake tomography at the Knipovich Ridge. *Geochemistry Geophysics Geosystems* 23. <https://doi.org/10.1029/2021GC010210>
- Peterson J (1993) Observation and modeling of seismic background noise, U.S. Geological Survey Technical Report 93-322:1–95.

### 3. NEREID UNDER ICE HYBRID AUV-ROV OPERATIONS

Molly Curran<sup>1</sup>, Michael Jakuba<sup>1</sup>, Victor Nacklicki<sup>1</sup>,  
Alissa Dalpe<sup>1</sup>, Matthew Silvia<sup>1</sup>, Rosemary Loer<sup>1</sup>,  
Laura Lindzey<sup>2</sup>, Andrew Klesh<sup>3</sup>, Andrew Branch<sup>3</sup>,  
Elmar Albers<sup>1</sup>, Jeffrey Seewald<sup>1</sup>, Maren Walter<sup>4</sup>,  
Christopher German<sup>1</sup>

not on board: Andrew Bowen<sup>1</sup>, Steve Chien<sup>3</sup>,  
Kevin Hand<sup>3</sup>, Wolfgang Bach<sup>4</sup>

<sup>1</sup>US.WHOI

<sup>2</sup>US.UW

<sup>3</sup>US.JPL

<sup>4</sup>DE.UNI-BREMEN

**Grant-No. AWI\_PS137\_04**

#### Objectives

This chapter describes the research aboard PS137 using WHOI's *Nereid Under Ice (NUI)* deep submergence vehicle to conduct hybrid AUV-ROV dives to the seafloor at selected target areas along the Gakkel Ridge as part of the ALOIS programme.

The main objectives of the *NUI* group on PS137 were linked to a complementary NASA-funded research project, with science and technology components, focussed on advancing the search for life on other ocean worlds (German et al., 2022a). *Scientifically*, our priority on PS137 was to collect samples of hydrogen-rich vent-fluids from the Aurora hydrothermal field, at a range of temperatures that cross the limits for life on Earth, to investigate the system's potential to host abiotic organic synthesis. We have demonstrated that such processes can arise on the similarly ultra-slow spreading Mid-Cayman Rise (McDermott et al., 2015) and there is preliminary evidence that similarly hydrogen-rich venting may also arise at the bottom of the ice-covered ocean of Saturn's moon Enceladus (Waite et al., 2017). On Earth, such seafloor fluid-flow environments provide energy for microbial metabolisms that underpin *chemosynthetic* ecosystems. Logically, similarly habitable environments could arise on other ocean worlds, expanding both the volume and diversity of habitable space within our own solar system (Hendrix et al., 2019) and among other ocean world exo-planets (Quick et al., 2020). *Technologically*, our use of *NUI* during PS137 will build on our past work to autonomously explore for, and localize, submarine vent-sites within unexplored oceans (Branch et al., 2018, 2019). On PS137, our goal was to advance autonomous strategies to the next level: to enhance the near-seafloor search for characterization and selection of seafloor target sites *within* an identified hydrothermal field. PS137 provided the opportunity of having autonomy experts at sea together with an experienced piloted-operations team to collect training data-sets for future research into autonomous sampling site approach and landing.

In the wider context of ALOIS, our team's contributions also pursued two further whole-project objectives: in AUV mode, our *NUI* mapping surveys of the Aurora vent-field and Lucky B areas will help to provide new perspectives to advance our understanding of the geological controls of venting in the Arctic; in ROV mode, *NUI* was able to conduct reconnaissance and sampling to help guide the seafloor geology, oceanography, microbiology and OFOBS teams at Lena Trough. Although we were only able to collect a single sulfide sample for mineralogy/microbiology at Aurora, as a complement to our geochemical research program, we were able to guide the *Kronprins Haakon* and ROV *Aegir* to the same sites in the hope that they would be able to conduct additional sampling at the targets we provided.

## Work at sea

- One engineering test and five deep NUI dives were attempted at sea with all but the first deep-dive attempt being very successful. While the 1°45'W and 3°00'W sites could not be accessed for planned work later in the cruise, three very successful dives to Aurora were completed (Fig. 3.1) plus a final dive at Lena Trough to search for a hydrothermal source in the Lucky B area, using the same strategy planned for 1°45'W.

**Tab. 3.1:** Summary statistics for all five dives

Dive	Max. Depth	Total Time	Bottom Time	Ship Drift	Max. Separation	Notes
041	121 m	03:38 hr	00:00 hr	n/a	n/a	Test dive.
042	1040 m	03:48 hr	00:00 hr	n/a	n/a	Aborted.
043	3901 m	09:50 hr	02:14 hr	3300 m	1500 m	
044	3922 m	09:23 hr	03:21 hr	4100 m	2100 m	
045	3970 m	09:35 hr	03:50 hr	3300 m	1400 m	
046	3398 m	10:23 hr	05:16 hr	7300 m	2700 m	

- PS137\_15-1 (*NUI* Dive 041). A successful test/engineering dive was completed en route to the Gakkel Ridge. This included deployment of *NUI* and its depressor to 100 m, unlatching of the vehicle from its depressor, engineering tests while submerged, and return to the ship with contact through *NUI*'s fiber optic microtether sustained throughout the dive.
- PS137\_23-1 (*NUI* Dive 042). This was the first planned dive to the Aurora hydrothermal field. Two factors contributed to this dive having to be abandoned before reaching the seafloor. First, the deployment of *NUI* and its depressor to 1,000 m proceeded as intended, but upon arrival at this greater depth/pressure, it was found that the vehicle was unable to detach its tow-body from the depressor and swim free to conduct its planned dive to the seafloor at 4,000 m. Second, during the 90 minutes spent descending to 1,000 m and then trouble shooting the engineering problem, a combination of ice conditions and drift at the ocean surface made it appropriate to return to the surface and recover the vehicle without further delay anyway. For all subsequent deployments at Aurora (*NUI* dives 043, 044, 045), the depressor was only deployed to 100 m prior to separation, as had worked flawlessly on Dive 041.
- PS137\_32-1 (*NUI* Dive 043). This was the first of three dives to the Aurora hydrothermal field and focussed on relocating the three known vent-sites reported from the *Kronprins Haakon*/ROV *Aurora* dives in 2021 (Ramirez-Llodra et al., 2023). During the dive, *NUI* relocated each of the **Hans Tore Vent**, the **Ganymede** vent and the **Enceladus** vent in sequence. Toward the end of the dive, a suitable low-temperature vent was identified suitable for sampling and *NUI* landed at this **Dragonfly** site (Fig. 3.2). Unfortunately, upon landing it was discovered that communications between the vehicle and the IGT vent-fluid samplers had ceased to function and no fluid sample could be taken. Using the vehicle's manipulator, however, it was possible to collect a sample of chimney wall material (NUI043-R1) from the **Dragonfly** vent and place it in its sample basket. Upon collection of that sample, the vehicle rose up and conducted multibeam mapping to the North East as it departed the site. Upon return to the ship the sulfide material was sub-sampled for mineral and microbiological studies. Contact through the microtether was sustained throughout the dive, up to and including shipboard recovery.
- PS137\_37-1 (*NUI* Dive 044). The second dive to the Aurora field, like the first, prioritized vent-fluid collection. During this dive a series of three new vents were discovered

(Fig. 3.2) – the **Walrus**, **Lander/OrbiLander** and **Polar Bear** sites. A conjugate pair of low temperature and high-temperature vent-fluid orifices were identified at the Lander/OrbiLander vent and *NUI* set down to sample the low temperature **Lander** orifice. It was not possible to collect a sample with the first of these IGTs (IGT#1) due to a problem with its valve rotation but the second bottle (IGT#2) did collect a high-quality vent-sample (Fig. 3.2). There was insufficient battery power remaining to collect a corresponding sulfide sample upon completion of IGT sampling prior to returning to the surface. Contact through the microtether was sustained throughout the dive, up to and including shipboard recovery.

- PS137\_50-1 (*NUI* Dive 045). The final dive to Aurora had a primary priority to conduct a systematic search for venting across the entire Aurora field followed by sampling of active vent-fluids and new locations away from what was already known. To start, a systematic mapping survey was planned that extended for ~400 m in a generally NE-SW orientation centered on the known vent-sites from KPH2021 and *NUI* Dive 044 results (Fig. 3.1). Three survey lines were planned, each approximately 400 m long and at 75 m separation, centered on the known sites. At the beginning of the central survey line, a distinct and pronounced temperature anomaly was detected in near real time and a series of steep sided topographic features were identified in the real-time bathymetry displays as *NUI* progressed along this line (Fig. 3.3). Accordingly, the extent of the mapping survey was adjusted to reach ~150 m farther to the South West prior to commencing seafloor sampling and exploration.
- Upon reaching the seafloor, the first action undertaken was to return to the location at which the temperature anomaly had been detected during the preceding mapping survey. There two black smoker vent systems from *NUI* dive 044 were re-located, **Polar Bear** and **Lander/OrbiLander** chimneys. First, a set of three vertical imaging transects of the **Polar Bear** vent were completed, to add to the first vertical transect completed as *NUI* left the seafloor at the end of *NUI* dive 044. To complement the clear low temperature fluid collected from the **Lander** orifice during the preceding dive, IGT#1 was used to collect a high-quality end-member vent-fluid sample from the **OrbiLander** orifice. After collecting this sample, a fault on the manipulator claw prevented any further sampling and the remainder of the dive was devoted to further reconnaissance and survey operations. Subsequently, *NUI* was oriented to traverse to the SW, starting at the **Walrus** site which had also been identified during *NUI* dive 044 and encountering four more “Black Smoker” vents (Fig. 3.4): **Beluga**, **Arctic Fox**, **Narwhal** and **QuiNUItuq**. During this transect, *NUI* also passed over multiple lower-temperature flow-sites characterized by bright yellow-orange mineral/microbial discoloration ± orifices discharging hot, clear fluids. At **QuiNUItuq**, a 20 m tall chimney, three vertical video-transects were completed. *NUI* then conducted a final line of mapping survey, from **QuiNUItuq** to the **Polar Bear** area before return to the surface. Contact through the microtether was sustained throughout the dive, up to and including shipboard recovery.
- PS137\_57-1 (*NUI* Dive 046). Toward the end of the cruise, a final *NUI* dive was conducted as the first operation in Lena Trough in pursuit of the source for the Lucky B plume detected during *Polarstern* cruise PS66 in 2004 (Budéus & Lemke, 2004). This was the most ambitious of our *NUI* dives because it involved three components: a fixed depth water column sensing survey at the depth of the plume reported in 2004 ( $3,225 \pm 25$  m) with *NUI* employed as a (micro)tethered AUV; a mapping survey with location to be informed by the results of the water-column survey, still in tethered AUV mode; and finally a video-reconnaissance ± sampling survey at the seafloor in ROV mode. The initial water-column survey followed a saw-tooth pattern with 1 km lines

extending toward and away from the 3,250 m contour, working from North to South at a constant depth of  $3,225 \pm 25$  m. [Note: Survey depth was picked from the PS66 Cruise Report (Budéus & Lemke, 2004) but subsequent CTD operations revealed that plume depth in this area was ~400 m shallower, at ~2,850 m].

- Following ~90 minutes of water-column survey, which revealed evidence for decreasing methane anomalies to south and west, but no compelling evidence for a local plume source, a mapping survey was conducted over a topographic feature identified during the plume survey from the multibeam sonar which was already powered on and logging data. This mapping survey, which lasted approximately 1h, covered an area of ~300 m x 300 m via a series of 5 survey lines, each at 50 m altitude and spaced 75 m apart. The mapping survey was centered on a location at  $81^{\circ}21.931'N$   $003^{\circ}24.267'W$ . Finally, upon completion of the mapping survey, *NUI* was lowered to the seafloor and, in ROV mode, drove to and ascended along the same transect as AUV Mapping Line 3. While no active sources of venting were observed throughout the ~1.5h of ROV operations, the strongest *in situ* methane (METS) anomalies observed throughout the entire dive were observed approximately 3 minutes after *NUI* left the seafloor, at ~70 m altitude.

### Preliminary results

**Mapping:** During the PS137 cruise we were able to conduct systematic mapping of the Aurora hydrothermal field (Fig. 3.1) and locate 7 new high-temperature vents in addition to the three sites that had already been identified from previous expeditions in 2014, 2019 and 2021 (German et al., 2022b; Ramirez-Llodra et al., 2023).

**Vent-Fluids:** We were also able to collect a conjugate pair of low- and high-temperature vent-fluids at **Lander/Orbi-Lander**. Hydrothermal vent fluids were collected using isobaric gas-tight (IGT) fluid samplers (Seewald et al., 2002) deployed from the ROV *NUI* (Fig. 3.2). The primary scientific objective of the fluid sampling programme was to examine fluid-rock interactions and magmatic processes that regulate the chemistry of hot-spring fluids at the Aurora vent field with a focus on abiotic reactions occurring during mixing of high temperature fluids with seawater in subseafloor upflow zones. Two samples were collected; the first at a  $126^{\circ}C$  vent (**Lander**) during *NUI* Dive 44 (Sample NUI044-IGT2) and the second at the conjugate  $\sim 350^{\circ}C$  vent (**OrbiLander**) during *NUI* Dive 45 (Sample NUI045-IGT1). Due to a malfunctioning thermocouple during collection of Sample NUI045-IGT1 there is significant uncertainty ( $\pm 10^{\circ}C$ ) associated with the measured temperature. Fluid samples were analyzed at sea for dissolved  $H_2$  and  $CH_4$  by gas chromatography, pH ( $25^{\circ}C$ ) using a Ag/AgCl combination reference electrode, and total dissolved  $H_2S$  by ion selective electrode. Fluid aliquots were archived for shore-based analysis of dissolved major and trace cations by inductively coupled plasma – mass spectrometry (ICPMS), the abundance and carbon isotopic composition  $CH_4$  and  $CO_2$  by isotope ratio monitoring – gas chromatography mass spectrometry (irm-GCMS), dissolved inorganic anions and cations and organic acids by ion chromatography, and ammonium using flow injection analysis. Aliquots of the same fluid samples were provided for noble gas analyses at UNI-Bremen (NUI044-IGT2 & NUI045-IGT1) and for use in microbial incubation experiments aboard ship (NUI045-IGT1).

**Autonomous Vent-Localization:** We successfully collected a dataset that will be used to develop algorithms for fully autonomous mapping of high-temperature and low-temperature hydrothermal venting and for autonomous selection of one or more vent locations for further sampling. The dataset collected consists of data from a Norbit MBES multibeam bathymetric sonar, scalar sensor data from 4 sensors (Seabird FastCAT49 CTD, Wetlabs ECO FLNTURTD dual-channel chlorophyll and turbidity fluorometer, Franatech METS methane sensor, and APS Eh/Redox electrode), and video from multiple high-definition and standard-definition cameras.

Dives 043 to 045 were completed at the Aurora Vent Site. Approximately 2.5 km of mapping surveys were completed in total over the hydrothermally active region and the surrounding area (see Fig. 3.3 as one example). Each dive also consisted of a camera survey at near-seafloor altitudes (0-5 meters) in the hydrothermally active region. Dive 046 was completed at the Lucky B Site. Data was acquired at three heights, a 3,225-meter fixed depth and a 50-meter altitude mapping survey and a seafloor level camera survey. This dataset will be used for two primary purposes with regards to algorithm development. First, it will assist in understanding the relationship between the response of the different available data streams and the corresponding hydrothermal venting. Included in this will be determining which of the available sensors are the most relevant for the task of mapping and worksite selection. The data collected at various altitudes reflects the current methodologies for mapping hydrothermal vent fields. The camera surveys provide ground truth information for the known vent locations relative to the collected data. Second, it will be used as a test case for the developed algorithms for autonomous mapping and worksite selection.

*Toward Autonomous Vent Site Approach:* Once a vent-site has been identified as suitable for more detailed characterization, pilots are required for *NUI* to approach the seafloor and set up to conduct sampling. The final component of our cruise work has been to acquire i) Stereo imaging for near-site mapping of selected worksites in AUV mode and ii) operational data from piloted-operations when setting up for sampling in ROV mode. Cameras developed for the Orpheus vehicle – with onboard Snapdragon processors and 1,300x1,600 grayscale focal plane arrays – were incorporated as a stereo pair on the “chin” of *NUI* for close-approach imaging of potential sampling sites. Imaging data was captured in several modes. During *NUI* dive 043, video was live-streamed to surface operators to evaluate the placement of the cameras vs real-time vehicle altitude. The RTSP compressed data stream was recorded simultaneously on each camera and on top-side computers. During *NUI* dive 044, high resolution video was recorded solely on the cameras as RAW8 video files (the high-resolution precluded streaming). During dive *NUI*045, video was recorded as higher-pixel-depth RAW12 image frames (which simplified timestamping of images to UTC time). Between dives, imaging data was evaluated for utility with feedback provided to the pilot for ideal approach altitude. In addition, data from the multiple SD cameras, the pan/tilt/zoom HD camera, and the 4K-fixed-position camera present on *NUI* were evaluated. Recordings from all cameras were used for preliminary 3D terrain reconstruction, including at several hydrothermal vents (see Fig. 3.5). These cameras, along with the telemetry streams, recorded pilot operations and decision making. Due to the varied terrain and multitude of vents discovered (aka, obstacles and hazards), AUV mode was only used at altitudes 30 m and higher, which (due to lighting) precluded simultaneous use of camera recording. Likewise, low-altitude approaches under ROV (piloted)-mode precluded the use of sonar, but necessitated cameras. By using the full complement of cameras on *NUI*, which provide varied imaging angles, including the stereo-pair, the 3D-reconstruction will be married with the higher-altitude bathymetric data to provide an environment reconstruction of the virtual Aurora vent site for future autonomy research.

#### **Data Management**

For this cruise *NUI* was equipped with a Seabird FastCAT49 CTD, a Wetlabs ECO FLNTURTD dual-channel chlorophyll and turbidity fluorometer, a Franatech METS methane sensor, an APS Eh/Redox electrode, a forward-looking Blueview imaging sonar, a Kongsberg internal pan/tilt/zoom HD video camera, a SubC Rayfin digital camera with 4K video, custom JPL recording stereo pair cameras, upward and a downward looking 300 kHz RDI ADCP/DVLs, and a Norbit MBES multibeam bathymetric sonar. A complete set of data from these systems, along with vehicle engineering data has been provided to the Chief Scientist Vera Schlindwein on external drives in native format for archival with the PANGAEA system in Germany.

Processed multibeam bathymetry and timeseries data (interpolated onto a 1 second timebase and including navigation) have also been provided as netCDF and CSV files, respectively. Duplicate sets of the same data will be returned to WHOI by Co-Chief Scientist Chris German where they will be archived (ideally within NSF's Marine Geosciences Data System) but can also be made available upon request.

In all publications based on this expedition, the **Grant No. AWI\_PS137\_04** will be quoted and the following publication will be cited:

Alfred-Wegener-Institut Helmholtz-Zentrum für Polar- und Meeresforschung (2017) Polar Research and Supply Vessel *POLARSTERN* Operated by the Alfred-Wegener-Institute. Journal of large-scale research facilities, 3, A119. <http://dx.doi.org/10.17815/jlsrf-3-163>.

Participation of the *NUI* Team from the USA on Cruise PS 137 was funded through the PSTAR Grant "Science and Technology for Ocean Worlds: Ice Covered Ecosystems:" from NASA's Astrobiology Program, Award Number: 80NSSC22K1312.

### Acknowledgements

The *NUI* team would especially like to acknowledge the strong support and generous opportunities provided to our dive operations by Chief Scientist Vera Schlindwein throughout a cruise that presented multiple challenges but where she remained calm, collected, cheerful and always ready with a new plan for us to pursue. Implementation of those plans would not have been nearly as productive as they were without the help of the Bridge team and we especially thank Dr.H.Jakob Bünger (Drift+Noise) for such care and attention to helping plan our dive trajectories and to Captain Moritz Langhinrichs and Chief Mate Jacob Langhinrichs for their exceptional seamanship in helping make our theoretical dream-deployments a reality. We thank Herrn Bootsman Sebastian Brück and his crew for their support in a series of safe deployments and recoveries of *NUI* at many unsocial hours of night and day and, finally, a sincere thanks to everybody aboard PS137 for making our team from the USA for feeling so welcome. For some of us it was our 3<sup>rd</sup> experience with *NUI* in the Arctic sailing aboard *Polarstern* and from the very first day, it felt like coming home. We hope you will invite us back!

### References

- Branch A, Xu G, Jakuba MV, German CR, Chien S, Kinsey JC, Bowen AD, Hand KP & Seewald JS (2018) Autonomous Nested Search for Hydrothermal Venting In Workshop on Planning and Robotics, International Conference on Automated Planning and Scheduling (ICAPS PlanRob 2018), Delft, Netherlands.
- Branch A, McMahon J, Xu G, Jakuba MV, German CR, Chien S, Kinsey JC, Bowen AD, Hand KP & Seewald JS (2019) Demonstration of Autonomous Nested Search for Local Maxima using an Unmanned Underwater Vehicle. IEEE Robotics and Automation Letters (RA-L). Paris, France, 2020, pp. 1888–1895. <https://doi.org/10.1109/ICRA40945.2020.9196625>.
- Budéus G & Lemke P (2004) The Expedition ARKTIS-XX/1 and XX/2 of the Research Vessel "*Polarstern*" in 2004. Cruise Report, 182pp.
- German CR, Blackman DK, Fisher AT, Girguis PR, Hand KP, Hoehler TM, Huber JA, Marshall JC, Pietro KR, Seewald JS, Shock EL, Sotin C, Thurnherr AM & Toner BM (2022a) Ocean system science to inform the exploration of ocean worlds. *Oceanography* 35:16–22. <https://doi.org/10.5670/oceanog.2021.411>.
- German CR, Reeves E, Türke A, Diehl A, Albers E, Bach W, Purser A, Ramalho SP, Suman S, Mertens C, Walter M, Ramirez-Llodra E, Schlindwein V, Bünz S & Boetius A (2022b) Volcanically hosted venting with indications of ultramafic influence at Aurora hydrothermal field on Gakkel Ridge. *Nat. Commun.*,13:6517.

- Hendrix A R, Hurford TA, Barge LM, Bland MT, Bowman JS, Brinkerhoff W, Buratti BJ, Cable M, Castillo-Rogez J, Collins G, Diniega S, German CR, Hayes AG, Hoehler T, Hosseini S, Howett C, McEwen A, Neish C, Neveu M, Nordheim TA, Patterson GW, Patthoff DA, Rhoden A, Schmidt B, Singer K, Soderblom J, and Vance SD (2019) Roadmap to Ocean Worlds. *Astrobiology* 19. <https://doi.org/10.1089/ast.2018.1955>.
- McDermott JM, Seewald JS, German CR & Sylva SP (2015) Pathways for abiotic organic synthesis at submarine hydrothermal fields. *Proc. Nat. Acad. Sci.* 112:7668–7672.
- Quick LC, Roberge A, Mlinar AB, and Hedman MM, Forecasting Rates of Volcanic Activity on Terrestrial Exoplanets and Implications for Cryovolcanic Activity on Extrasolar Ocean Worlds, *Publications of the Astronomical Society of the Pacific*, 132:084402 (27pp), 2020 August, <https://doi.org/10.1088/1538-3873/ab9504>
- Ramirez-Llodra E, Argentino C, Baker M, Boetius A, Costa C, Dahle H, Denny EM, Dessandier P, Eilertsen MH, Ferre B, German CR, Hilário A, Jamieson JW, Mall A, Panieri G, Purser A, Ramalho SP, Reeves EP, Rolley L, Pereira SI, Ribeiro PA, Sert MF, Steen IH, Stetzler M, Stokke R, Victorero L, Vulcano F, Vâgenes S, Waghorn KA & Buenz S (2023) Hot vents beneath an icy ocean: The Aurora Vent Field, Gakkel Ridge, revealed. *Oceanography* 36:8–19. <https://doi.org/10.5670/oceanog.2023.103>.
- Seewald JS, Doherty KW, Hammer TR & Liberatore SP (2002) A new gas-tight isobaric sampler for hydrothermal fluids. *Deep Sea Res.* 49:189–196.
- Waite JH, Glein CR, Perryman R, Teolis BD, Magee BA, Miller G, Grimes J, Perry ME, Miller KE, Bouquet A, Lunine JI, Brockwell T & Bolton SJ (2017) Cassini finds molecular hydrogen in the Enceladus plume: Evidence for hydrothermal processes. *Science* 356:155–159.

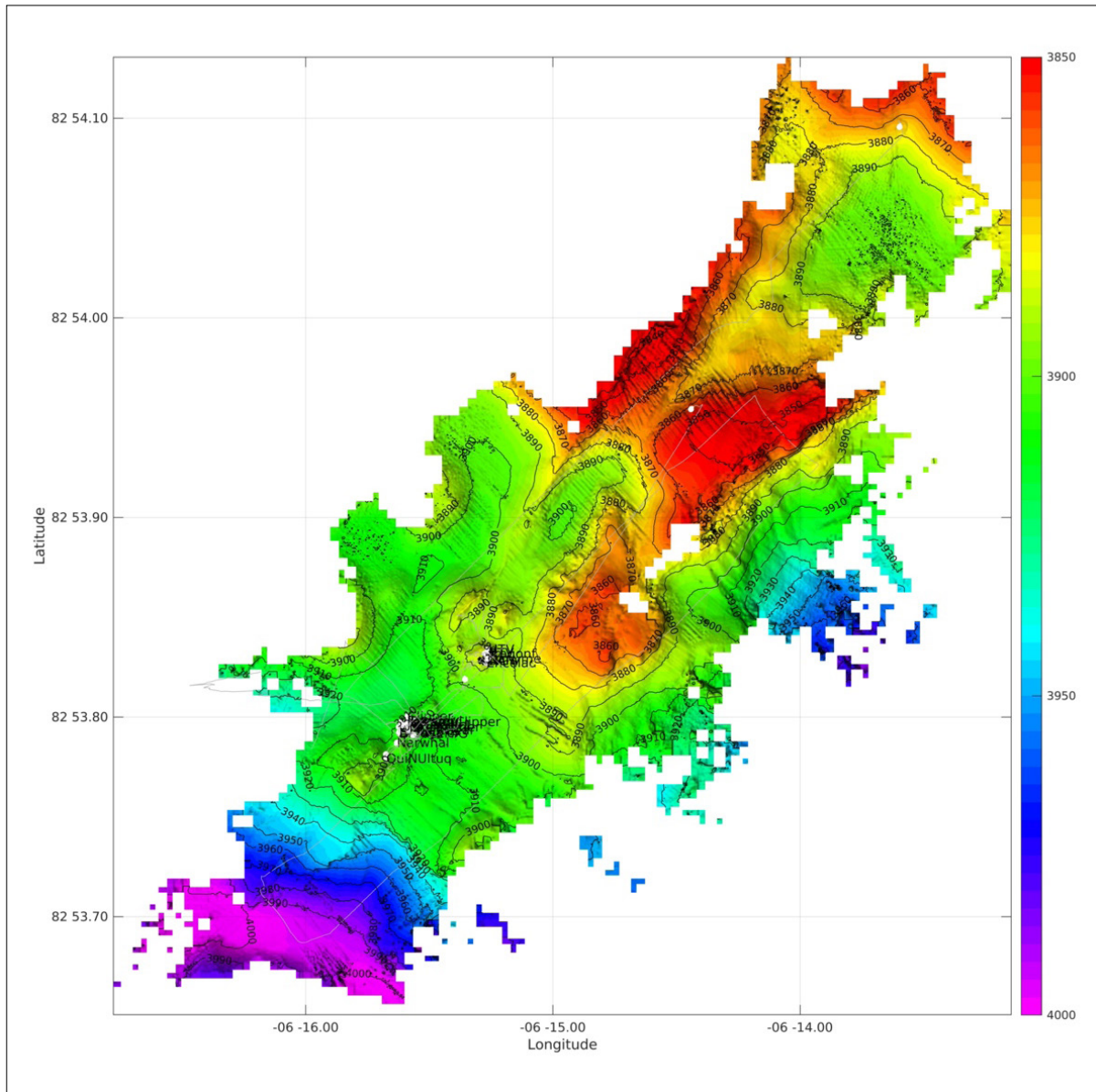


*Fig. 3.1 High resolution multibeam bathymetric map (working version) of the seafloor at the Aurora hydrothermal field Gakkel Ridge compiled from data collected during NUI Dives 043, 044 and 045 (vehicle tracklines are shown in pale grey). Previously known vents (Hans Tore Vent, Ganymede, Enceladus; Ramirez-Llodora et al., 2023) are clustered at  $\sim 82^{\circ}53.83'N$ ,  $6^{\circ}15.20'W$ . Seven additional vents discovered during this cruise were aligned NE-SW along strike from those vents starting at approximately  $82^{\circ}53.79'N$ ,  $6^{\circ}15.50'W$ .*

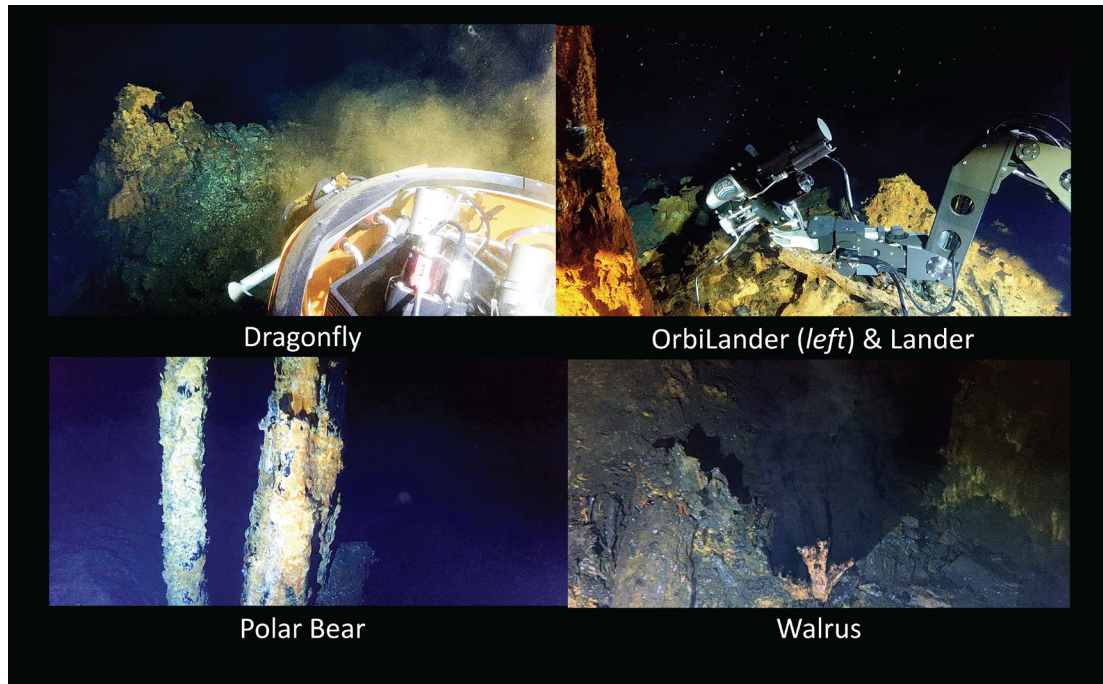


Fig. 3.2: Still images of 4 sites located and sampled during NUI Dives 043 and 044 (clockwise from top left): **Dragonfly** (sampled for sulfides on N43); **OrbiLander & Lander** showing the **Lander** orifice being sampled by IGT during N44 [the conjugate high temperature fluids from **OrbiLander** were collected on N45]; **Walrus** and **Polar Bear**.

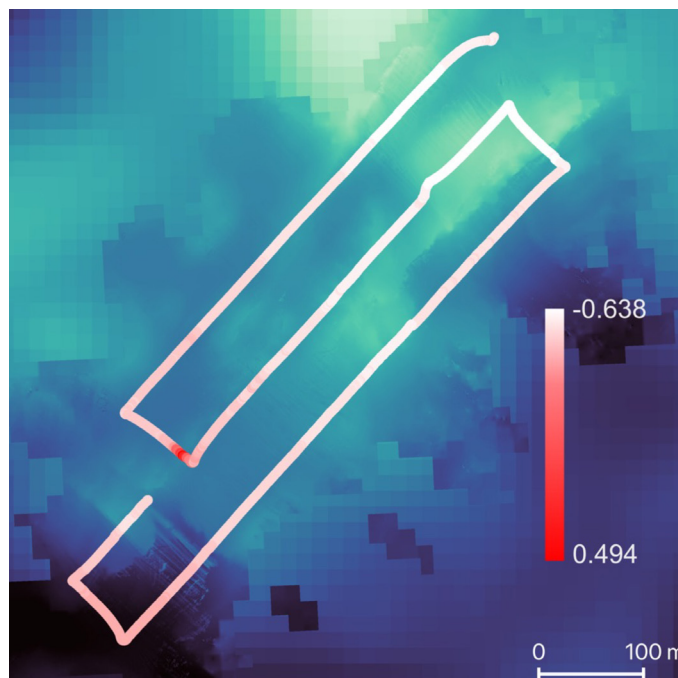


Fig. 3.3: A map of in situ temperature values detected in real-time while conducting the multibeam survey at 50 m altitude during the first phase of NUI dive 045. A series of high temperature hydrothermal vents was located along a NE-SW traverse starting directly beneath the pronounced temperature anomalies.

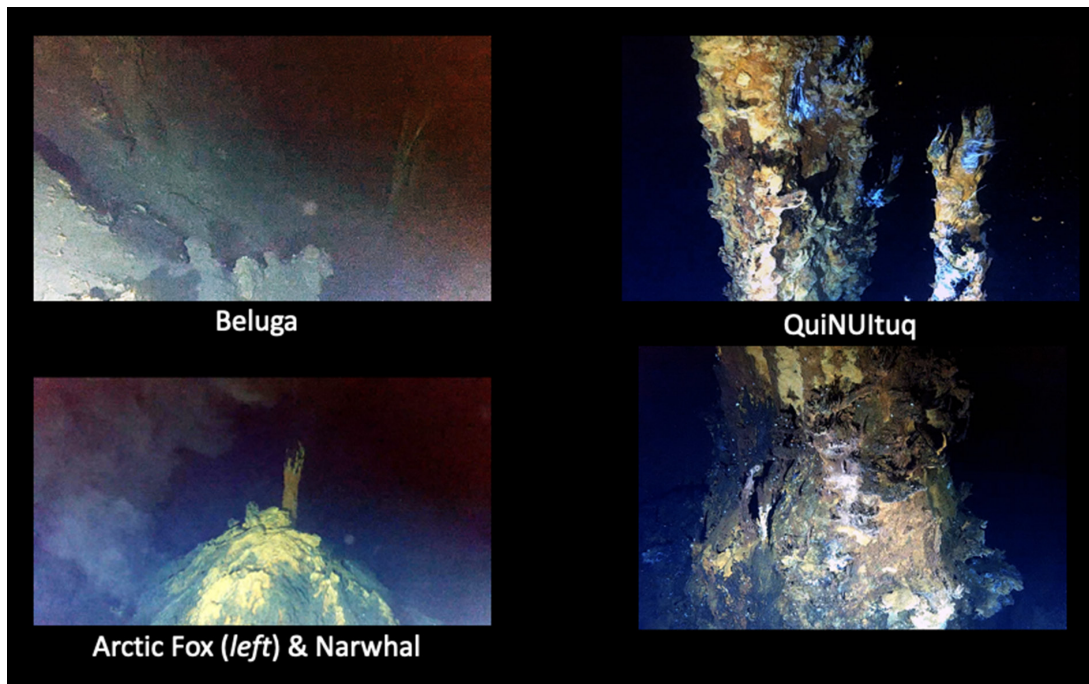


Fig. 3.4: Still images of 4 “black smoker” sites located during NUI Dive 045 (counter-clockwise from top left): **Beluga**; **Arctic Fox & Narwhal**; and **QuiNUItuq** (near its base & near its summit).

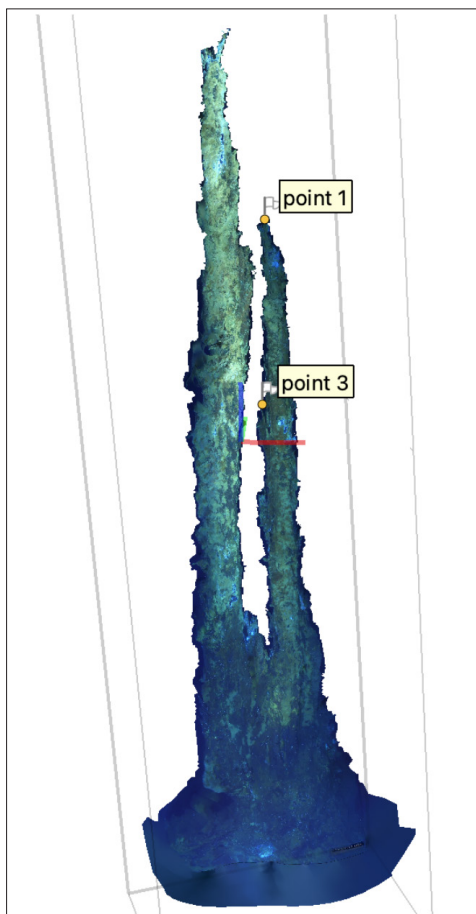


Fig. 3.5: Preliminary 3D reconstruction of the entire ~20 m tall **QuiNUItuq** vent using 213 images from the NUIHD camera. As a monocular camera, no scale information is provided. Images from the stereo camera pair used in this effort will be combined with these images (and additional views/telemetry) to provide scale and a more detailed vent reconstruction. These reconstructions will be combined with bathymetric data for environment reconstruction of the full Aurora site.

## 4. HYDROACOUSTICS

Fynn Warnke<sup>1</sup>, Ellen Unland<sup>1</sup>, Laura K. Höppner<sup>1</sup>; <sup>1</sup>DE.AWI  
not on board: Boris Dorschel<sup>1</sup>, Simon Dreutter<sup>1</sup>

**Grant-No. AWI\_PS137\_03**

### Objectives

Accurate knowledge of the seafloor topography, hence high-resolution bathymetry data, is a basic key information and necessary to understand many marine processes. It is of particular importance for the interpretation of scientific data in a spatial context. Bathymetry, hence geomorphology is furthermore a basic parameter for the understanding of the general geological setting of an area and tectonic landforms. Even information on tectonic processes and potential off-axis sources for earthquakes can be inferred from bathymetry.

While world bathymetry maps give the impression of a detailed knowledge of worldwide seafloor topography, most of the world's ocean floor remains unmapped by hydroacoustic systems. In these areas, bathymetry is modelled using satellite altimetry with a corresponding low resolution. Satellite-altimetry-derived bathymetry, therefore, lack the resolution necessary to resolve small- to mesoscale geomorphological features (e.g. sediment wave, glaciogenic features or small seamounts). Ship-borne multibeam data provide bathymetric information at a resolution sufficient to resolve these features and enable site selection for the other scientific working groups on board.

During the last shipyard stay, the hull-mounted transducers of the HydroSweep system were removed and reinstalled, which might result in different angular alignments. If not corrected accordingly, these alignment offsets can significantly impact the correct beam forming and could lead to systematic offsets in the data. Therefore, a calibration survey and subsequent patch test will be conducted during the cruise.

Accordingly, the main tasks of the bathymetry group on board *Polarstern* during PS137 were:

- calibration of multibeam system (patch test)
- collection of bathymetric data, including calibration and correction of the data for environmental circumstances (sound velocity, systematic errors in bottom detection, etc.)
- post-processing and cleaning of the data
- data management for on-site map creation
- collection of sediment echo-sounder data
- support for other working groups for site selection and station planning

## Work at sea

### *Technical description*

During expedition PS137 the bathymetric surveys and a patch test were conducted with the hull-mounted Multibeam Echosounder (MBES) Teledyne Reson HydroSweep DS3 (HSDS3). The HydroSweep is a deep-water system for continuous mapping with the full swath potential. It operates on a frequency of ~14 kHz. On *Polarstern*, the MBES transducer arrays are arranged in a Mills Cross configuration of 3 m (transmit unit) by 3 m (receive unit). The combined motion, position (Trimble GNSS), and time data comes from an iXBlue Hydrins system and the signal is directly transferred into the Processing Unit (PU) of the MBES to carry out real-time motion compensation in Pitch, Roll and Yaw. With a combination of phase and amplitude detection algorithms the PU computes the water depth from the returning backscatter signal. The maximum opening angle is 140° (70° to each side of the nadir). In water depths deeper than 2,000 m and during heavy ice transit, the maximum opening angle is reduced to approx. 50° to each side of the nadir.

The hullmounted subbottom profiling system PARASOUND generates two primary frequencies, of which the lower frequency is selectable between 18 and 23.5 kHz transmitting in a narrow beam of 4° at high power (PHF). As a result of the non-linear acoustic behavior of water, the so-called “parametric effect”, two secondary harmonic frequencies are generated, one of which is the difference (e.g. 4 kHz, SLF) and the other the sum (e.g. 40 kHz, SHF). As a result of the longer wavelength, the difference parametric frequency (SLF) allows sub-bottom penetration up to 200 m (depending on sediment conditions) with a vertical resolution of about 30 cm. The primary advantage of parametric echosounders is based on the fact that the sediment-penetrating pulse is generated within the narrow beam of the primary frequencies, thereby providing a very high lateral resolution compared to conventional 4 kHz systems. For vertical beam transmission, this capability, however, limits good survey results on seafloor slopes, which are inclined to more than 4° relative to horizontal.

### *Data acquisition and processing*

Data acquisition was carried out throughout the entire cruise after leaving the territorial waters (12 nm zone) of Norway with the exception of a stop in Longyearbyen (Svalbard). Data acquisition was paused before entering Svalbard’s territorial waters and resumed afterwards. In addition, data logging was stopped during station work while pinging continued to provide accurate depth control. Repeated surveys at the Aurora vent field allowed to switch off the logging after achieving a dense data coverage for the site. A more detailed overview of the operating times is listed in Table 4.1. PARASOUND acquisition was only conducted during ice-free transit and for selected station work (e.g., heatflow, dredging and OBS deployment).

The HydroSweep was operated with Hydromap Control and for online visualization, Teledyne PDS was used. The bathymetric data was stored in ASD, PDS and S7K raw files. Subsequent data processing was done with Caris HIPS and SIPS. For generating maps, the data were exported to QGIS in GeoTIFF raster format.

The PARASOUND was also operated with Hydromap Control and the data was visualized in Parastore. Both PHF and SLF traces were visualized as online profiles on screen and stored in the following formats:

- PHF (ASD format)
- PHF (PS3 format; carrier frequency with geographic coordinates)
- SLF (ASD format)

- SLF (PS3 format; carrier frequency with geographic coordinates)
- Navigation and auxiliary data (60 seconds interval; ASCII format)

**Tab. 4.1:** Operating times of the HydroSweep DS3 system during cruise PS137.

Start [UTC]	Comment (Start)	Stop [UTC]	Comment (Stop)
2023-06-22 07:55:58		2023-06-23 19:06:29	Territorial waters of Svalbard (12 nm)
2023-06-24 10:31:49	Leaving territorial waters	2023-06-24 13:26:59	CTD for patch test (PS137/1-1)
2023-06-24 15:58:39	Swath Width: 175% of depth	2023-06-24 19:41:01	
2023-06-24 19:41:03	Swath Width: 150% of depth	2023-06-25 09:55:17	PS137/2-1 (Mooring)
2023-06-25 11:56:35		2023-06-25 12:22:30	PS137/3-1 (Mooring) and PS137/4-1 (CTD)
2023-06-25 17:46:47		2023-06-25 18:49:07	PS137/5-1 (Ice station)
2023-06-25 21:20:03		2023-06-26 08:31:20	PS137/6-1 (CTD)
2023-06-26 08:59:50		2023-06-26 11:04:55	PS137/7-1 (Mooring)
2023-06-26 12:49:20		2023-06-26 13:06:21	PS137/8-1 (Mooring)
2023-06-26 19:02:15		2023-06-27 05:28:17	PS137/10-1 (CTD) and PS137/11-1 (Mooring)
2023-06-27 13:54:26		2023-06-28 01:11:02	PS137/12-1 (CTD)
2023-06-28 05:47:06		2023-06-28 12:56:20	PS137/14-1 (CTD) and PS137/15-1 (NUI)
2023-06-28 20:17:16		2023-06-29 03:02:48	Temporary depth finding issue (~1 min)
2023-06-29 03:10:21		2023-06-29 08:20:00	
2023-06-29 14:32:42		2023-06-30 09:56:52	PS137/16-1 (Dredging)
2023-06-30 21:22:18		2023-06-30 23:24:39	PS137/18-1 (CTD)
2023-07-01 07:37:10		2023-07-01 08:28:45	PS137/20-1 (Heatflow)
2023-07-01 15:55:18		2023-07-02 22:02:21	PS137/21-1 (Mooring)
2023-07-04 09:09:54		2023-07-04 10:18:11	
2023-07-04 11:34:34		2023-07-04 14:03:12	OBS (AUR07) recovery
2023-07-04 21:39:24	Transit to CTD station at Aurora	2023-07-05 03:32:04	

Start [UTC]	Comment (Start)	Stop [UTC]	Comment (Stop)
2023-07-05 07:15:59		2023-07-05 09:35:51	Pinging OBS (AUR02)
2023-07-05 09:47:43		2023-07-05 11:21:22	
2023-07-05 11:34:16		2023-07-05 12:11:12	
2023-07-05 13:47:22		2023-07-05 13:51:11	
2023-07-05 15:46:30		2023-07-05 20:10:59	
2023-07-06 08:12:43	Transit to OBS (AUR08)	2023-07-06 10:56:02	Pinging OBS (AUR08)
2023-07-06 23:29:22		2023-07-07 08:04:51	Drifting in position for NUI/CTD
2023-07-08 08:38:36	Transit to CTD station at Aurora	2023-07-08 13:55:28	
2023-07-08 22:00:01	Transit to OBS (AUR04)	2023-07-08 22:45:00	
2023-07-08 23:36:53	Transit to OBS (AUR04)	2023-07-09 00:28:26	
2023-07-09 09:41:01	Transit to vent site	2023-07-09 11:09:26	
2023-07-11 10:16:13		2023-07-11 16:07:26	Drifting in position for OBS recovery
2023-07-11 20:14:30		2023-07-11 21:46:09	
2023-07-11 22:21:21		2023-07-11 22:49:51	Drifting in position for OBS recovery
2023-07-12 00:14:20	Transit to OBS position	2023-07-12 00:33:41	
2023-07-12 03:32:59		2023-07-12 06:19:35	
2023-07-12 14:13:06		2023-07-12 17:10:00	
2023-07-13 16:40:04		2023-07-13 19:55:19	PS137/42-1 (OFOBS)
2023-07-14 03:44:30		2023-07-15 09:40:09	at proposed heatflow station
2023-07-15 10:07:04		2023-07-16 22:35:44	stuck between ice floes
2023-07-16 22:50:24		2023-07-18 05:52:10	
2023-07-18 15:08:09		2023-07-20 14:17:22	
2023-07-23 10:06:26		2023-07-23 16:35:07	
2023-07-23 22:00:13		2023-07-24 19:52:49	

Start [UTC]	Comment (Start)	Stop [UTC]	Comment (Stop)
2023-07-24 21:09:08	Moving into position for NUI dive	2023-07-24 21:57:24	PS137/57-1 (NUI)
2023-07-25 14:34:58		2023-07-25 15:19:49	
2023-07-25 20:34:56	Transit to OFOBS station	2023-07-25 22:01:57	PS137/59-1 (OFOBS)
2023-07-26 04:36:40	Transit to dredging station	2023-07-26 05:37:08	PS137/60-1 (Dredging)
2023-07-26 10:11:14	Transit to CTD station	2023-07-26 10:33:18	PS137/61-1 (CTD)
2023-07-26 22:53:52	Transit to Jotul	2023-07-30 14:03:40	Finished survey

### *Sound velocity profiles*

For best survey results and to correct HydroSweep depths for changes of the sound velocity (SV) in the water column, SV profiles were generated from Conductivity Temperature Depth (CTD) data that were collected and provided by the oceanography group. This is essential, as the acoustic signal travels down the water column from the transducer to the seafloor and back to the surface through several different layers of water masses with each a different sound velocity. The SV is influenced by density and compressibility, both depending on pressure, temperature and salinity. Wrong or outdated sound velocity profiles lead to refraction errors and reduced data quality.

The SV profiles obtained by the CDT were immediately processed and applied within the MBES for correct beamforming during the survey. Additionally, these profiles were combined/extended with WOA18 (World Ocean Atlas 2018) data to create full ocean depth SV profiles. In cases where no CTD data was available, the SV profiles were extracted from the WOA18 database for the appropriate geographic position.

During PS137, a total of 37 SV profiles were applied to the MBES. This includes 17 SV profiles from the CTD data and 20 profiles generated using the WOA18 database. The SVP from station PS137/53-1 was not applied since the CTD cast was canceled a few meters below the sea surface.

### *Stations*

Data collection with the HydroSweep received the number PS137\_0\_Underway-54 throughout the expedition. HydroSweep and CTD stations are listed in Table 4.2. After leaving the port of Longyearbyen, a calibration survey (patch test) was conducted to verify and adjust the angular offsets of the hull-mounted transducer and receiver arrays if necessary.

Tab. 4.2: List of bathymetry-related stations during cruise PS137.

Station Number	Description	Device	Start [UTC]	Start LAT/ LON [deg]	End [UTC]	End LAT/ LON [deg]
PS137_0_0 Underway-54	Underway multibeam data acquisition	HydroSweep DS3	2023-06-22 07:55	71.605, 19.1838	2023-07-30 14:00	71.5966, 18.8802
PS137_1-1	Sound velocity profile (SVP)	CTD	2023-06-24 13:38	78.3159, 8.1091	2023-06-24 15:33	78.3161, 8.1102
PS137_1-2	patch test (calibration of installation parameters)	HydroSweep DS3	2023-06-24 15:56	78.3088, 8.1095	2023-06-24 19:40	78.4159, 8.3473
PS137_4-1	SVP	CTD	2023-06-25 16:46	80.4224, 10.1617	2023-06-25 17:40	80.4241, 10.1928
PS137_6-1	SVP	CTD	2023-06-26 08:51	80.9609, 8.6307	2023-06-26 09:53	80.9596, 8.6604
PS137_10-1	SVP	CTD	2023-06-27 05:30	81.4998, 7.2234	2023-06-27 09:49	81.5016, 7.1062
PS137_12-1	SVP	CTD	2023-06-28 01:13	81.319, 3.2375	2023-06-28 05:18	81.3136, 3.1268
PS137_14-1	SVP	CTD	2023-06-28 17:25	81.3585, 1.0676	2023-06-28 19:51	81.3643, 1.0969
PS137_18-1	SVP	CTD	2023-06-30 23:33	82.6058, -5.9714	2023-07-01 05:27	82.6143, -5.7407
PS137_22-1	SVP	CTD	2023-07-03 02:09	82.8981, -6.2553	2023-07-03 05:28	82.8949, -6.2148
PS137_26-1	SVP	CTD	2023-07-05 03:25	82.8944, -6.2213	2023-07-05 06:57	82.8898, -6.1855
PS137_26-1	SVP	CTD	2023-07-05 03:25	82.8898, -6.1855	2023-07-05 06:57	82.9104, -6.4152
PS137_28-1	SVP	CTD	2023-07-05 20:22	82.9104, -6.4152	2023-07-06 05:07	82.9012, -6.3616
PS137_33-1	SVP	CTD	2023-07-08 13:47	82.9087, -6.4027	2023-07-08 21:34	82.878, -6.2772
PS137_36-1	SVP	CTD	2023-07-10 07:09	82.9252, -6.2374	2023-07-10 14:19	82.8857, -6.2615
PS137_40-1	SVP	CTD	2023-07-12 18:13	82.9054, -6.2977	2023-07-12 20:40	82.8997, -6.4514
PS137_41-1	SVP	CTD	2023-07-13 10:39	82.9006, -6.2467	2023-07-13 13:54	82.8929, -6.2351
PS137_49-1	SVP	CTD	2023-07-18 12:12	83.8101, -3.4282	2023-07-18 15:03	83.8017, -3.4042

Station Number	Description	Device	Start [UTC]	Start LAT/ LON [deg]	End [UTC]	End LAT/ LON [deg]
PS137_52-1	SVP	CTD	2023-07-21 20:38	82.8983, -6.4104	2023-07-21 22:13	82.8969, -6.3758
PS137_53-1	SVP	CTD	2023-07-22 05:34	82.8982, -6.2933	2023-07-22 10:52	82.8957, -6.2487
PS137_55-1	SVP	CTD	2023-07-22 15:34	82.9015, -6.271	2023-07-22 18:22	82.8954, -6.2246
PS137_58-1	SVP	CTD	2023-07-25 15:20	81.3753, -3.3883	2023-07-25 20:28	81.3506, -3.4073
PS137_61-1	SVP	CTD	2023-07-26 10:40	81.3913, -3.4387	2023-07-26 16:18	81.3678, -3.3905

### Preliminary results

During 39 days of survey, a track length of 2,323 nmi (4,303 km) was surveyed by the swath bathymetry (Tab. 4.1). While on transit data gaps were closed, following along edges of already existing bathymetry data as permitted by the sea-ice conditions. Figure 4.1 shows an overview map of the collected bathymetry data for the entire cruise.

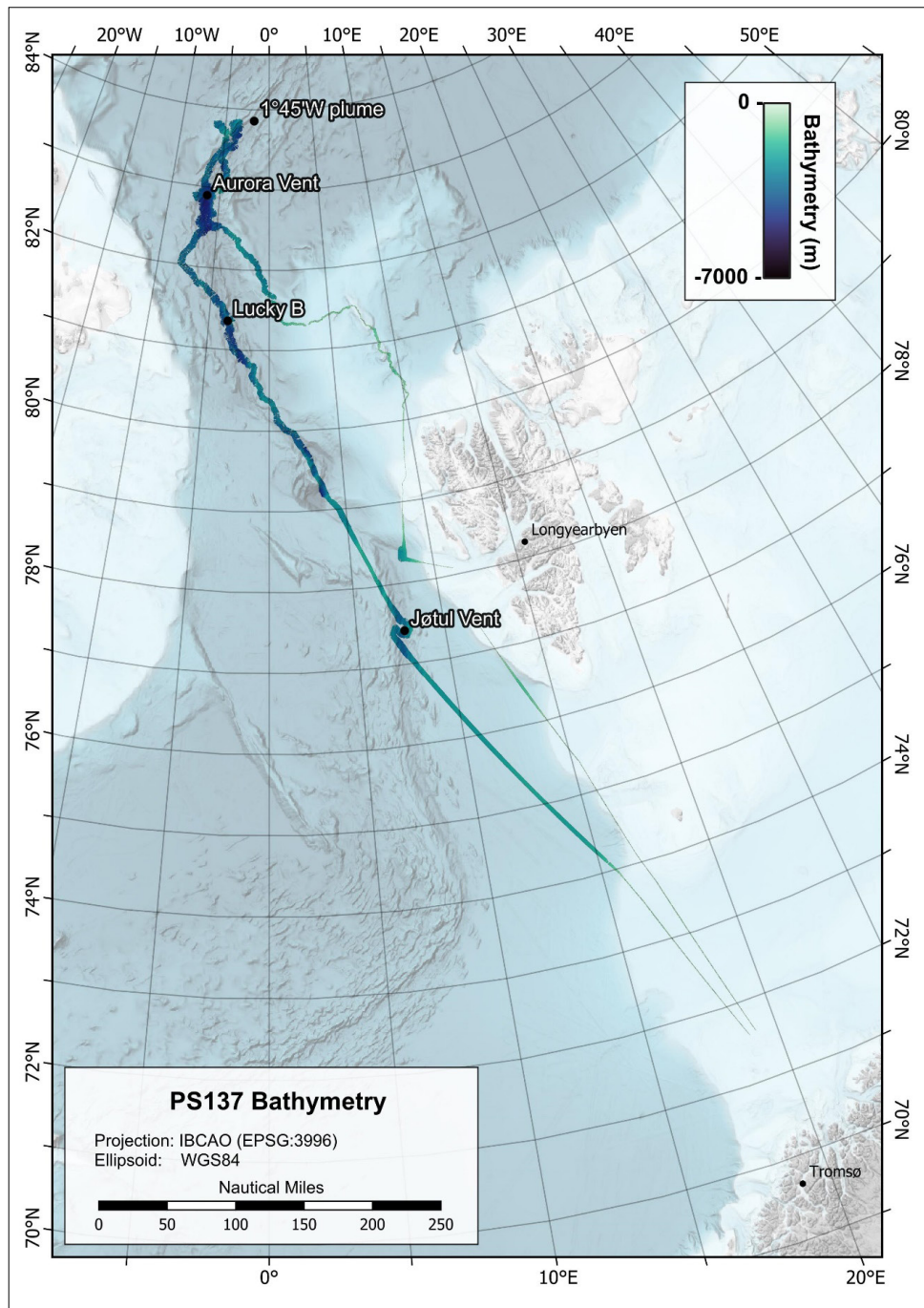


Fig. 4.1: Overview map of the bathymetric data coverage acquired during cruise PS137

For the Aurora vent site, repeated visits allowed the acquisition of an extensive amount of multibeam data as presented in Figure 4.2.

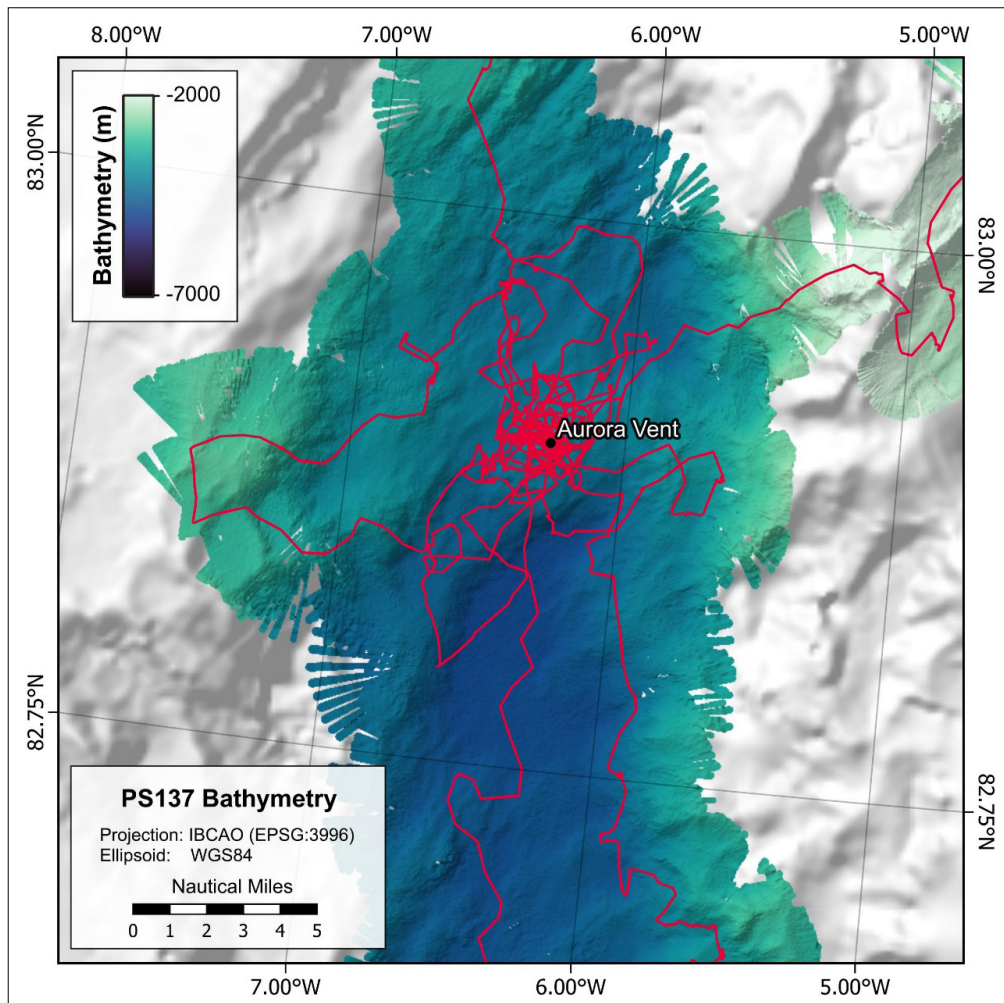


Fig 4.2: Aurora vent site data coverage (50 x 50 m grid resolution) with PS137 cruise track (red lines)

### Data management

Bathymetric data collected during PS137 will be archived, published and disseminated according to international standards by the World Data Centre PANGAEA Data Publisher for Earth & Environmental Science (<https://www.pangaea.de>) within two years after the end of the cruise. By default, the CC-BY license will be applied. Furthermore, the data will be provided to mapping projects and included in global bathymetry compilations such as the International Bathymetric Chart of the Arctic Ocean (IBCAO) and the General Bathymetric Chart of the Ocean (GEBCO) within the framework of the Nippon Foundation – GEBCO Seabed 2030 Project. Once georeferenced, the data will be linked for external accessibility in PANGAEA.

This expedition was supported by the Helmholtz Research Program “Changing Earth – Sustaining our Future” Topic 2, Subtopic 3.

In all publications based on this expedition, the **Grant No. AWI\_PS137\_03** will be quoted and the following publication will be cited:

Alfred-Wegener-Institut Helmholtz-Zentrum für Polar- und Meeresforschung (2017) Polar Research and Supply Vessel Polarstern Operated by the Alfred-Wegener-Institute. Journal of large-scale research facilities, 3, A119. <http://dx.doi.org/10.17815/jlsrf-3-163>.

## 5. HABITAT MAPPING

Lilian Böhringer<sup>1</sup>, Tea Isler<sup>1</sup>  
not on board: Autun Purser<sup>1</sup>, Boris Dorschel<sup>1</sup>

<sup>1</sup>DE.AWI

**Grant-No. AWI\_PS137\_03**

### Objectives

Benthic megafauna inhabit the sediment-water interface and are closely associated with their physical environment. Highly variable geo-morphologies found along the ultra-slow spreading Gakkel Ridge therefore provide diverse seafloor habitats which harbor different benthic communities. Previous research expeditions visited the location of the Aurora vent field (PS86, HK19 and HK21) and the Polaris vent site (PS101). During those expeditions, a rough topography featuring different benthic communities was reported for the Aurora vent field (Boetius, 2015). And on a nearby seamount a distinct sponge community with motile sponges was observed (Morganti et al., 2021).

In order to increase our knowledge on such unique ecosystems the OFOBS (Fig. 5.1) was used as a platform to investigate different seafloor habitats and the associated benthic fauna. The OFOBS is a towed camera sled capable of being deployed in moderately ice-covered regions collecting acoustic as well as video and still image data from the seafloor (Purser et al., 2019).

### Work at sea

The OFOBS is a towed camera sled equipped with a high-resolution still camera and a high-definition video camera. In addition to collecting image data, the OFOBS also collected in parallel high-resolution topographical information from the seafloor by using a side scan sonar system. The sidescan system allowed a ~100 m swath of the seafloor to be investigated acoustically at the same time as the collection of still- and video-camera images. A CTD was additionally mounted on the OFOBS and provided real-time information on salinity, temperature and depth.

The set up and application of the OFOBS was similar to investigations in other polar regions such as in the Weddell Sea, Antarctica (Hellmer, 2020) and followed the description in Purser et al. (2019).

The OFOBS was deployed from the side of *Polarstern* and towed at speeds of less than 1 knots (depending on the drift speed of the ice) at an altitude of 1.5 to 2.5 m. The OFOBS transects were planned in such a way to use existing holes in the ice sheet which would drift over the target location at a specific time.

In total, 5 OFOBS dives were planned, of which 4 dives were successfully carried out (Tab. 5.1). The transects were conducted in the proximity of the Aurora vent location and the Lucky B vent location (Fig. 5.2). The first dive followed the western ridge of the Aurora vent field. The second dive followed the eastern ridge of the Aurora vent field. The other two dives followed along the eastern ridge of the Lucky B vent location and along the foot of the ridge system, where hydrothermal activity was suspected.



Fig. 5.1: The Ocean Floor Observation and Bathymetry System (OFOBS) on board Polarstern;  
Photo: L. Boehringer

Tab. 5.1: Overview of OFOBS deployments.

Station Number	Date/Time [UTC]	Action	Ship position	Depth [m]	# Images	Length [m]	Bottom time [h]
PS137_39-1	12.07.2023 08:08	Profile start	82° 52,087' N 7° 33,130' W	2810	972	2132	4:20
	12.07.2023 12:28	Profile end	82° 50,995' N 7° 31,562' W	3006			
PS137_42-1	13.07.2023 22:21	Profile start	82° 58,086' N 5° 03,286' W	1709	1014	1244	4:11
	14.07.2023 02:32	Profile end	82° 57,441' N 5° 02,232' W	1949			
PS137_47-1	18.07.2023	failed	83° 50,750' N 3° 28,379' W	2464	-	-	-
PS137_59-1	25.07.2023 23:23	Profile start	81° 22,282' N 3° 05,261' W	2285	955	2158	4:07
	26.07.2023 03:30	Profile end	81° 21,210' N 3° 05,915' W	2611			

Station Number	Date/Time [UTC]	Action	Ship position	Depth [m]	# Images	Length [m]	Bottom time [h]
PS137_62-1	26.07.2023 17:58	Profile start	81° 22,732' N 3° 24,337' W	3273	923	2117	3:35
	26.07.2023 21:33	Profile end	81° 21,659' N 3° 23,367' W	3216			

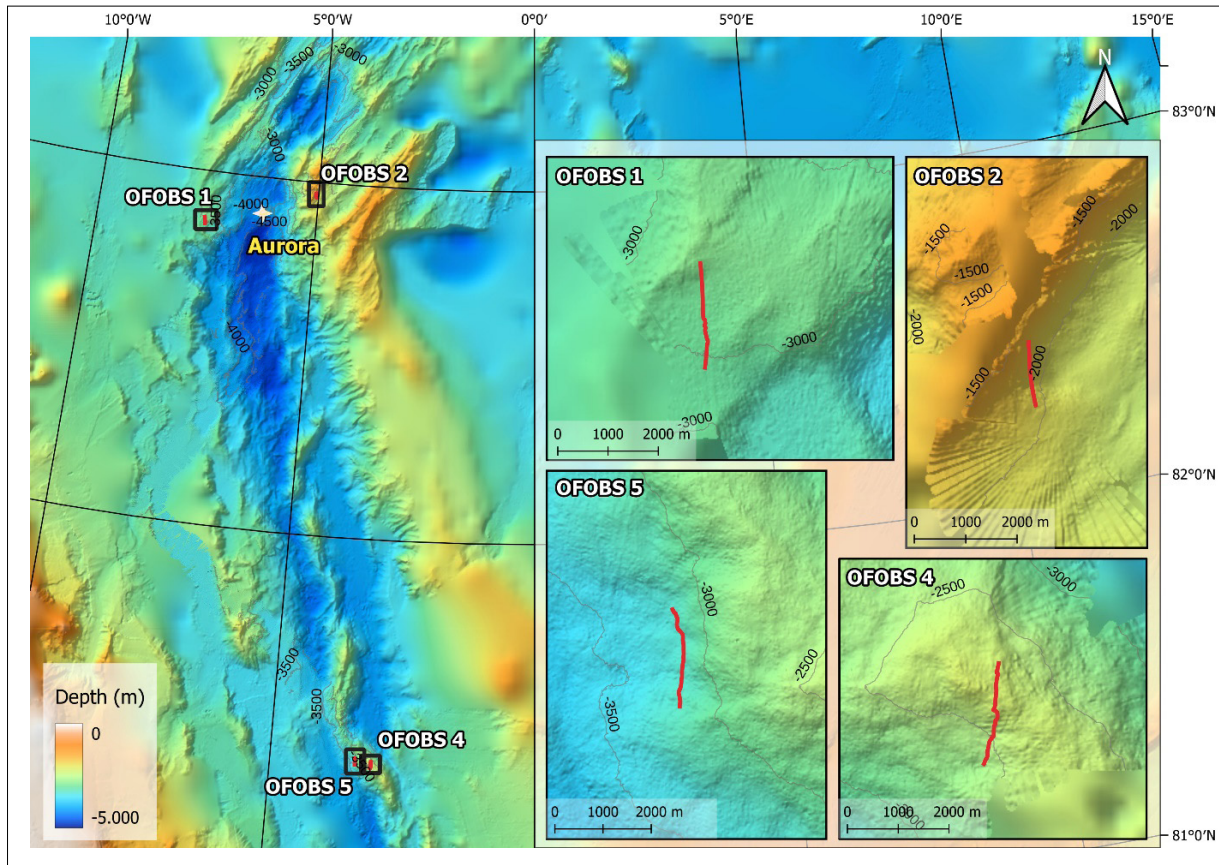


Fig. 5.2: Map of the OFOBS transects conducted during PS137. High resolution bathymetry: PS137, background map IBCAO

### Preliminary (expected) results

For all dives during PS137 the signal of the POSIDONIA transponder was only received for the first 1,000 m depth but was subsequently lost. During the ascent, the signal was received again, typically at around 2,000 m depth. For the entire bottom time, for all OFOBS dives, there was no signal from the POSIDONIA transponder. For reconstruction of the positions of the image and acoustic data sets the ship's position is provided in Table 5.1.

### Bathymetry

For all deployments during PS137, the forward-looking sonar was not responding and was therefore taken off the OFOBS frame after the third deployment. The side scan sonar was not working for the first deployment but for the following deployments full side scan data sets were collected. The side scan sonar provided real time information on habitat types of up to 100 m to the port and starboard sides of the OFOBS. It was additionally used to identify different seafloor structures and as an indicator of the topography of the surrounding seafloor (Fig. 5.3).

Alongside the side scan data, bathymetry data was collected as well which will be used in order to create high resolution maps of the transects. The bathymetry and side scan data sets will be processed using Caris Hips and Sips 11.4 to create GEOTIFF images which may be useful for future dive planning.

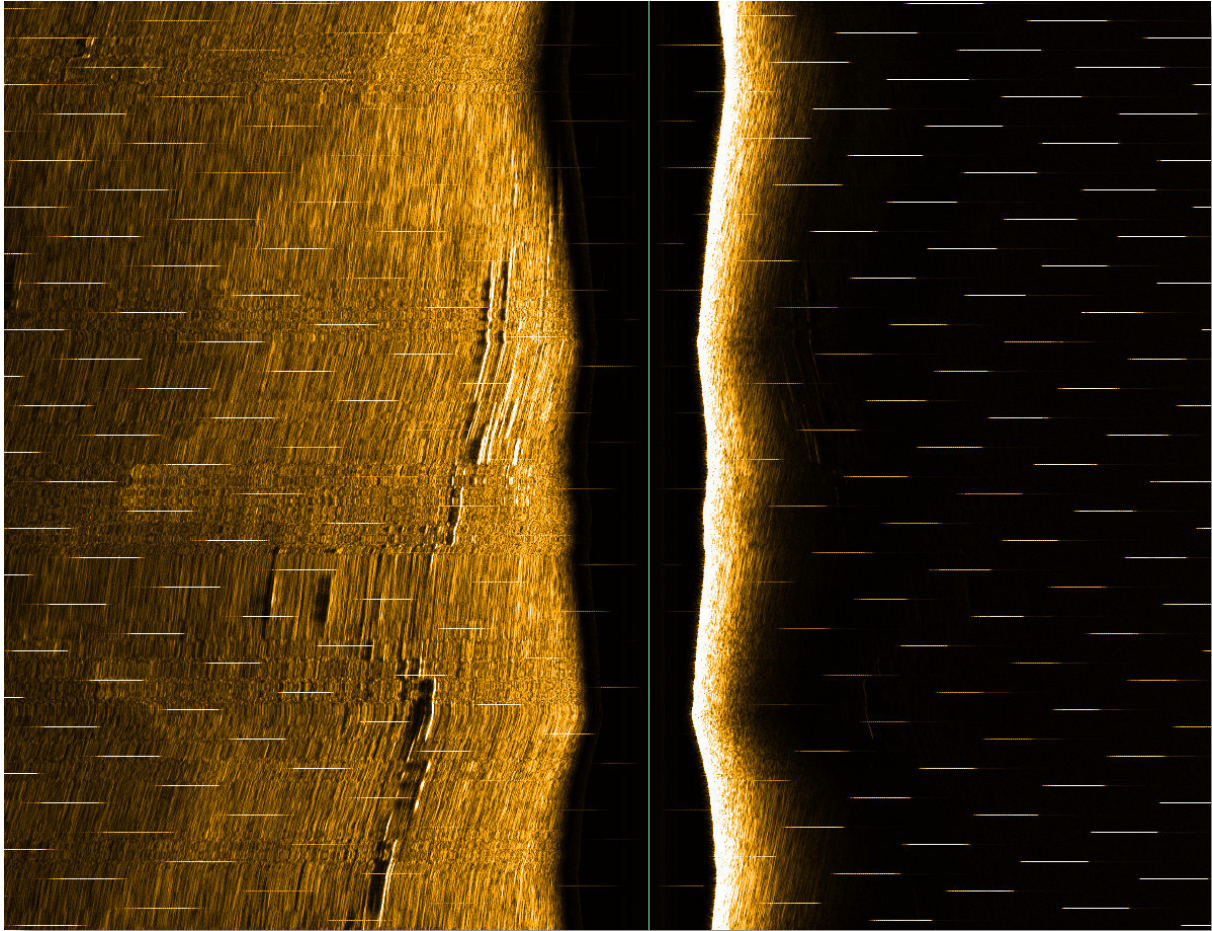


*Fig. 5.3: Example of side scan sonar data set collected at station PS137\_42-1. The green line represents the path the OFOBS was towed. To the right-hand side, a steep incline reflects the acoustic signal represented in white. To the left-hand side, a downward slope was observed.*

### Imagery

#### *PS137\_39-1\_OFOBS-01*

The first OFOBS dive was conducted on 12 July 2023 west of the Aurora vent field at a depth of approx. 3,000 m. The transect was oriented southward as the ship was drifting with the ice floes. The seafloor was predominantly flat and covered with soft and muddy sediments (Fig. 5.4). Dropstones were not observed in this area. The inhabiting benthic megafauna were mostly sea cucumbers, sea anemones and shrimps. Occasionally, octagonal traces, identified as feeding traces of dumbo octopuses (Golikov et al. 2023), could be observed as well.



*Fig. 5.4: Example of the seafloor at station PS137\_39-1. The soft sediments provide a habitat for sea cucumbers, sea anemones and shrimps. On the lower part of the image, an octagonal trace can be observed indicating octopus feeding behaviour at the seafloor.*

#### *PS137\_42-1\_OFOBS-02*

The OFOBS was deployed for the second time on 13 July 2023 on a ridge system east off the Aurora vent field. The transect followed the eastern flank of the ridge system downwards at an approx. depth of 1,800 m. During this dive, many different habitat types were observed. Sandy patches followed steep cliffs which were mostly made up of basaltic rocks (Fig. 5.5). Big and small boulders occurred as well. Different species of demosponges were observed to inhabit the rocky areas. On sandy patches, large stalked crinoids could be seen.



*Fig. 5.5: Example of the seafloor at station PS137\_42-1. Small rocks and boulders were observed, as well as soft sediments. Demosponges were observed associated with rocky structures.*

#### *PS137\_47-1\_OFOBS-03*

The third OFOBS dive on 18 July 2023 was planned to be conducted in the northern working area along a ridge system in the western part of the Gakkel Ridge. This dive was aborted at 20m depth due to technical problems within the OFOBS.

#### *PS137\_59-1\_OFOBS-04*

On 25 July 2023, the fourth OFOBS dive was conducted in the proximity of the Lucky B vent site. The dive was planned to follow as southward direction crossing a seamount east of the Lucky B vent site. The seafloor on the seamount showed diverse habitat types, with small rocks and boulders being interlaced with soft sediment. Locally light-coloured banked outcrops of rocks occurred (Fig. 5.6). Steep cliffs were observed predominately on the northern side of the seamount. Different species of demosponges, sea anemones and brittle stars were typically observed on the rocks and boulders.



*Fig. 5.6: Example of the seafloor at station PS137\_59-1. The seamount was covered with basaltic outcrops and rocks, as well as boulders providing a habitat to sea anemones.*

#### *PS137\_62-1\_OFOBS-05*

The OFOBS was deployed one last time during the PS137 expedition on 26 July 2023. This OFOBS transect was conducted in the area where the Lucky B vent site was suspected at approx. 3,200 m depth. The transect followed a southward direction. During this dive, a diverse seafloor with steep rock formations followed by areas with soft sediments were observed. Hydrothermally affected and discoloured rocks and sediments were observed as well (Fig. 5.7). The soft sediments were inhabited by brittle stars and in between rocks purple anemones were found. On top of the rocks white-pink anemones and shrimps were observed. In areas with suspected hydrothermal activity more crustaceans and fishes could be found.



*Fig. 5.7: Example of the seafloor at station PS137\_62-1. During parts of the transect hydrothermally affected, discoloured sediments and rock structures were observed.*

### Data management

Environmental data will be archived, published and disseminated according to international standards by the World Data Centre PANGAEA Data Publisher for Earth & Environmental Science (<https://www.pangaea.de>) within two years after the end of the cruise at the latest. By default, the CC-BY license will be applied. All of the data will be made available to all other cruise participants at the end of the cruise.

This expedition was supported by the Helmholtz Research Programme “Changing Earth – Sustaining our Future” Topic 2, Subtopic 3 and Topic 6, Subtopic 1.

In all publications based on this expedition, the **Grant No. AWI\_PS137\_03** will be quoted and the following publication will be cited:

Alfred-Wegener-Institut Helmholtz-Zentrum für Polar- und Meeresforschung (2017) Polar Research and Supply Vessel POLARSTERN Operated by the Alfred-Wegener-Institute. Journal of large-scale research facilities, 3, A119. <http://dx.doi.org/10.17815/jlsrf-3-163>.

### References

Boetius A (2015) The Expedition PS86 of the Research Vessel POLARSTERN to the Arctic Ocean in 2014. Reports on Polar and Marine Research, Alfred-Wegener-Institute for Polar and Marine Research 685. [https://doi.org/10.2312/BzPM\\_0685\\_2015](https://doi.org/10.2312/BzPM_0685_2015).

- Golikov AV, Stauffer JB, Schindler SV, Taylor J, Boehringer L, Purser A, Sabirov RM, Hoving H-J (2023) Miles down for lunch: deep-sea *in situ* observations of Arctic finned octopods *Cirroteuthis muelleri* suggest pelagic-benthic feeding migration. Proceedings of the Royal Society B 290. <https://doi.org/10.1098/rspb.2023.0640>.
- Hellmer H (2020) Expedition Programme PS124 Polarstern, Stanley-Stanley, 4 February 2021 - 30 March 2021, Continental Shelf Multidisciplinary Flux Study (COSMUS). Alfred-Wegener-Institute for Polar and Marine Research.
- Morganti TM, Purser A, Rapp HT, German CR, Jakuba MV, Hehemann L, Bendl J, Slaby BM, & Boetius A (2021) In situ observation of sponge trails suggest common sponge locomotion in the deep central Arctic. Current Biology 31, R368–R370.
- Purser A, Marcon Y, Dreutter S, Hoge U, Sablotny B, Hehemann L, Lemburg J, Dorschel B, Biebow H, & Boetius A (2019) Ocean floor observation and bathymetry system (OFOBS): A new towed camera/sonar system for deep-sea habitat surveys. IEEE Journal of Oceanic Engineering 44(1):87–99. <https://doi.org/10.1109/JOE.2018.2794095>.

## 6. HEATFLOW

Josefa Lotte Ritter<sup>1</sup>, Hannah Plötz<sup>1</sup>, Norbert Kaul<sup>2</sup>

<sup>1</sup>DE.AWI

<sup>2</sup>DE.UNI Bremen

**Grant-No. AWI\_PS137\_01**

### Outline

Little is known about the geothermal heat flow in the Arctic Basin. The heat flow across the Amundsen Basin was found to be abnormally high exceeding predictions of global lithospheric cooling models by a factor of two (Urlaub et al., 2009), deduced from just one research cruise, the AMORE expedition. Heat flow data from further transects of the Eurasian Basin are lacking. Newer heat flow values concentrate on ridge features like Aurora vent field and Karasik seamount.

In recent times, a relationship between seismicity and hydrothermal activity has been found. One of our aims is to reveal locations where fluid flow responds to seismic disturbances and thus constrain circulation patterns.

### Objectives

At 3°E there is a boundary of unknown origin. We measure heat flow profiles to understand heat input into Arctic Ocean in its dependence to different styles of lithosphere formation. This is in combination with magnetic surveying to test the stability of the boundary in time and a seismic refraction survey. The question is: does the lithospheric structure and thermal regime of the lithosphere change across this boundary?

Fridtjof Nansen already realized the oceanographic situation in the central Arctic Basin during his Fram expedition in 1893–1896. He observed a temperature increase in the very deep part of the basin (> 4,000 m) and related this to the high pressure. We use high precision temperature measurements to distinguish between pressure related temperature increase and additional geothermal heat input into the deep and confined Arctic Basin.

### Work at sea

The planned two heat flow transects across the Nansen Basin to either side of the 3°E boundary could not be acquired due to the dense ice conditions. Five heat flow profiles could be measured instead along the eastern and western rim of Lena Trough and the northern extension at the Gakkel Ridge. At each site the intention was to investigate the transition from younger to ageing crust.

We used the 6 m Bremen heat flow probe (MEM488) in memory mode on the 18 mm dredge-wire. In total, 31 sites were tested, three failed due to hard ground or steep slope.



Fig. 6.1: Deployment of the 6 m heat flow probe was carried out over the stern. Very calm sea conditions made this a smooth operation. (Photo: J. Ritter)

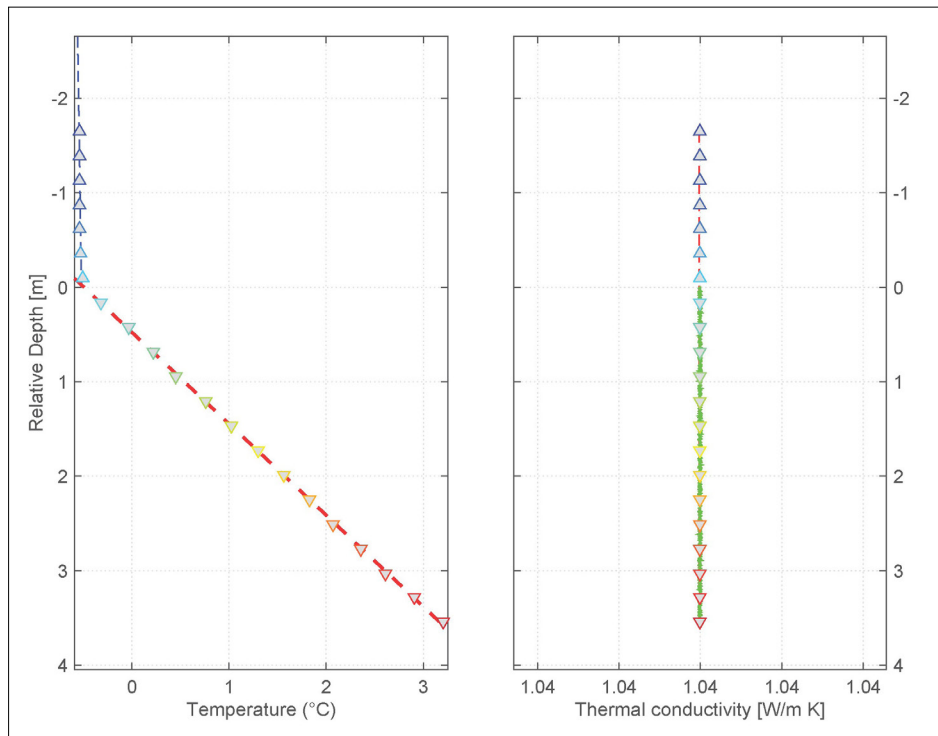


Fig. 6.2: The most exceptional gradient, observed during this cruise: 1,032 mK/m at a western Lena Trough site (HF2346P07). We use a regional mean of 1.04 W/m\*K as thermal conductivity.

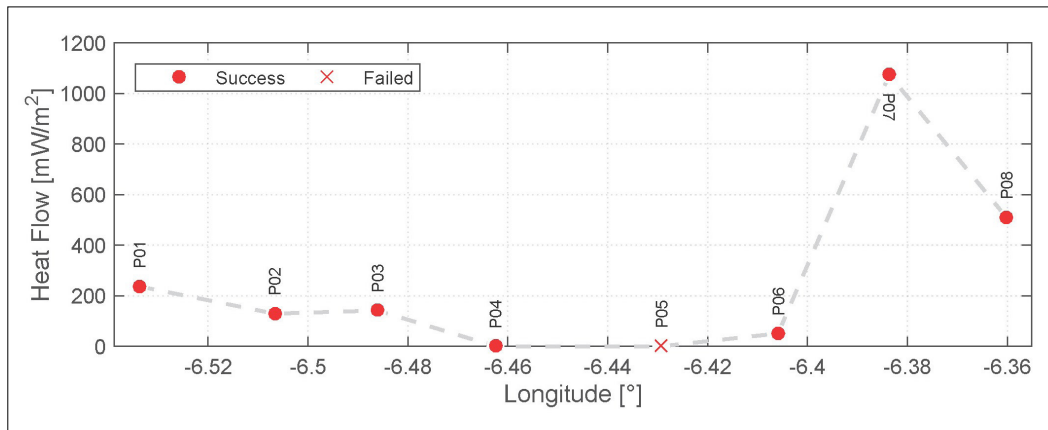


Fig. 6.3. Heat flow profile PS137-56 (HF2346) on the western margin of Lena Trough. When descending to the foot of the lower terrace, heat flow values increase rapidly.

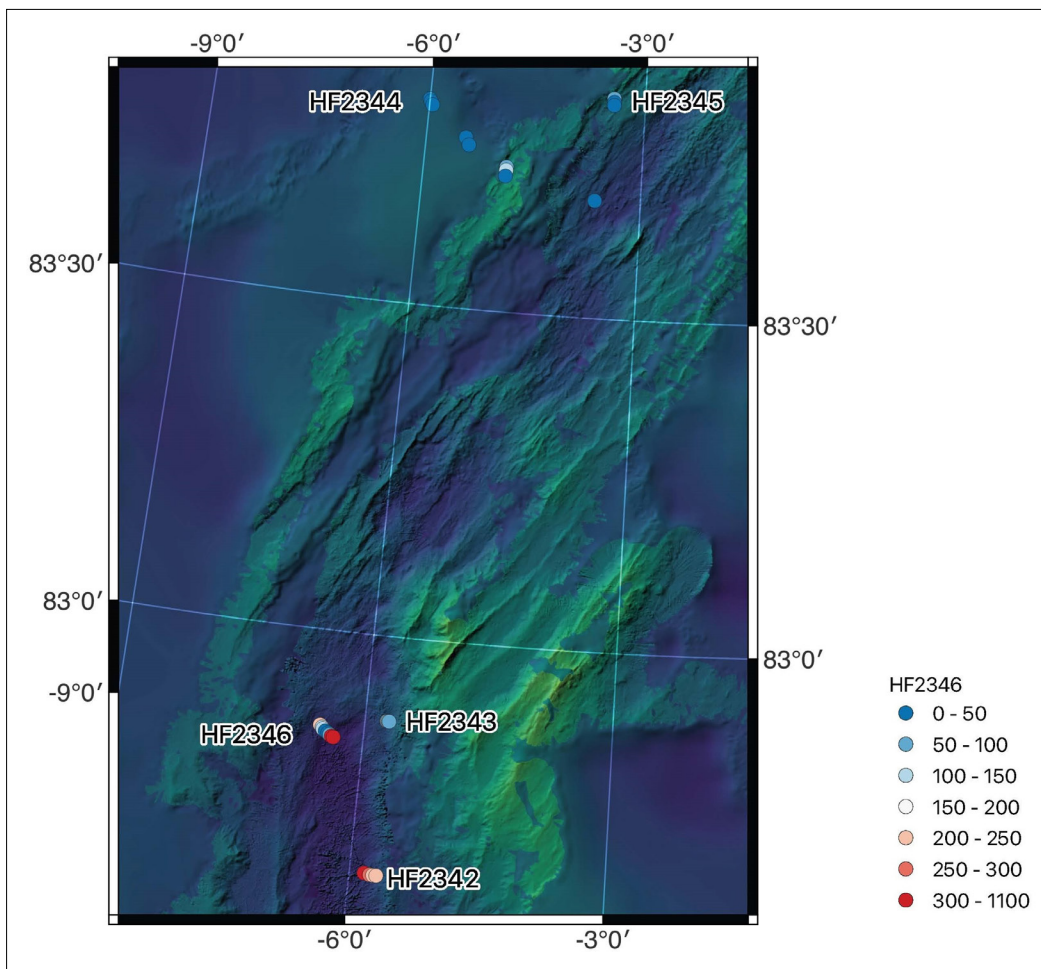


Fig. 6.4. Location map heat flow sites

Tab. 6.1: Preliminary results of heat flow determinations

PS-Name	HF-Name	DD	MM.MMM	DDD	MM.MMM	gradT	k	q
PS137_20	HF2342P01	82	38.551	-005	49.530	340.5	1.12	374.3
PS137_20	HF2342P02	82	38.450	-005	47.821	NaN	0.90*	NaN
PS137_20	HF2342P03	82	38.453	-005	45.480	261.3	1.10*	287.4
PS137_20	HF2342P04	82	38.431	-005	43.217	192.6	1.07	204.5
PS137_20	HF2342P05	82	38.424	-005	40.945	227.1	1.10*	249.9
PS137_30	HF2343P01	82	52.379	-005	43.955	138.2	1.08	149.1
PS137_30	HF2343P02	82	52.374	-005	43.401	121.6	1.10*	133.7
PS137_30	HF2343P03	82	52.361	-005	42.899	115.3	1.04	119.1
PS137_30	HF2343P04	82	52.350	-005	42.441	79.5	1.04*	82.7
PS137_43	HF2344P01	83	48.536	-006	00.076	34.8	1.23	41.3
PS137_43	HF2344P02	83	48.339	-005	59.109	22.7	1.10*	25.0
PS137_43	HF2344P03	83	48.035	-005	57.507	37.6	1.10*	41.4
PS137_44	HF2344P04	83	45.400	-005	27.178	53.3	0.88	40.5
PS137_44	HF2344P05	83	45.039	-005	25.694	9.1	0.90*	8.2
PS137_44	HF2344P06	83	44.756	-005	24.111	28.0	0.90*	25.2
PS137_45	HF2344P07	83	43.074	-004	51.589	97.4	0.90*	87.7
PS137_45	HF2344P08	83	42.783	-004	51.699	163.2	0.90*	146.9
PS137_45	HF2344P09	83	42.247	-004	51.907	11.8	1.10*	13.0
PS137_46	HF2344P10	83	40.611	-003	37.369	6.4	1.10*	7.0
PS137_46	HF2344P11	83	40.554	-003	39.646	NaN	1.10*	NaN
PS137_48	HF2345P01	83	49.902	-003	26.202	41.0	1.34	54.8
PS137_48	HF2345P02	83	49.584	-003	26.012	24.5	1.30*	31.9
PS137_48	HF2345P03	83	49.307	-003	25.980	28.2	1.42	40.3
PS137_56	HF2346P01	82	51.417	-006	32.027	224.1	1.06	237.3
PS137_56	HF2346P02	82	51.220	-006	30.401	123.3	1.05*	129.5
PS137_56	HF2346P03	82	51.080	-006	29.164	136.5	1.04*	141.9
PS137_56	HF2346P04	82	50.910	-006	27.750	0.4	1.03	0.4
PS137_56	HF2346P05	82	50.757	-006	25.758	NaN	1.04*	NaN
PS137_56	HF2346P06	82	50.621	-006	24.354	49.1	1.04*	51.1
PS137_56	HF2346P07	82	50.502	-006	23.018	1032.6	1.04*	1073.9
PS137_56	HF2346P08	82	50.435	-006	21.610	514.3	1.03	509.6

### Data management

Heat flow data will be archived, published and disseminated according to international standards by the World Data Center PANGAEA Data Publisher for Earth & Environmental Science (<https://www.pangaea.de>) within two years after the end of the expedition at the latest. By default, the CC-BY license will be applied.

Any other data will be submitted to an appropriate long-term archive that provides unique and stable identifiers for the datasets and allows open online access to the data.

This expedition was supported by the Helmholtz Research Programme “Changing Earth – Sustaining our Future” Topic 2, Subtopic 3.

In all publications based on this expedition, the **Grant No. AWI\_PS137\_01** will be quoted and the following publication will be cited:

Alfred-Wegener-Institut Helmholtz-Zentrum für Polar- und Meeresforschung (2017) Polar Research and Supply Vessel POLARSTERN Operated by the Alfred-Wegener-Institute. Journal of large-scale research facilities, 3, A119. <http://dx.doi.org/10.17815/jlsrf-3-163>

### References

Urlaub M, Schmidt-Aursch MC, Jokat W et al. (2009) Gravity crustal models and heat flow measurements for the Eurasia Basin, Arctic Ocean. Mar Geophys Res 30:277–292. <https://doi.org/10.1007/s11001-010-9093-x>

## 7. GEOLOGY AND PETROLOGY

Elmar Albers<sup>1,2</sup>, Felix Genske<sup>3</sup>;  
not on board: Wolfgang Bach<sup>2,4</sup>

<sup>1</sup>US.WHOI  
<sup>2</sup>DE.MARUM  
<sup>3</sup>DE.UNI Münster  
<sup>4</sup>DE.UNI Bremen

**Grant-No. AWI\_PS137\_07**

### Objectives

#### *Objective 1: The Aurora vent field*

In order to further our understanding of hydrothermal systems at ultraslow-spreading ridges, we will comprehensively study the geological setting of the Aurora vent field as well as of other vent sites, which we hope to locate during PS137. The style of the hydrothermalism is shaped by underlying geologic processes, i.e., by local geology at the respective sites that determine fluid pathways and seawater–rock reactions. At ultraslow-spreading ridges, particularly diverse types of hydrothermal systems result from the interplay between tectonic seafloor spreading and magmatic activity. Specific questions we aim to answer include: How deep do fluids circulate through the lithosphere at Aurora and which rock types do they interact with? What provides the heat source that drives hydrothermal circulation away from the spreading axis, within the deep rift-valley floor?

#### *Objective 2: The 3°E boundary*

We will investigate the lithospheric structure across the prominent 3°E boundary, where the seafloor spreading mode markedly changes from robust magmatic spreading to dominantly tectonic spreading. Rock sampling will help to test the hypothesis that ridge segmentation is controlled by mantle domains, and scientific questions that will be addressed are: Does the lithospheric structure and thermal regime of the lithosphere change across this boundary? Are there petrological and geochemical affinities between melt on either side? How is melt flow along axis either enabled or blocked by the boundary?

### Work at sea

One hydrothermal precipitate sample was collected at the Aurora hydrothermal field with the *NUI* vehicle (see Chapter 3). The precipitate is composed of sulfides and orange–brown Fe oxides/oxyhydroxides (Fig. 7.1).

Due to heavy ice conditions, no rock dredging was possible at Aurora or further to the east. A single dredge haul in the central Lena Trough was unsuccessful as the dredge's weak link broke and the dredge came up empty. A dredge haul in the southern Lena Trough, on the western slope of the Lucky Ridge in the vicinity of the "Lucky B" hydrothermal field, yielded ~35 kg recovery (Tab. 7.1). Rocks were cut onboard. About 85 % of the recovery is of ultramafic composition. All samples are strongly serpentinized, commonly showing mesh texture serpentine, multiple generations of serpentine veins, and/or bastite textures (Fig. 7.2). Except

for spinel, no primary phases were observed. A number of samples are heavily brecciated. Some samples are heavily weathered whereas others show little evidence of low-temperature interaction with seawater. In addition, the recovery comprised two small cobbles that may be basaltic (samples 21 and 22; Fig. 7.3). They are fine-grained and gray in color. Further, one well-rounded sample, possibly a carbonaceous metamorphic rock, is part of the recovery (sample 15). This sample likely represents ice-rafted debris. Most samples are coated with a submillimetric Mn crust.



*Fig. 7.1: Hydrothermal precipitate composed sulfides and Fe oxides/oxyhydroxides recovered by the NUI vehicle. Sample size is approximately 15 cm.*



Fig. 7.2: Representative photographs of ultramafic dredge recovery. (a) Serpentinized peridotite with several generations of serpentine veining. Sample PS 137/60-1-005. (b) Brecciated serpentinite with cm-sized clasts. Sample Sample PS 137/60-1-016. (c) Highly weathered and oxidized serpentinite. Sample PS 137/60-1-014. The white label is 9 cm long.



Fig. 7.3: Fine-grained cobbles of potentially basaltic composition. Samples 21 (a) and 22 (b). The white label is 9 cm long.

Tab. 7.1: List of rocks and precipitates.

Station	Device	Sample #	Description	Weight
PS137/32-1	NUI		chimney piece, composed of sulfides and Fe oxides/ oxyhydroxides; strong S smell	0.6
PS137/60-1	dredge	1	serpentinite breccia with several-cm-large-clasts; matrix weathered, clasts serpentinized but less strongly weathered	2.4
PS137/60-1	dredge	2	serpentinite breccia (fault gauge?) with mm-sized clasts; light brownish to gray in color	0.3
PS137/60-1	dredge	3	serpentinite; several generations of mm-wide veins green in color (lizardite?) and chrysotile; up to 5 mm-large black pyroxene pseudomorphs	0.4
PS137/60-1	dredge	4	serpentinite; several generations of mm-wide veins of light green-gray serpentine and few of chrysotile; up to 5 mm-large black pyroxene pseudomorphs; brown mesh serpentine in center	0.8
PS137/60-1	dredge	5	unweathered serpentinite of mesh texture serpentine w/ abundant bastite textures; several generations of serpentine, with abundant magnetite, and some chrysotile	6.2
PS137/60-1	dredge	6	serpentinite similar to sample 005 but slightly more abundant magnetite veins; sample overall more strongly weathered with zoning towards outside	8.5
PS137/60-1	dredge	7	strongly weathered serpentinite	0.4

Station	Device	Sample #	Description	Weight
PS137/60-1	dredge	8	unweathered serpentinite similar to sample 005 but less bastite	0.3
PS137/60-1	dredge	9	unweathered serpentinite similar to sample 008	1.0
PS137/60-1	dredge	10	serpentinite breccia similar to sample 001	1.0
PS137/60-1	dredge	11	weathered serpentinite	0.4
PS137/60-1	dredge	12	serpentinite breccia similar to sample 001 but much less weathered	0.4
PS137/60-1	dredge	13	foliated serpentinite with some larger clasts, weakly weathered	1.2
PS137/60-1	dredge	14	strongly weathered serpentinite with several weathering zones from the outside inwards; abundant pyroxene pseudomorphs	2.3
PS137/60-1	dredge	15	potentially metamorphic rock (dropstone?) composed of dark, crystalline domains and light brownish-gray patchy domains	2.7
PS137/60-1	dredge	16	serpentinite breccia similar to sample 001 but apparently unweathered	0.6
PS137/60-1	dredge	17	unweathered serpentinite similar to sample 008	0.6
PS137/60-1	dredge	18	unweathered serpentinite similar to sample 005 but slightly more oxidized	0.3
PS137/60-1	dredge	19	weathered serpentinite w/ slight zonation	0.2
PS137/60-1	dredge	20	serpentinite breccia similar to sample 016	0.2
PS137/60-1	dredge	21	fine crystalline unaltered basalt(?)	0.1
PS137/60-1	dredge	22	fine crystalline unaltered basalt(?)	0.1

### Preliminary (expected) results

The hydrothermal precipitate will be used to characterize phase assemblages and mineral compositions at the loci of fluid emission. The results will be combined with fluid geochemical data to provide comprehensive insight into sub-seafloor processes, to estimate fluxes of metabolic energy that is provided when the discharging fluids enter the oxic overlying water column.

The dredge recovery will be investigated petrologically and geochemically. Bulk and mineral chemical compositions of the mafic samples are of particular interest since mafic recovery from the Lucky Ridge is very sparse. The samples may hence close the existing gap between the southern and northern ends of the Lucky Ridge. Spinel and relict pyroxene compositions will provide information on the extent of melting of the ultramafic samples.

### Data management

The sample will be archived for long-term access in the repository of the MARUM, Bremen. Interested onshore scientists can request sample splits for related research.

In all publications based on this expedition, the **Grant No. AWI\_PS137\_07** will be quoted and the following publication will be cited:

Alfred-Wegener-Institut Helmholtz-Zentrum für Polar- und Meeresforschung (2017) Polar Research and Supply Vessel POLARSTERN Operated by the Alfred-Wegener-Institute. Journal of large-scale research facilities, 3, A119. <http://dx.doi.org/10.17815/jlsrf-3-163>.

## 8. PHYSICAL OCEANOGRAPHY AND BIOGEOCHEMISTRY OF HYDROTHERMAL PLUMES

Maren Walter<sup>1</sup>, Jonathan Mette<sup>1</sup>, Elmar Albers<sup>1,3</sup>,  
Chris German<sup>3</sup>, Jeff Seewald<sup>3</sup>, Gunther Wegener<sup>1</sup>  
not on board: Christian Mertens<sup>2</sup>,  
Jürgen Sültenfuß<sup>2</sup>; Wolfgang Bach<sup>1</sup>

<sup>1</sup>DE.MARUM  
<sup>2</sup>DE.IUP  
<sup>3</sup>US.WHOI

**Grant-No. AWI\_PS137\_06**

### Objectives

The main objective of the work on hydrothermal signals in the water column (plumes) was to conduct hydrothermal plume surveying and sampling of the Aurora vent site on the ultraslow spreading Gakkel Ridge in the Arctic Ocean. Plume surveys conducted by research vessels are, by necessity, snapshots of the actual hydrothermal activity. Therefore, to obtain a more solid estimate of the hydrothermal activity, a mooring (AURORA-1) was deployed in 2022 during the cruise *Polarstern* PS131 (ATWAICE), designed to monitor the hydrothermal plume (characterized by its distinct temperature anomaly) and its dispersal (current directions) close to the vent.

These time series were complemented by a plume survey at the Aurora vent site, with observations of plume parameters as temperature anomaly, turbidity, redox potential, and geochemical anomalies, as well as environmental parameters as background flow and stratification. The aim of these observations is to estimate the long-term flux of the hydrothermal plume coming out of Aurora, to understand temporal changes in the activity of the hydrothermal system and to determine the interconnection between seismic events and potential perturbations of the water column plume.

The second aim of the plume oceanography was reconnaissance of hydrothermal activity at yet unknown sites, i.e. exploratory work and follow ups on previously observed water column anomalies and seafloor observations. From hydrogen, methane, metal, heat, and turbidity data collected in these surveys, inferences can be made about the nature of the vent which, prior work from PS86 and PS101 has revealed, can reveal important new insights into the style of venting at the seafloor, beyond what can be determined from *in-situ* sensing, alone (Edmonds et al. 2003; Baker et al., 2004; German et al., 2022; Albers et al., *in prep*, Walter et al., *in prep*).

### Work at sea

The main tool for the plume surveys was the CTD-Rosette equipped with additional geochemical sensors for redox potential and turbidity to allow for online plume detection and targeted sampling, geo-referenced by a POSIDONIA transponder. For the general setup and operation of the CTD-Rosette system, see Chapter 10. To detect and map a hydrothermal plume, the CTD system is lowered and heaved during the (known or suspected) plume depth range, while the ship is slowly (>1 kn) moving (tow-yo), or, in our case, drifting with the ice (floe-yo). Standard (vertical) CTD casts have been carried out to sample background profiles and to

obtain high resolution sampling of the water column at the Aurora site. Below the CTD-Rosette system, a McLane *in-situ* pump was installed that was switched on and off according to the real time data of the CTD via the releaser system for the Niskin bottles. A second pump that could be operated this way could be attached to the CTD wire up to a vertical distance of up to 40 m above the CTD. Depending on the sampling strategy, up to two more pre-programmed pumps were installed on the wire during *in-situ* pump stations. Details can be found in Chapter 9.

Miniature Autonomous Plume Recorders (MAPR, Baker and Milburn, 1997) record (offline) temperature, pressure, turbidity, and oxygen reduction potential. Up to three MAPR have been attached to the CTD/Rosette system during plume casts in order to increase the spatial coverage and to capture possible plume signals, typically one at the wire 15 m above the CTD, and additional ones above the *in-situ* pumps. MAPR were also installed on the NUI and the OFOBS system during dives/deployments. A custom-built Seapoint Turbidity Meters (5x normal gain), the same sensor that is used on the MAPR, was attached to the CTD system to obtain online turbidity data. However, due to technical problems with the turbidity sensor and cables, we relied during operations on the beam transmission measured by the transmissometer. Oxygen reduction potential was monitored in real time using the NOAA/PMEL ORP sensor, again the same sensor that is build into the MAPR. The MAPR and the ORP sensor have been provided by S. Walker, NOAA/PMEL.

Direct current measurements have been carried out at selected profiles using an acoustic current meter (Nortek Aquadopp) attached to the CTD instrument package. The instrument was set to a sampling frequency of 60 s and an averaging interval of 10 s with the main goal to record the current strength and direction during the times of the *in-situ* pumping.

Fluids collected using the Niskin rosette were analyzed for dissolved methane by gas chromatography with flame ionization detection and a 5Å molecular sieve separation column following a headspace extraction of dissolved gases. Aliquots of fluid were subsampled in duplicate from selected Niskin bottles in 60 ml plastic syringes fitted with on/off valves. For each analysis, gases were extracted from 25 ml of fluid. A total of 44 samples were analyzed with concentrations ranging from below detection ( $\leq 1$  nmol/L) to 250 nmol/L in a plume at Lucky B. Hydrothermal plume samples collected with the CTD-rosette system have been analyzed for H<sub>2</sub> onboard (see Chapter 9 for details). The sampling and measurement routine includes collecting air-free aliquots in syringes from the Niskin bottles, equilibration at room temperature, and immediate analyzes via headspace extraction gas chromatography using flame ionization detection.

Water samples (69 samples, incl. 6 duplicates) from the CTD-rosette system have been taken in gas-tight copper tubes to be analyzed post cruise in the Bremen Mass Spectrometer Laboratory (Sültenfuß et al., 2009) for concentrations and isotopic ratios of the noble gases helium and neon. Hydrothermal plumes are highly enriched in helium (isotopes: <sup>3</sup>He and <sup>4</sup>He), leading to elevated He/Ne ratios, as well a a higher  $\delta^3\text{He}$  due to the higher proportion of the isotope <sup>3</sup>He in the primordial helium from the hydrothermal vents. The helium isotopic composition is an important tracer for the distribution of vent fluids in the water column, since the inert gas helium is non-reactive and detectable over long distances away from the source. At selected stations all together 20 samples for the analysis of tritium (<sup>3</sup>H) have been taken to determine the background signal of tritiogenic <sup>3</sup>He. Tritium is the unstable isotope of hydrogen, and decays into <sup>3</sup>He.

Samples from the CTD-rosette have also been taken for post-cruise measurements of dissolved metals, specifically Fe and Mn. Aliquots of the fluid samples have been filtered (0.45 µm) and acidified with nitric acid to a pH of 1.7 and stored at 4°C for the remainder of the cruise. Dissolved and particulate metal concentrations will be measured post-cruise by ICP-MS at the Faculty of Geosciences at the University of Bremen.

CTD casts for plume observation started with a background station in Lena Trough (PS137/18-1). All together, 11 vertical casts, floe/tow-yos, and pump stations were carried out in the vicinity of the Aurora mound (Fig. 8.1, left), with varying degrees of success of mapping and sampling of the plume signal (due to the difficult ice situation). An additional exploratory station was carried out north-east of the Aurora site at the northern wall of the rift valley. Two more floe-yo stations were carried out at the Lucky B site in Lena Trough (Fig. 8.1, right), where previously indications of hydrothermal activity had been reported. For an overview of the sampling and observations, see Table 8.1. Details of the CTD operation as well as times and coordinates can be found in Table 10.3.

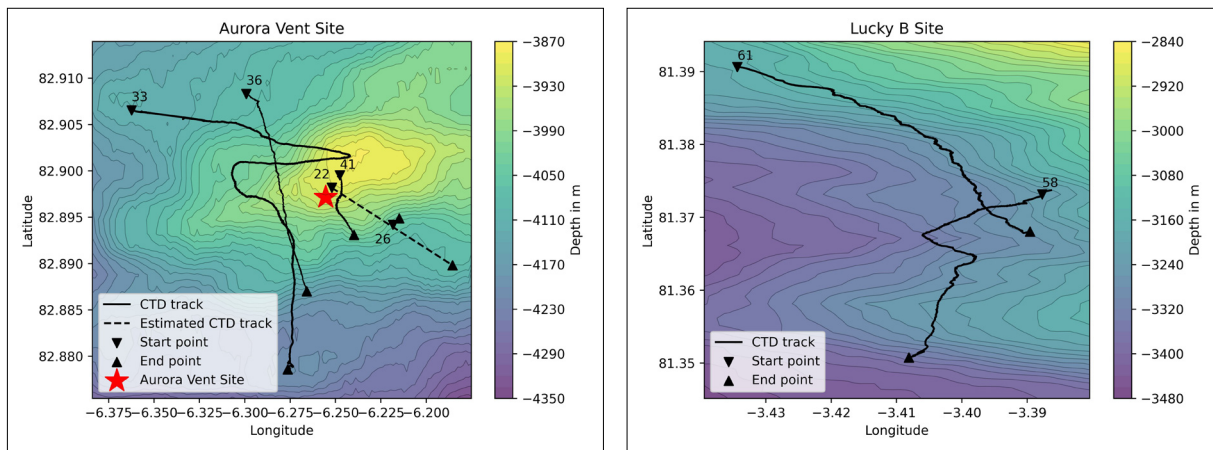


Fig. 8.1: Location of CTD stations/profiles at the Aurora site (left) and the Lucky B site (right).

Tab. 8.1: Overview of water samples collected from CTD casts

Station	Location	Tow-yo	In-situ pump	MAPR	Current meter	Samples & experiments
PS137/1-1						
PS137/4-1						
PS137/6-1						
PS137/10-1						
PS137/12-1						
PS137/12-1a						
PS137/14-1						Salinity
PS137/18-1	Lena Trough		x	x	x	Salinity, He, $^3\text{H}$ , $\text{H}_2$ consumption, $\text{CH}_4$ , DNA, DOC, POC, FISH, DIC, $^{14}\text{C}$ -tracer experiment, EEA
PS137/22-1	Aurora					Fe, Mn, He, $\text{CH}_4$ , $\text{H}_2$ , $\text{H}_2$ consumption, DNA, DOC, POC, FISH, DIC, $^{14}\text{C}$ -tracer experiment, EEA
PS137/26-1	Aurora			x	x	Salinity, $\text{CH}_4$ , $\text{H}_2$ , $\text{H}_2$ consumption, DNA, DOC, POC, FISH, DIC, $^{14}\text{C}$ -tracer experiment, Dual labeling experiment, Amino acid labeling experiment
PS137/28-1	Aurora	x	x	x	x	$\text{CH}_4$ , $\text{H}_2$ , $\text{H}_2$ consumption, DNA, DOC, POC, FISH, DIC, Dual labeling experiment

Station	Location	Tow-yo	<i>In-situ</i> pump	MAPR	Current meter	Samples & experiments
PS137/33-1	Aurora	x	x	x	x	Salinity, Fe, Mn, He, CH <sub>4</sub> , H <sub>2</sub> , H <sub>2</sub> consumption, DNA, DOC, POC, FISH, DIC, <sup>14</sup> C-tracer experiment, EEA
PS137/36-1	Aurora	x	x	x	x	Fe, Mn, He, CH <sub>4</sub> , H <sub>2</sub> , H <sub>2</sub> consumption, DNA, DOC, POC, FISH, DIC, <sup>14</sup> C-tracer experiment, EEA
PS137/40-1	Aurora					
PS137/41-1	Aurora		x	x		Fe, Mn, He, CH <sub>4</sub> , H <sub>2</sub> , H <sub>2</sub> consumption, DNA, DOC, POC, FISH, DIC, <sup>14</sup> C-tracer experiment, EEA, Dual labeling experiment
PS137/49-1	Gakkel (3.3°W)			x	x	Salinity, He, <sup>3</sup> H
PS137/52-1	Aurora					Salinity
PS137/53-1	Aurora			x	x	
PS137/54-1	Aurora		x	x	x	Fe, Mn, CH <sub>4</sub> , H <sub>2</sub> , H <sub>2</sub> consumption, DNA, DOC, POC, FISH, DIC, <sup>14</sup> C-tracer experiment, Dual labelling, Amino acid labeling
PS137/55-1	Aurora			x	x	
PS137/58-1	Lucky B	x				Salinity, Fe, Mn, He, <sup>3</sup> H, CH <sub>4</sub> , H <sub>2</sub> , H <sub>2</sub> consumption, DNA, DOC, FISH
PS137/61-1	Lucky B	x	x	x	x	Fe, Mn, He, CH <sub>4</sub> , H <sub>2</sub> , H <sub>2</sub> consumption, DNA, DOC, POC, FISH, DIC, <sup>14</sup> C-tracer experiment, EEA

### Preliminary results

At Aurora, the AURORA1 mooring deployed during the ATWAICE expedition (PS131, 2022), was successfully recovered (Chapter 10). The time series of temperature anomalies and current velocities from the 5 temperature recorders (SBE 37) and the 4 current meters (RCM 11) will be used to estimate the long-term flux of the hydrothermal plume coming out of Aurora, and in combination with the data from the OBS (Chapter 2) will be used to understand the temporal changes in the activity of the hydrothermal system, and its interconnection with seismic events.

The observations of the Aurora plume confirmed the ongoing hydrothermal activity in the area, with the main plume signal with water column temperature anomalies of a few mK in a depth range between 3,400 m and 3,600 m (Figs. 8.2, 8.3), and occasional interception of a shallower and thinner plume centered around 3,100 m water depth. Both signals were most frequently observed north of the known vents, but a systematic mapping of the plume was hindered by the variable ice drift. Whether the two plume signals are both originating from the known vent site and are caused by environmental variability (as changing current direction), or whether there is a further (unknown) site nearby remains unclear at this point. However, this question can potentially be addressed with upcoming analysis of (a) the above mentioned time series from the mooring deployment, as well as (b) the geochemical data. To determine the endmember concentrations for the noble gases helium and neon, fluid samples have been taken from clear low temperature fluids (NUI 44, PS137/37-1) as well as hot fluids (NUI45, PS137/50-1) during the NUI dives with the IGTs (Chapter 3); these samples will be analysed post cruise for concentrations and isotopic ratios in the Bremen Mass Spectrometer Laboratory. An expository CTD station east of Aurora (PS137/49-1, 3.3°W, at the northern wall of the rift valley) showed signs of hydrothermal activity in the vicinity.

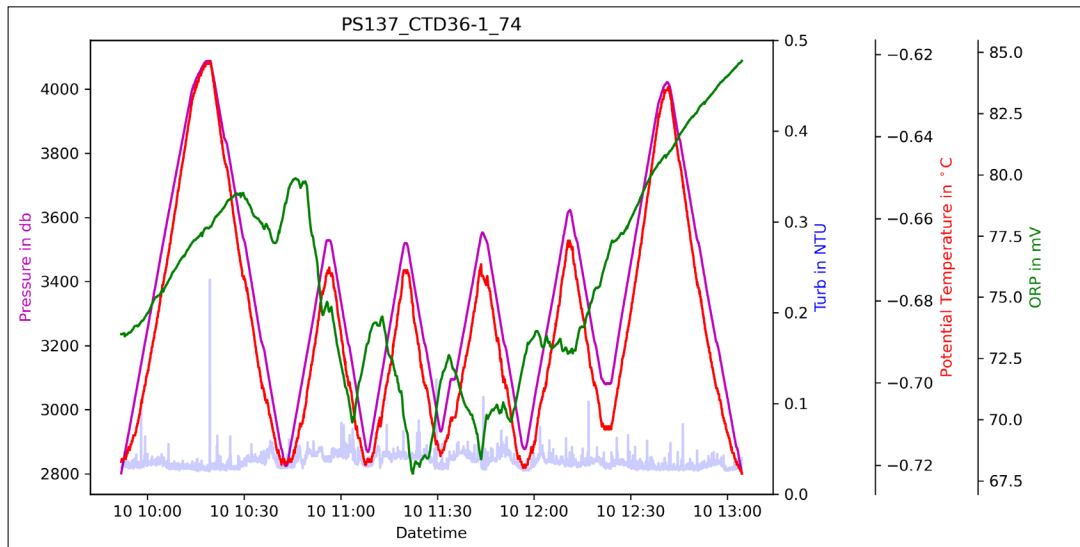


Fig. 8.2: Time series of pressure (dbar), potential temperature ( $^{\circ}\text{C}$ ), turbidity (NTU), and oxygen reduction potential (mV) during floe-yo PS137/36-1 from MAPR mounted 40 above the CTD/Rosette system.

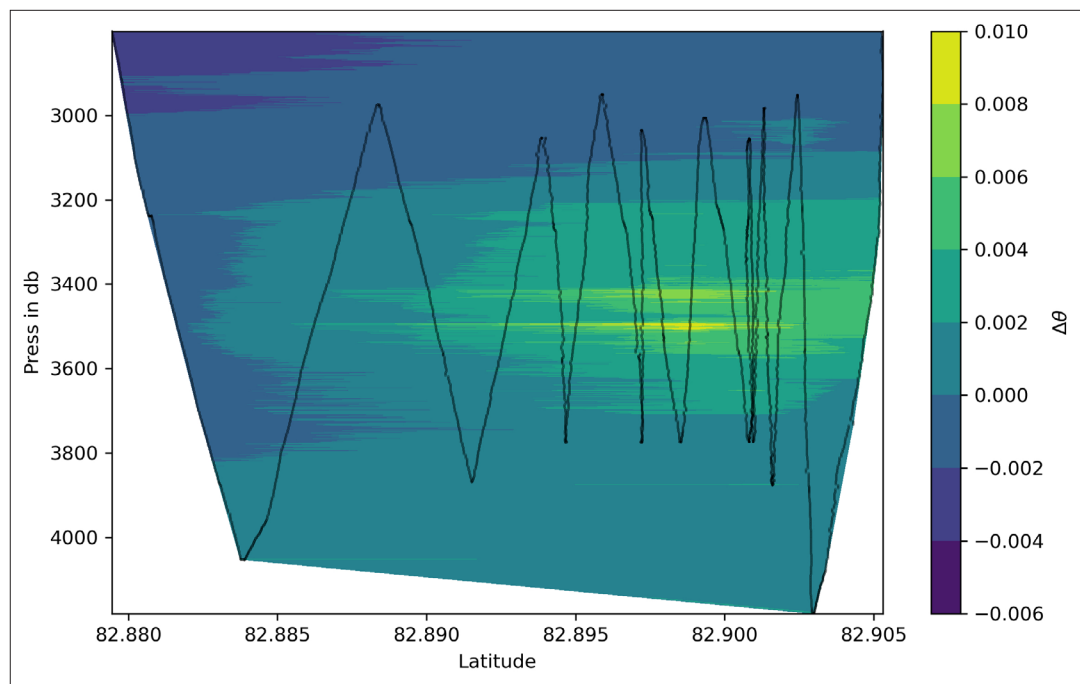


Fig. 8.3: Anomaly of potential temperature ( $\theta$ , in  $^{\circ}\text{C}$ ) along floe-yo CTD station PS137/33-1 across the Aurora vent site.

At the Lucky B site, prior information about sulphites in dredge samples and water column anomalies were indicative of hydrothermal activity. Based on these, a NUI dive was carried out (Chapter 3), and subsequently a CTD floe-yo station (PS137/58-1) was targeted at the position of the NUI dive (Fig. 8.1), drifting from there to the south. During this first floe-yo, a weak plume signal was found at the start of the drift, but not further south. Accordingly, a second floe-yo (PS137/61-1) was carried out further north, that intercepted a plume to the north of the formerly reported dredge and CTD positions. Temperature, turbidity and Eh signals were found

in a water depth between 2,850 and 3,000 m, with  $\Delta\theta$  up to 5 mK.  $\text{CH}_4$  was measured to be up to 250 nmol/L, and  $\text{H}_2$  to be 418 nmol/L in the plume layer. During the cast, we followed the plume to the south, yo-yoing between 3,000 m and 2,800 m while pumping (Fig. 8.4). Current velocity in the plume range as measured by the Aquadopp was between 10 and 15 cm/s to the north over this time, consistent with a northward dispersing plume. A follow up OFOBS deployment (Chapter 5) followed the track of this CTD, and was equipped with a MAPR on the instrument frame. The MAPR data confirmed hydrothermal activity, with a sharp drop in oxygen reduction potential of  $\sim 70$  mV and a concurrent increase in turbidity at approximately 20:20 UTC (Fig. 8.5), approximately at the southern limit of the observed water column plume, in a water depth of 3,300 m.

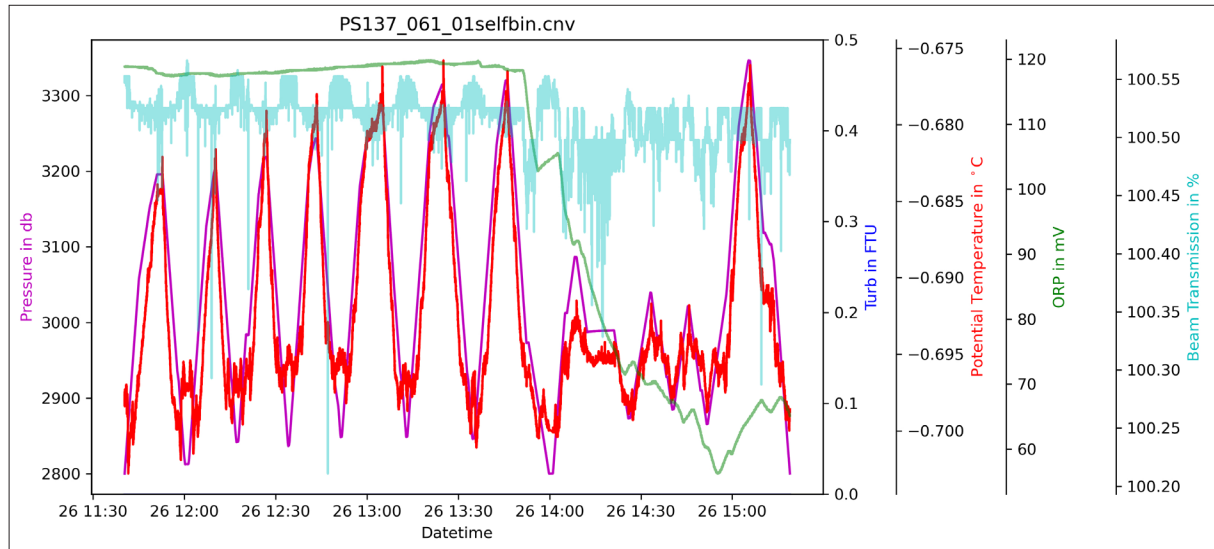


Fig. 8.4: Time series of CTD data during PS137/61-1 north of the Lucky B plume site. The plume was first encountered about 13:50 UTC, a few hundred m north of the previously reported site on the way south.

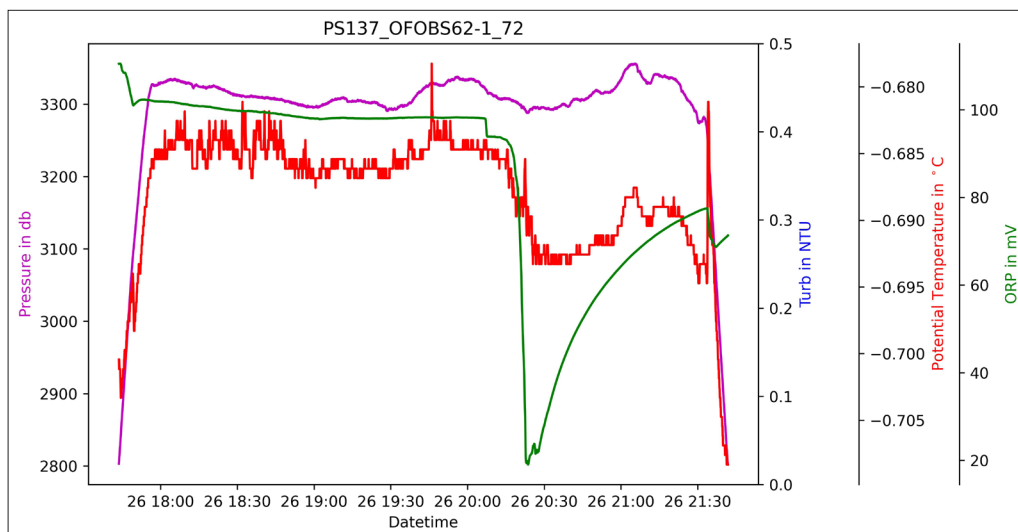


Fig 8.5: Time series of pressure (dbar), potential temperature ( $^{\circ}\text{C}$ ), turbidity (NTU), and oxygen reduction potential (mV) from MAPR mounted on OFObS, dive PS137/62-1 at the Lucky B site, along the same track as CTD PS137/61-1.

### Data management

CTD and MAPR data were made available for all cruise participants on board; all data will be archived, published and disseminated according to international standards by the World Data Center PANGAEA Data Publisher for Earth & Environmental Science (<https://www.pangaea.de>) within two years after the end of the expedition at the latest. By default, the CC-BY license will be applied.

This expedition was supported by the DFG Cluster of Excellence “The Ocean in the Earth System” at the University of Bremen, grant 49926684.

In all publications based on this expedition, the **Grant No. AWI\_PS137\_06** will be quoted and the following publication will be cited:

Alfred-Wegener-Institut Helmholtz-Zentrum für Polar- und Meeresforschung (2017) Polar Research and Supply Vessel POLARSTERN Operated by the Alfred-Wegener-Institute. Journal of large-scale research facilities, 3, A119. <http://dx.doi.org/10.17815/jlsrf-3-163>.

### References

- Baker ET, Edmonds HN, Michael PJ, Bach W, Dick HJB, Snow JE, Walker SL, Banerjee NR & Langmuir CH (2004) Hydrothermal venting in a magma desert: The ultraslow-spreading Gakkel and Southwest Indian Ridges. *Geochem. Geophys. Geosys.* 5(8):Q08002. <https://doi.org/08010.01029/02004GC000712>
- Baker ET & Milburn H (1997) MAPR: a new instrument for hydrothermal plume mapping. *Ridge Events* 8(1):23–25.
- Edmonds HN, Michael PJ, Baker ET, Connelly DP, Snow JE, Langmuir CH, Dick HJB, Mühe R, German CR & Graham DW (2003). Discovery of abundant hydrothermal venting on the ultraslow-spreading Gakkel ridge in the Arctic Ocean. *Nature* 421:252–256. <https://doi.org/10.1038/nature01351>
- German CR, Reeves E, Türke A, Diehl A, Albers E, Bach W, Purser A, Ramalho SP, Suman S, Mertens C, Walter M, Ramirez-Llodra E, Schlindwein V, Bünz S & Boetius A (2022) Volcanically hosted venting with indications of ultramafic influence at Aurora hydrothermal field on Gakkel Ridge. *Nat. Commun.* 13:6517.
- Sültenfuß J, Rhein M & Roether W (2009) The Bremen Mass Spectrometric Facility for the Measurement of Helium Isotopes, Neon, and Tritium in Water. *Isotopes Environ. Health Stud.* 45(2):1–13.

## 9. HYDROTHERMAL PLUME MICROBIOLOGY

Gunter Wegener<sup>1</sup>, Massimiliano Molari<sup>2</sup>,  
Qing-Zeng Zhu<sup>1</sup>, Christopher Klaembt<sup>2</sup>

<sup>1</sup>DE.UNI Bremen  
<sup>2</sup>DE.MPIMM

**Grant-No. AWI\_PS137\_05**

### Objectives

Microorganisms are key players in the pelagic carbon cycle. Autotrophic bacteria are primary producers of biomass, and heterotrophic bacteria degrade particulate and dissolved organic matter in the water column. Within the dark oceans energy sources supporting autotrophic carbon fixation are limited, however hydrothermal vents plumes may provide energy sources for autotrophic activity such as hydrogen, methane, and reduced sulfur species. The vent temperature and its geological setting determine the concentrations of the different potential electrons in the plume, and vice versa the plume composition gives insights into the vent chemistry. Deviations from the expected ratios indicate a potential microbial consumption of compounds. The Microbiology group aims to measure the *in-situ* concentrations of hydrogen and methane, the likely most accessible microbial energy sources as the Aurora vents, across the plume. During onboard experiments, we measure the influence of hydrogen and other reduced compounds on microbial activity parameters such as carbon fixation and enzymatic turnover of substrates. Moreover using different onboard and *in-situ* filtration techniques we sample microbial biomass to determine microbial community compositions of the Aurora vent plume and at reference sites. With these experiments, the aims of the microbiology team (i) quantify the emissions of hydrogen and methane (ii) track the consumption of hydrogen as the most important anticipated energy source; (iii) determine the effect of plume compounds on autotrophic carbon fixation and heterotrophic microbial activity. For further analysis in the home laboratory, we collected chemically fixed and frozen cell material filtered from CTD bottle water and via *in-situ* pumping.

### Work at sea

The main *in-situ* tools to retrieve samples for the Microbiology team are (i) the CTD rosette, which will be used to sample the water column of the hydrothermal plumes of Aurora and new vent systems, (ii) the *in-situ* pumps, which allows to receive larger amounts of particulate matter from the water column. Together with the Oceanography team, we investigated the position and size of the hydrothermal plume of the Aurora vent. During the expedition, we sampled the plumes and comparison samples with the CTD rosette and *in-situ* pumps. The CTD rosette will provide highly defined samples from specific units in the plume. After recovery, the plume water was split for the different methods see below. In addition, we sampled large amounts of water-derived particles using up to 4 McLane *in-situ* pumps in parallel which pumped up to 2 hours and resulted in the filtration of particles with a 300 L for each pump deployment.

*Hydrogen concentrations:* For plume hydrogen concentration measurement the CTD water was collected with 60 mL syringes. 40 ml seawater was collected and 10 ml headspace of ultrapure air was added on top. After that, the water is allowed to heat to room temperature,

and agitation is used to transfer the hydrogen into the gas phase. Hydrogen is measured using an RCP-GC Peak Performer 1 (Peak laboratories; Paolo Alto, CA, USA).

*Hydrogen consumption measurements:* To determine consumption rates, 256 ml serum bottles were filled with seawater (N=10, headspace-free is necessary) from plumes and reference sites. These bottles were incubated for defined times (i.e. 0,1,2,3 and 5 days) at *in-situ* temperatures. At these time points an air headspace was applied, bottles were agitated, and hydrogen was measured from the headspace. For samples that did not contain substantial amounts of hydrogen (references; or after hydrogen was consumed), 1 ml 0.25 or 0.5 atm H<sub>2</sub> saturated seawater was added to the serum bottles.

*Cultivation experiments:* Samples with the most-pronounced hydrogen consumption were processed in two ways: **1)** Provide a 50 ml headspace with 1,000 ppm hydrogen with atmospheric or lower O<sub>2</sub>:N<sub>2</sub> ratios. The development of the hydrogen headspace was measured after diluting the 1 ml headspace with 9 ml air. **2)** Provide 5 ml H<sub>2</sub> saturated seawater with no headspace. The development of the hydrogen concentration was measured by mixing a 2 ml water sample with 10 ml air.

*Biomolecular analyses:* For DNA extraction defined volumes of seawater (usually 10 L) were filtered using Sterivax filtration operated with peristaltic pumps. Filters were immediately stored at -80° C to preserve the DNA/RNA. DNA extraction and analysis will be performed in the home laboratory. To retrieve large sufficient amounts of microbial cells for transcriptomic and genomic analyses, CTD rosette casts were equipped with *in-situ* pumps (WTS-LV Large Volume Pumps, McLane), which were equipped with polycarbonate filters (142 mm diameter; 0.2 µm pore size; Millipore). The pumps were operated at different water depths: one *in-situ* pump was located inside the CTD frame to filter seawater inside the plume, another one at ca. 40 m above the CTD to filter seawater inside the plume, and the other two attached to the CTD cable to filter seawater above the plume. The two pumps for plume sampling had a multi-event trigger system to remotely control the switching on and off of the pump via the CTD deck unit. Start time and duration of pumping of the other two *in-situ* pumps above the CTD was pre-programmed before deployment on board.

*Cell counts and in-situ hybridization:* To determine absolute cell numbers and numbers of specific taxa, unit (applying fluorescence *in-situ* filtration) defined volumes of water (1 L) will be fixed with prefiltered formalin solution (2 % final concentration and 6 to 8 h fixation). After that, the water will be collected with 47 mm diameter/ 0.2 µm pore size polycarbonate filters using vacuum filtration. Filters will be washed with 0.2-µm filtered seawater and ethanol (70 % in water), and stored at -20° C.

*Carbon fixation:* Water samples were collected with 60 mL glass syringes, which were sealed with stopcocks and kept at *in-situ* temperature. In the radioisotope lab, defined amounts of pH10 buffered, carrier-free <sup>14</sup>C sodium bicarbonate (100 kBq per sample) are added via a syringe, and incubated in the dark at *in-situ* temperature. Incubation times will range between 6 to 48 hours. The water is filtered and the filters are exposed to an HCl atmosphere. The remaining radioactivity in the particulate fraction is measured from the filters.

*Leucine uptake:* For each sample replicates of 40 mL of seawater collected in glass syringes will be amended with 3H-leucine and leucine mix (1:4) at a final concentration of 10 nM, and incubated in the dark at *in-situ* temperature. Incubation times will range between 1 to 12 hours. The incubations will be stopped with the addition of formaldehyde (2 % final concentration). The samples will be filtered through a 0.2-um polycarbonate filter (Millipore) and rinsed three times with 5 mL of 5 % TCA (ice-cold). The remaining radioactivity in the particulate fraction is measured from the filters.

*Extracellular enzymatic activity:* The hydrolysis of the fluorogenic substrate analogous  $\beta$ -glucoside (MUF- $\beta$ ), N-acetyl-glucosamine (MUF-N-Ac), leucine (MCA), and fluorescein diacetate (FDA) will be measured to estimate potential activity rates of  $\beta$ -glucosidase, chitinase, aminopeptidase, and esterase enzymes in the seawater samples. Seawater samples (3 mL) will be incubated in the dark at a final concentration of 10  $\mu$ M for FDA, 20-500  $\mu$ M for MUF-B and 1-500  $\mu$ M for MUF-N-Ac, and 500  $\mu$ M MCA. The incubations will be stopped at four different interval times (0, 12, 24, 48 h) and the fluorescence will be measured with a fluorometer. Each enzyme is measured under saturating concentrations of the artificial substrate, which was assessed with saturation curves. All substrates, which are pre weighed before the cruise, were dissolved in approximately 2 ml of 2-Metoxyethanol by sonication for 30 seconds at 72/D and cycle of 30 %, while keeping the vial on ice. The substrates are then split up into aliquots of 200  $\mu$ l each and stored at -20°C. For the calibration, stock solutions of 5 mM (Stock 1) are prepared for every Fluorochrome by dissolving 8.75 mg MCA (MW: 175.18), 8.8 mg MUF (MW: 176.17) and 16.6 mg Fluorescein (MW: 332.31) in 10 ml 2-Metoxyethanol. Another stock solution with a concentration of 50  $\mu$ M (Stock 2) is prepared from the previous solutions by diluting 1 ml thereof with 2-Metoxyethanol to a final volume of 100 ml. A calibration curve for every fluorochrome is measured for each station by preparing working solutions from the stock solutions with the sample water from the respective station. A table of all working solutions can be found in Table 9.2. The slope of the linear regression gives the factor for the calculation of the relative fluorescence units into molar amounts of hydrolysed molecular bonds ( $\mu$ M). These can be converted into hydrolysed C in  $\mu$ g l<sup>-1</sup> by using the factor 72 for amino acids and glycosides with 6 C atoms. For the extracellular enzymatic activity, at least one sample was collected from a Niskin bottle at every station with a CTD deployment. The sample volume for every EEA sample is 0.5 litres. Before sampling, the 0.5 litre Duran bottles were autoclaved and then rinsed with the sea water from the Niskin bottle attached to the CTD before sample collection. The samples are then stored in a fridge at ca. 4°C until further processing. The fluorescence of MUF and MCA is detected at 365 nm excitation and 445 nm emitted, while the fluorescence of FDA is detected at 470 nm excitation and 510 nm emitted wavelength. Every substrate is measured in triplicate using a dedicated cuvette, which is rinsed with MilliQ water after every measurement, and reused for every timepoint.

*Lipid stable isotope probing:* Large amounts of water (20 L) are transferred into gas-tight bags made of aluminum-coated two-component welding foil. Specific amounts of energy substrates (1  $\mu$ M hydrogen final concentration; or no substrate) and labeled compounds (<sup>13</sup>C-bicarbonate (5 % final conc; and D2O 0.1 % D2O; final concentration) are added. The concentration of hydrogen development is tested by gas chromatography (see above). After defined incubation times (3 days) the experiments are stopped by filtration of the cells onto 0.3  $\mu$ m filters. Filters are immediately frozen. In the home laboratory assimilation of <sup>13</sup>C and deuterated water will be measured using the dual-stable isotope approach (Wegener et al., 2012; Wegener et al., 2017). This approach aims to identify the lipids and lipid production pathways of the yet uncultured hydrogen oxidizers in the water column.

*Amino acid stable isotope probing:* 10 L seawater was incubated either with 2  $\mu$ M <sup>13</sup>C-labeled or <sup>15</sup>N-labeled alanine to explore the heterotrophic activities (Zhu et al., 2022). After defined incubation times (3 days) the experiments are stopped by filtration of the cells onto 0.3  $\mu$ m filters. Filters are immediately frozen. In the home laboratory assimilation of <sup>13</sup>C and <sup>15</sup>N into lipids and protein will be measured using GC-IRMS.

*Retrieval of large amounts of plume biomass with in-situ pumps:* The *in-situ* pumps will be charged with batteries and the filtration units are loaded with 0.2  $\mu$ m pore-size polycarbonate filters. We used 2 CTD-triggered *in-situ* pumps of which one was mounted into the CTD and one was attached 40 m above CTD to the wire. Two time-programmed pumps were attached sometimes attached to the CTD wire. The pumps pumped up to 300 l in different partly plume-influenced water bodies. After the CTD dive the filters were rapidly harvested, cut into six

sections, and transferred to 15 ml centrifugation tubes. The tubes were immediately shock-frosted in liquid nitrogen and stored at  $-80^{\circ}\text{C}$ . In the home laboratory samples will be used for metagenomic sequencing, transcription analysis, or mineral phases are analyzed by the Petrology group.

*Cultivation of Ca. S. pluma*: Onboard, plume water bottles with strong hydrogen consumption and DCF rates will receive additional hydrogen or hydrothermal fluids. Bottles with increasing hydrogen consumption are subsampled and transferred to a synthetic growth medium. The culture will be taken home, and further enrichment/isolation steps will be performed in the home laboratories.

### Preliminary results

During this mission, we aimed to deepen our understanding of hydrogen and methane fluxes from the Gakkel Ridge and in particular from the Aurora hydrothermal vent. We measured hydrogen in the water column, performed water incubation experiments, and hydrogen pulse incubations. To obtain a mechanistic understanding of the microorganisms using hydrogen in the water column, we sampled the water column for microscopy and the analysis of cellular DNA and RNA. To measure autotrophic and heterotrophic activity we measured carbon fixation and enzymatic activity. Samples for the cultivation of the main hydrogen oxidizer were obtained. The main sampling instrument was the CTD rosette and *in-situ* pumps that were attached to the rosette and the CTD wire. Sampling locations' depths were determined together with the Oceanography group, using parameters such as turbidity and temperature anomalies as key indicators for vent plumes. Due to difficult ice conditions, only a small number of CTD stations was performed.

*Hydrogen and methane profiles in the water column*: In total, we retrieved hydrogen concentration from seven sites at Aurora and reference sites. Some samples exhibit hydrogen: methane ratios close to the endmember fluid sampled from the hydrothermal vent of 22:1. Those samples are likely from the buoyant plume, where the residence time of the dissolved gases was very short. The second group of samples exhibits much lower hydrogen: methane ratios or hydrogen was entirely depleted, whereas methane remained in detectable concentrations. This shows that hydrogen is quickly metabolized by microorganisms, whereas methane remains inert, despite quite similar thermodynamic yields for the oxidation of both compounds. Most samples showed hydrogen and methane concentrations  $< 2\text{ nmol/l}$  and therefore were considered as non-plume influenced.

*Hydrogen consumption in the plume water*: The dynamics of hydrogen consumption by the plume microorganisms cannot be directly assessed from the environmental concentrations of this compound. However, the deep water current was about  $2.5\text{ cm s}^{-1}$  (about 2 km per day), and hydrogen was not detectable anymore at a distance of  $> 2\text{ km}$ . Hence the microorganisms should have oxidized all hydrogen within one or two days. To directly measure hydrogen consumption, we filled seawater collected from the different depths into 256 ml cultivation bottles, sealed the bottles headspace-free with gas-tight butyl rubber stoppers, and measured the development of hydrogen concentrations over time. Only some samples contained notable natural hydrogen concentrations to measure the development of hydrogen concentrations over time. For the other samples, we injected defined amounts of hydrogen by exchanging small amounts of water with hydrogen-saturated seawater. In the beginning, we used 1 ml of 25 %  $\text{H}_2$  saturated seawater (resulting in 1,000 nM) in up to 10 replicate bottles for sample depth. Samples from reference sites / non-plume depths) showed only minor hydrogen consumption (Fig. 9.1). In contrast, samples from the plume depth (3,200 mbsl) showed immediate hydrogen consumption with rates up to  $100\text{ nmol/L per day}$ . This indicates the presence of large numbers of hydrogen oxidizers in the plume. Water from active plume depths supports active microbial

communities. Because the hydrogen was rapidly depleted in experiments, we added 1 ml 50 % hydrogen-saturated seawater (2,000 nM) hydrogen in the incubated water, hopefully, to get microbial enrichments.

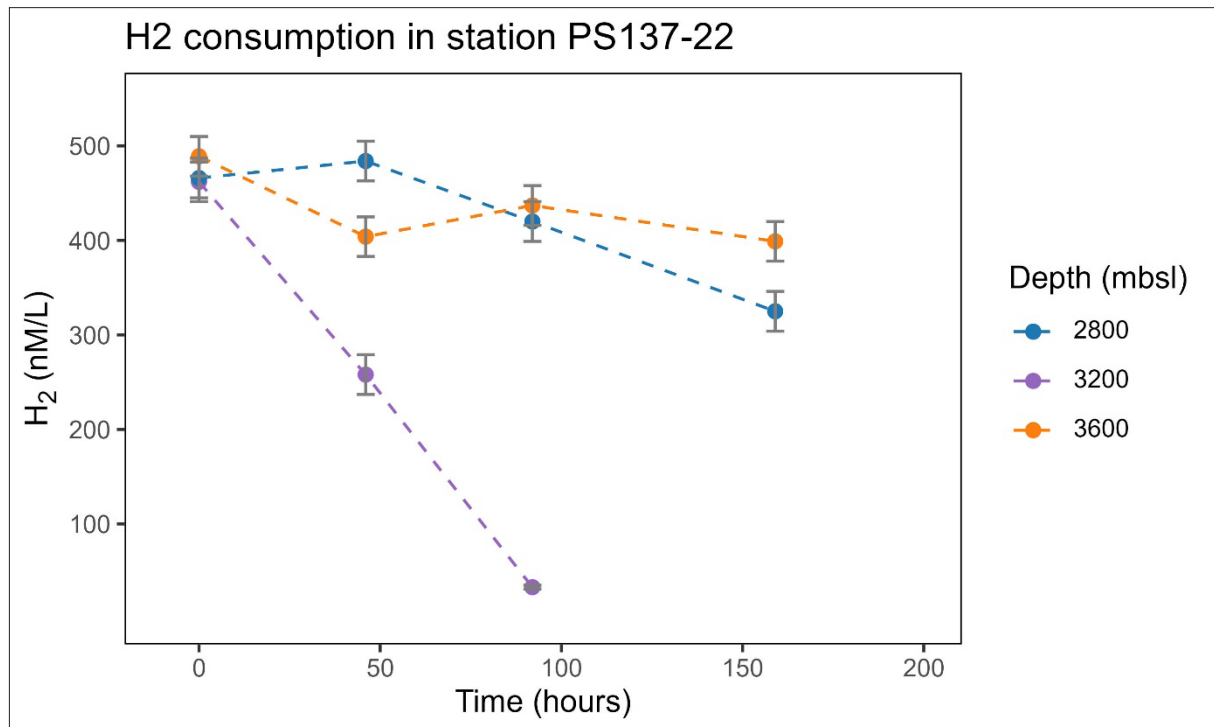


Fig.9.1: H<sub>2</sub> consumption at different water depths in station PS137-22. 3,200 mbsl is the Plume depth.

**Cultivation of the hydrogen oxidizers:** To assess possible ways to culture the hydrogenotrophic from the plume water, we supplied 1,000 ppm hydrogen in an air atmosphere (final supply: 8  $\mu$ mol H<sub>2</sub> per liter water) to the headspace of select plume water incubations, which showed highest hydrogen oxidation rates and we measured the development of hydrogen concentrations in the headspace. In the course of the experiment, most waters showed rather linear than exponential hydrogen consumption. We hypothesized that the intense oxygen supply (0.2 atm) had an inhibitory effect on the growth of hydrogen oxidizers. The most likely candidate for hydrogen oxidation in the plume is *Candidatus Sulfuriomas pluma*, an organism that has a carbon fixation pathway that functions best at low oxygen concentrations. Water samples with high hydrogen content were selected for further cultivation attempts in the home laboratory. Samples from hydrothermal plume with evidence of increased microbial activity were mixed with 0.2  $\mu$ m-filtered seawater (collected at Aurora field) oxygen depleted and amended with hydrogen or hydrothermal fluids (collected during NUI dives). These samples will be processed in the home MPI and MARUM lab (H<sub>2</sub> measurement) for further cultivation attempts.

**Quantification of dark carbon fixation:** We measured the uptake of dissolved inorganic carbon and leucine into biomass from 7 plume samples and 2 non-plume samples using the DI<sup>14</sup>C carbon and 3H-leucine assays. Several incubation times were tested to find the most appropriate. For leucine uptake, several increasing concentrations of substrates were tested to find at which one the system reach saturation. The plume samples showed carbon fixation

rates of 283 to 2,607 pmol C L<sup>-1</sup> d<sup>-1</sup>, and leucine uptake ranging between 2.9 and 0.3 pmol leucine L<sup>-1</sup> d<sup>-1</sup>. In contrast, carbon fixation and leucine uptake in non-plume samples were lower than 300 pmol C L<sup>-1</sup> d<sup>-1</sup> and than 0.9 pmol leucine L<sup>-1</sup> d<sup>-1</sup>, respectively. Hence the tested plume samples showed a remarkably higher increase of carbon fixation (up to 10 times) than leucine (up to three times) background samples (Fig. 9.2). To test the influence of hydrogen on carbon fixation we performed additional experiments with water from stations 137-41-6 that we equilibrated with 1,000 ppm of hydrogen headspace. No significant increase in carbon fixation was observed for these samples.

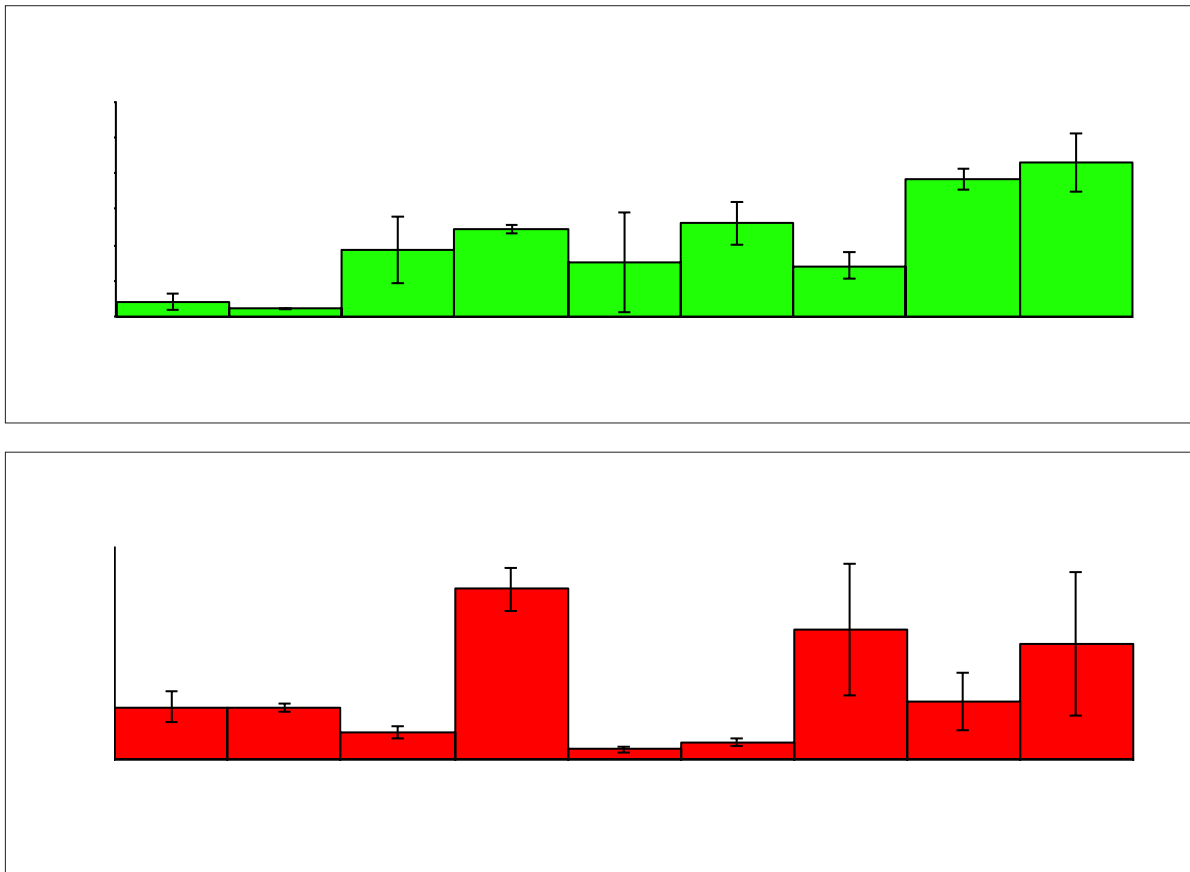


Fig. 9.2: Dissolved inorganic carbon and leucine uptake rates in different types of seawater collected during PS-137. BG: background water; P-500m: hydrothermal plume 500 m distance from Aurora vents field; BW-115m: bottom water (ca. 10 m above the seafloor) 115 m distance from Aurora vents field; P-200m: hydrothermal plume 200 m distance from Aurora vents field; BW-500m: bottom water (ca. 10 m above the seafloor) 500 m distance from Aurora vents field; P-Lucky B: hydrothermal plume north Lucky-B site.

**Microbial community analysis:** For DNA sequencing in the home laboratory, about **300** polycarbonate filters for particles > 0.2 µm have been prepared from 10 liters each (stations/depth see Appendix A.4). For RNA sequencing about 14 samples were collected with *in-situ* pumps. *In-situ* pumps were used to filter a large volume of seawater (44-228 L) in background stations (n=6), and in the hydrothermal plume or proximity of the Aurora vent field (n=8).

**Cell counts/Flourescence *in-situ* hybridization:** For phylogenetic fluorescence-specific in quantitative community analysis *n* samples have been prepared from environmental samples

by filtration of 1 l formalin-fixed samples. For gene expression analysis samples have been retrieved by *in-situ* filtration.

**Enzymatic activities in water samples:** We tested the turnover of three fluorescence-labeled substrates in water enzymes in the plume and non-plume waters from 7 different sites. For all samples beta-glucosidase, chitinase, and aminopeptidase exhibit very low rates, ranging between 0 and 0.2 nM per hour for both concentrations, indicating very low activity of these enzymes in the Aurora- and Lucky-B area (Fig. 9.3). Only Esterase showed higher rates of around 0.8 to 1.5 nM per hour (Fig. 9.3). The rates of the plume samples (station PS137/36-1 and PS137/41-1) are significantly higher for Esterase in comparison to the background samples, indicating a higher activity for Esterase in the Aurora plume. The rates of the Lucky B vent samples are significantly lower than those of the Aurora vent sites. With values of around 0.9 nM h<sup>-1</sup> the rates of Esterase at Lucky B are more comparable with the background samples from the Aurora vent (Fig. 9.3).

Altogether enzyme activities were low, which was expected given the low cell numbers.

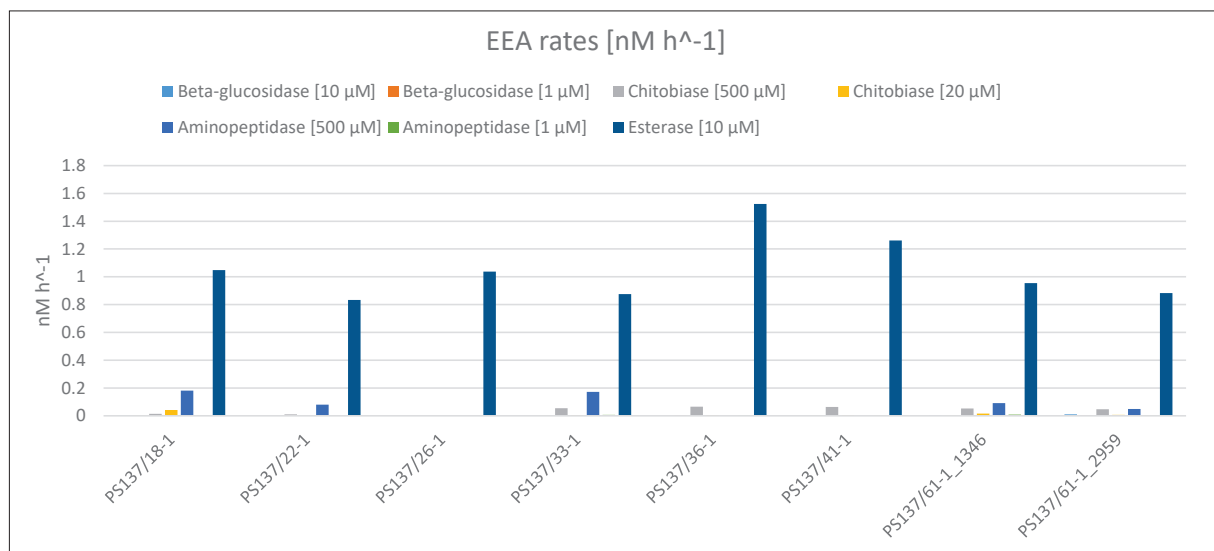


**Fig. 9.3.** Rates of extracellular enzymatic activities (EEA) determined for different water samples. Water samples were incubated with fluorogenic substrate analogues for defined times, and the fluorescence was measured after excitation at different wave lengths (see work at sea). The enzyme activity in plumes was indistinguishable from that of non-plume environments, suggesting only minor roles of heterotrophy in plumes.

### Data management

Environmental and experimental data will be archived, published and disseminated according to international standards by the World Data Center PANGAEA Data Publisher for Earth & Environmental Science (<https://www.pangaea.de>) within two years after the end of the expedition at the latest. The CC-BY license will be applied.

Molecular data (DNA and RNA data) will be archived, published and disseminated within one of the repositories of the International Nucleotide Sequence Data Collaboration (INSDC, [www.insdc.org](http://www.insdc.org)) comprising of EMBL-EBI/ENA, GenBank and DDBJ).

**References**

- Molari M, Hassenrueck C, Laso-Pérez R, Wegener G, Offre P, Scilipoti S and Boetius A (2023) A hydrogenotrophic *Sulfurimonas* is globally abundant in deep-sea oxygen-saturated hydrothermal plumes. *Nature Microbiology* 1–15.
- Wegener G, Bausch M, Holler T, Thang N M, Prieto Mollar X, Kellermann M Y, Hinrichs K-U and Boetius A (2012) Assessing sub-seafloor microbial activity by combined stable isotope probing with deuterated water and <sup>13</sup>C-bicarbonate. *Environmental Microbiology* 14:1517–1527.
- Wegener G, Kellermann M Y and Elvert M (2016) Tracking activity and function of microorganisms by stable isotope probing of membrane lipids. *Current Opinion in Biotechnology* 41:43–52.
- Zhu Q-Z, Wegener G, Hinrichs K-U. and Elvert M (2022) Activity of ancillary heterotrophic community members in anaerobic methane-oxidizing cultures. *Front. Microbiol.* 13.

## 10. PHYSICAL OCEANOGRAPHY AND OCEAN-SEA ICE COUPLING IN THE MARGINAL ICE ZONE

Simon Reifenberg<sup>1</sup>, Carina Engicht<sup>1</sup>,  
Nicolas Dettling<sup>1</sup>;  
not on board: Torsten Kanzow<sup>1</sup>, Wilken-Jon von  
Appen<sup>1</sup>, Mario Hoppmann<sup>1</sup>, Sandra Tippenhauer<sup>1</sup>,  
Ilker Fer<sup>2</sup>

<sup>1</sup>DE.AWI  
<sup>2</sup>NO.UIB

Grant-No. AWI\_PS137\_09

### Objectives

This physical oceanography group mainly continued work carried out during the PS131 expedition in summer 2022. The expedition PS131 **AT**lantic **W**ater pathways to the **ICE** in the Nansen Basin and Fram Strait (**ATWAICE**) addressed, amongst other objectives, ocean controls on sea-ice melt and the couplings to biogeochemistry, biology and the atmosphere in the Marginal Ice Zone (MIZ) north of Svalbard (Kanzow 2023). Our respective objective represents the major focus of ATWAICE related to key mechanisms of rapid Arctic sea-ice decline and Arctic Amplification. These include processes affecting heat fluxes in the air-ice-ocean system, ocean mixed layer-halocline coupling, ice melt and ice-edge dynamics in the MIZ. We posit that oceanic eddies, fronts and tidal mixing shape the sea-ice distribution in the MIZ which leads to locally enhanced ice melting as well as to the generation of stratified areas with suppressed melting. These processes result in sea-ice characteristics that can be distinguished by different gradients of sea-ice floe size, concentration, roughness and thickness. Our study also aims to understand the complex physical-chemical-biological interactions that control biogeochemical cycling and ecosystem functioning. Our guiding questions in the MIZ are:

Q1: What are the pathways and processes in the inflow regions of warm AW to the Arctic Ocean that transport heat and nutrients to the sea ice and into the euphotic layer in the MIZ?

Q2: How does the dynamic structure (stratification, mixing rates, (sub-)mesoscale activity) of the upper ocean change spatially from open ocean across the MIZ to the pack ice? How does it change seasonally with strongly varying atmospheric forcing?

Q3: What is the fate of sea ice in the summer melting season? And how does it change over time as oceanic mixing and atmospheric fluxes change over time?

Q4: How do the physical (sub-) mesoscale structures (fronts, ice-edge, eddies, etc.) and sea-ice properties (e.g., melt ponds, light transmission) impact biological production?

During the cruise PS131, high-resolution towed sections (velocity, stratification) by means of the Triaxus topAWI platform (von Appen et al. 2020) have been performed across the MIZ, revealing frontal characteristics and submesoscale dynamics, and several moorings were deployed, which are expected to provide year-round Eulerian observations of stratification and ocean currents (yielding daily to seasonal under-ice stratification and heat fluxes). The main objective for the present cruise is the recovery of said moorings.

## Work at sea

### Mooring recoveries

A total of seven ocean moorings were recovered over the course of PS137 (Fig. 10.1). At the Yermak Plateau study site, four out of seven moorings were completely recovered and two moorings were partially recovered. One mooring recovery was not attempted due to sea ice conditions (details are discussed below). At the Aurora study site, one mooring was successfully recovered.

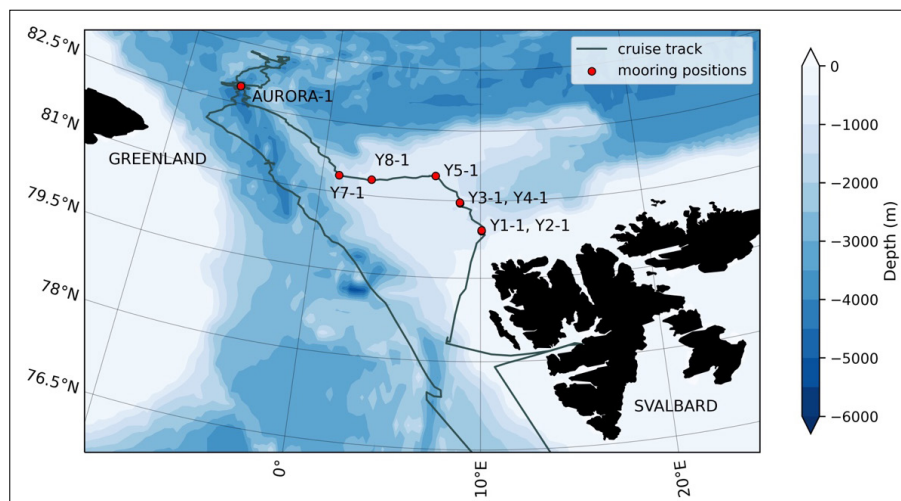


Fig. 10.1: Locations of mooring recovery sites (red) and PS137 cruise track (grey).

The moorings were instrumented to measure physical water properties (e.g. temperature, salinity, current velocity), chemical properties (e.g. oxygen), biogeochemical and biological parameters. Some sensors also collected biological and sedimentary material or recorded acoustic signals.

The moorings recovered on Yermak Plateau were placed during the ATWAICE expedition PS131. The objective of this array is to determine the influence of the upper ocean on sea ice melt and its coupling to biology and biochemistry in this region. The instrumentation was chosen to provide continuous Eulerian observations of stratification and ocean currents and reveal the temporal evolution of frontal and submesoscale structures. The mooring data thus complements the measurements taken at high spatial resolution during the ATWAICE cruise.

Two of the moorings deployed during PS131 ATWAICE were instrumented by collaborators from the University of Bergen (Y7-1, Y8-1). Through high vertical resolution particularly at the top and bottom of the mooring, the array is expected to have captured the signal of non-linear internal tides known to cause intense mixing close to sloping bathymetry. The continuous measurements thus provide context for the microstructure profiles obtained during PS131.

The mooring at the AURORA hydrothermal vent site (AURORA-1) was by collaborators from the University of Bremen. For a detailed description of the scientific objective, the reader is referred to Chapter 8.

At each mooring location, a CTD cast for calibration was obtained. In case of moorings Y1-1, Y2-1, Y3-1 and Y4-1, only two CTD casts were taken in between the moorings since the moorings had been deployed in pairs separated only by a short distance. The CTD work is discussed in detail in the next section.

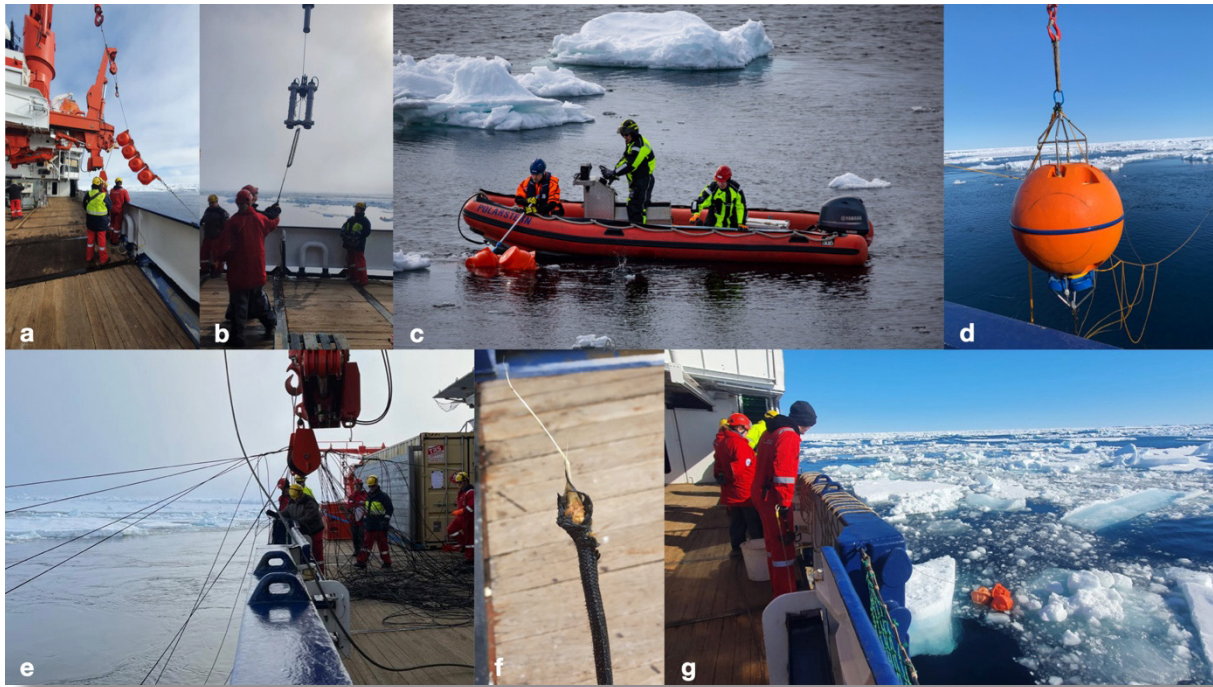


*Fig. 10.2: Examples from mooring recoveries: Recovery of a buoyancy package (a) and Develogic Sonovault (b) from mooring Y2-1. Recovery of mooring Y3-1 supported by a Zodiac for manoeuvring between floating ice (c). Entanglement of lines during recovery of mooring Y7-1 (d) and AURORA-1 (e). Severed mooring line on mooring Y3-1 where instrumented top tube was lost (f). Buoyancy package surfacing in between sea-ice floes (g). Photographs (a), (b), (e), (f), (g) are from S. Reifenberg, (c) is from T. Hecken, (d) is from N. Dettling.*

The sea state was generally calm during the mooring recoveries. At most of the recovery sites however, dense sea ice cover required to wait for a patch of open water or to extensively clear a suitable working area (Fig. 10.2).

Of the total of 7 moorings, 5 were retrieved without any complications. At times, lines and floatation devices had to be pulled around or under ice debris or got entangled during heaving operations which however did not damage any of the attached sensors.

For the recovery of mooring Y2-1, the upper 56 m containing a profiling winch system were released first. A Zodiac was then deployed to safely detach the profiler from the top of the mooring. By the time the upper part had been recovered, the sea ice conditions had become unfavourable to release the lower part of the mooring for which it had to be left behind.

After releasing mooring Y3-1, the 30 m long plastic tube that was mounted at the top of the mooring did not surface as expected. Instead, the mooring was recovered from the bottommost benthos package. When reaching the top, a damaged line end appeared close to where the tube was attached indicating the complete loss of the top tube (Fig. 2f). Inspection of the line damage suggests that the tube did not break off during recovery but at an earlier point in time. All instruments placed in the tube (3 x SBE56, 3 x SM37, 2 x RBR Wave, 1 x NORTEK ADCP, 1 x ECO Triplet) were lost, all other sensors were retrieved undamaged. Preliminary inspection of the pressure readings of the remaining instruments suggest that the tube was lost in early February 2023.

When arriving at the location of mooring Y8-1, the sea-ice cover was found to be too dense to be able to perform a recovery within a reasonable amount of time. A recovery was therefore not attempted.

**Tab. 10.1:** For further information please see the end of this chapter.

During recovery of mooring Y7-1, the mooring line was heavily entangled. Various flotation devices containing ADCPs had to be pulled under ice floes and at least one temperature sensor was subjected to heavy force when disentangling the line. Nevertheless, visual inspection did not reveal any damage to the recovered instruments.

Similarly, heavy entanglement of the lines of mooring AURORA-1 occurred during recovery, again without any visible damage to the instrumentation.

A total of 88 instruments were recovered containing amongst others 24 SBE037 MicroCATs, 26 SBE056 temperature loggers, three RDI 300kHz WorkHorse ADCPs and two 75kHz ADCPs (not counting mooring Y7-1 instrumented by University of Bergen). From these instruments, all data were downloaded, stored and repeatedly backed up. Three of the recovered SBE037 MicroCATs (serial numbers 1605, 2086, 7792) prematurely stopped logging due to low batteries. All three recovered RDI 300 kHz WorkHorse ADCPs stopped logging prematurely due to low batteries, and external batteries had to be used for the data download. From the remaining instruments, full data coverage is expected.

All MicroCATs and temperature loggers were deployed again during two calibration CTD casts which will allow a quality control and correction later in time (see next paragraph for a detailed description).

### *Hydrography*

Hydrographic measurements during PS137 were conducted using a CTD system. The sensors of the base configuration and rosette were provided by the ship.

Two sensor configurations of the CTD system were used throughout the cruise. The base configuration (*conf1*) consisted of two temperature sensors, two conductivity cells, a pressure sensor, two oxygen sensors, one fluorescence sensor, and a transmissiometer (see Tab. 10.2 for more details). For the oceanographic surveys at the plume sites, the configuration was changed (*conf2*) by adding two additional sensors for turbidity and oxidation/reduction potential (ORP) to the CTD system, and attaching up to three Miniature Autonomous Plume Recorders (MAPRs) to the cable above the CTD.

The general procedure of performing a CTD cast is the following. First, the rosette is lowered to 20 m. After the pumps turn on, the CTD is lifted back up to the surface, and then lowered again to the maximum depth of the cast.

In the vicinity of the vent sites, so-called Tow-Yos were performed during which the Rosette was lifted and lowered repeatedly in a zig-zag fashion around depths of interest. During some of these casts, several *in-situ* pumps were added to the CTD rosette and to the CTD cable. Additionally, MAPRs were mounted to the CTD cable close to the rosette or the insitu pumps. For a detailed discussion, the reader is referred to Chapters 8 and 9.

Due to a ship-wide problem with the NMEA system, one CTD cast (PS137\_010\_01) was performed without the NMEA input. To which extent this outage affects the vessel-mounted ADCP data needs yet to be determined.

Two CTD casts, 049\_01 and 052\_01, were designed and performed to later recalibrate the SBE037 MicroCATs and SBE056 temperature loggers deployed on the moorings. To this end,

we attached the MicroCATs and temperature loggers to the frame of the CTD rosette. During the first cast (049\_01), we stopped for five minutes each at 1,000 m, 750 m, 500 m, and 250 m depth. At the lower three depths, we collected water samples for high precision salinometry.

During cast 052\_01, we stopped for ten minutes each at the same depths, again taking water samples for high precision salinometry. The longer stops accommodate the lower sampling rates of MicroCATs with oxygen sensors (approx. 77 s). The remaining MicroCATs without oxygen sensors and the SBE056 temperature loggers were set to sample every 10 s.

All obtained CTD data were preliminarily processed on board using the ManageCTD software. For the Tow-Yos, only the first downcast was processed. Further data processing and recalibration using high precision salinometry will be performed on land after the cruise. An on-board comparison of primary and secondary sensors (see Fig. 10.3, for instance) did not indicate considerable sensor malfunctions or offsets.

Aside from the water sampling for salinometry, there was additional water sampling to measure the abundance of noble gases, hydrogen, methane and other chemical compounds. Again, we refer the reader to Chapters 8 and 9 for further information.

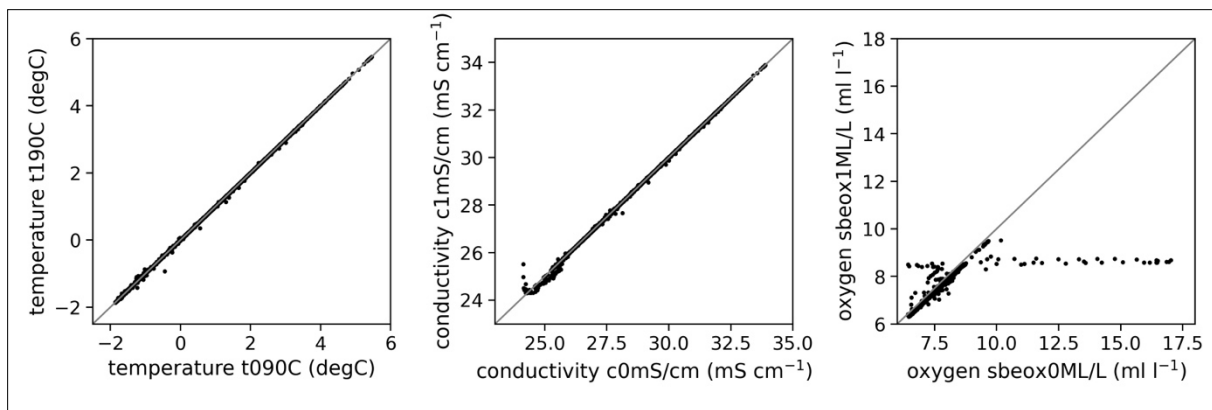


Fig. 10.3: Comparison of data from the respective primary and secondary sensors for temperature (left), conductivity (middle) and oxygen (right) from all downcasts during the cruise. The diagonal line marks the 1-1 relation.

**Tab. 10.2:** Sensor configurations for the CTD system used during PS137. The configuration *conf1* consisted of all sensors listed below, except for the turbidity meter. For the configuration *conf2*, which was used for hydrothermal plume surveying, the turbidity and oxidation/reduction sensors were added.

	SN	Calibration Date	Channel	Description
CTD				SBE 911plus
Temperature (primary)	2460	30-Jun-2022	F0	SBE3plus
Conductivity (primary)	2055	30-Jun-2022	F1	SBE4c
Pressure	0485	14-Nov-2017	F2	SBE9
Temperature	2417	30-Jun-2022	F3	SBE3plus
Conductivity	2054	30-Jun-2022	F4	SBE4c

## 10. Physical Oceanography and Ocean-Sea Ice Coupling in the Marginal Ice Zone

	SN	Calibration Date	Channel	Description
Beam Transmission	814	24-Oct-2011	V0	WETLabs C-Star
Fluorescence	1670	11-Dec-2009	V1	WETLabs ECO-AFL/FL
Altimeter	1228	--	V2	
--	--	--	V3	free
Oxygen	0880	09-Aug-2022	V4	SBE43
Oxygen	4016	19-Jan-2023	V5	SBE43
			V6	free (conf1)
			V7	free (conf1)
Turbidity	n.a.	--	V6	Seapoint Turbidity Meter (conf2)
ORP	4	--	V7	Oxidation/Reduction Potential (conf2)

**Tab. 10.3:** Meta-data of all CTD stations from PS137. The first line of the respective station names refer to the file numbers of the CTD data. The station names given with parentheses are referring to the corresponding station logged in the DSHIP system; note that both have “PS137\_” as a prefix which is omitted for simplicity here. When a depth is marked with an asterisk (\*), the CTD station was a Tow-Yo station, see Chapter 8. All casts up to PS137\_014\_01 were made with the sensor configuration *conf1*, all remaining casts, starting with PS137\_018\_1, were done with the configuration *conf2*.

Station <CTD file> <DSHIP>	Time [UTC]	Lat [°N]	Lon [°E]	Depth [dbar]	Description	Comments
001_01 (1-1)	24-Jun-2023 13:43	78.3158	8.1105	2385		Niskin #1 leaking, Niskin #14 did not close at bottom due to a plastic ball being stuck in the bottle handle
004_01 (4-1)	25-Jun-2023 16:50	80.4223	10.1648	720	Y1-1 & Y2-1 recovery	
006_01 (6-1)	26-Jun-2023 08:55	80.9607	8.6318	774	Y3-1 & Y4-1 recovery	
010_01 (10-1)	27-Jun-2023 08:23	81.5030	7.0965	486	Before Y5 recovery	ship-wide problem with NMEA, positions are from paper protocol
012_01 (12-1)	28-Jun-2023 01:25	81.3192	3.2355	377		profile was aborted due to ice conditions
012_01a (12-1)	28-Jun-2023 04:37	81.3125	3.1268	807		second cast at station
014_01 (14-1)	28-Jun-2023 17:46	81.3597	1.0578	1528	Y7-1 recovery	
018_1 (18-1)	30-Jun-2023 23:40	82.6053	-4.0303	4590		

Station <CTD file> [<DSHIP>]	Time [UTC]	Lat [°N]	Lon [°E]	Depth [dbar]	Description	Comments
022_1 (22-1)	03-Jul-2023 02:33	82.8982	-5.7480	3995	AURORA-1 recovery	
026_1 (26-1)	05-Jul-2023 03:46	82.8942	-5.7817	4143		
028_01 (28-1)	05-Jul-2023 20:36	82.9100	-5.5840	4263*		
033_01 (33-1)	08-Jul-2023 13:47	82.9087	-5.5975	4181*	Aurora vent site	
036_1 (36-1)	10-Jul-2023 08:30	82.9138	-5.6827	4137*		
040_01 (40-1)	12-Jul-2023 18:40	82.9040	-5.7040	1654		
041_01 (41-1)	13-Jul-2023 11:02	82.8995	-5.7545	3960		
049_01 (49-1)	18-Jul-2023 12:14	83.8100	-2.5720	3134		SBE037 calibration cast, 5 min stop at four target depths
052_01 (52-1)	21-Jul-2023 20:45	82.8983	-5.5920	1015		SBE037 & SBE056 calibration cast, 10 min stop at four target depths
053_01 (53-1)	22-Jul-2023 06:28	82.8968	-5.7287	174*		
054_01 (54-1)	22-Jul-2023 10:52	82.8980	-5.6878	4055*		
055_01 (55-1)	22-Jul-2023 15:40	82.9010	-5.7310	3929*		
058_01 (58-1)	25-Jul-2023 15:27	81.3748	-2.6126	3392*	Lucky B site	
061_01 (61-1)	26-Jul-2023 10:43	81.3913	-2.5628	3347*		

### Salinometry

We obtained high precision salinity measurements with an Optimare Precision Salinometer (OPS, SN 006) for recalibration of the conductivity data. Table 10.4 shows an overview of all taken samples as well as the results from the salinometry. All samples were taken from the Niskin bottles following the same procedure: Before taking the actual sample, the bottles were filled twice until the water spilled over in order to rinse them. After rinsing the rubber cap and emptying the rinsing water, the actual sample was taken. The bottles were then closed, rinsed from the outside with fresh water, sealed with an aluminum cap, and stored.

We processed the samples in two batches of 14 and 20 bottles, i.e. 34 samples in total. The day before each session, the salinity bottles were heated in a water bath to approximately 30° C, and then let cool down for about 20 h. After heating, the samples were degassed by releasing the pressure in the bottle with a syringe needle. Before the OPS measuring, the samples were shaken thoroughly to overcome any stratification in the bottle. While sampled by the OPS, the opening of the bottles was sealed with parafilm to avoid evaporation. The metal inlet tube of the OPS was cleaned with a Kim-wipe in between samples.

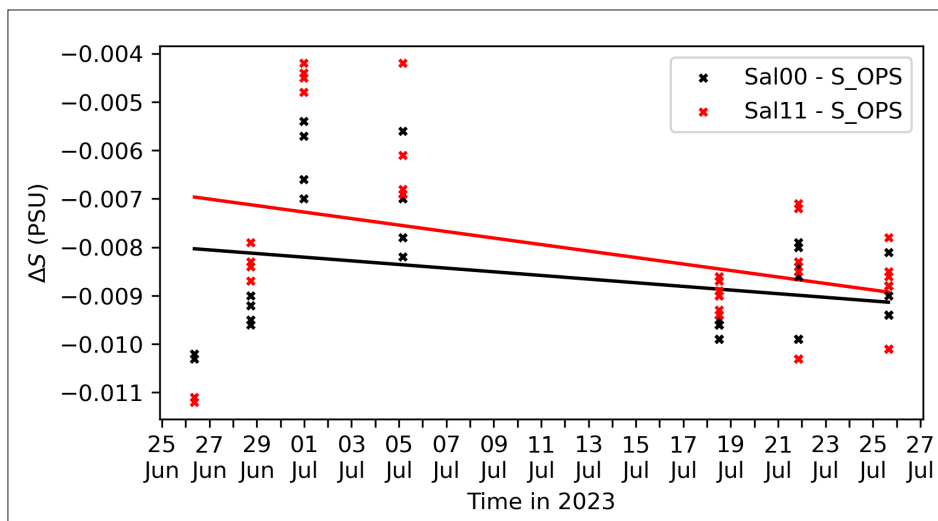


Fig. 10.4: Difference of practical salinity observed from the primary (Sal00, black) and secondary (Sal11, red) conductivity cell with respect to the salinity measured with the OPS (S OPS) over time. The red and black line indicate a linear fit to the respective data.

All salinometry session started with the standardization of the OPS with standard seawater. The respective bottle was then sealed with the original cap and sampled at the end of each session again. The salinity of the standard increased slightly in all sessions due to evaporation. This behaviour is expected and indicates that the standard water had not been contaminated.

Overall, a preliminary analysis shows absolute differences in the order of 0.001 to 0.01 PSU between both salinity measurements from the CTD and the OPS salinity. The comparably low values from the samples taken on 01 July 2023 can potentially be explained by the time delay caused by the insitu pumping during the cast. In consequence the water in the Niskin bottle may have stratified until the sampling, so that the observed salinity is not representative of the water sample.

**Tab. 10.4:** Results from OPS high-precision salinity measurements. The samples were measured in two sessions, indicated by the batch number in the remarks column.

Station	Date of water sampling	OPS salinity [PSU]	Sal00 salinity [PSU]	Sal11 Salinity [PSU]	Remarks
PS137_006_01	26-Jun-2023	34.9112	34.9010	34.9001	Batch 1
PS137_006_01	26-Jun-2023	34.9113	34.9010	34.9001	
PS137_014_01	28-Jun-2023	34.9148	34.9052	34.9061	

Station	Date of water sampling	OPS salinity [PSU]	Sal00 salinity [PSU]	Sal11 Salinity [PSU]	Remarks
PS137_014_01	28-Jun-2023	34.9144	34.9052	34.9061	
PS137_014_01	28-Jun-2023	34.9139	34.9044	34.9055	
PS137_014_01	28-Jun-2023	34.9134	34.9044	34.9055	
PS137_018_01	30-Jun-2023	34.9312	34.9255	34.9267	
PS137_018_01	30-Jun-2023	34.9309	34.9255	34.9267	
PS137_018_01	30-Jun-2023	34.9207	34.9141	34.9163	
PS137_018_01	30-Jun-2023	34.9211	34.9141	34.9163	
PS137_026_01	05-Jul-2023	34.9322	34.9252	34.9261	
PS137_026_01	05-Jul-2023	34.9330	34.9252	34.9261	
PS137_026_01	05-Jul-2023	34.9225	34.9169	34.9183	
PS137_026_01	05-Jul-2023	34.9251	34.9169	34.9183	
PS137_049_01	18-Jul-2023	34.9068	34.8969	34.8978	Batch 2
PS137_049_01	18-Jul-2023	34.9068	34.8969	34.8978	
PS137_049_01	18-Jul-2023	34.8985	34.8889	34.8896	
PS137_049_01	18-Jul-2023	34.8985	34.8889	34.8896	
PS137_049_01	18-Jul-2023	34.9309	34.9214	34.9216	
PS137_049_01	18-Jul-2023	34.931	34.9214	34.9216	
PS137_049_01	18-Jul-2023	34.9071	34.8975	34.8984	
PS137_049_01	18-Jul-2023	34.907	34.8975	34.8984	
PS137_052_01	21-Jul-2023	34.906	34.8961	34.8957	
PS137_052_01	21-Jul-2023	34.906	34.8961	34.8957	
PS137_052_01	21-Jul-2023	34.8971	34.8885	34.8886	
PS137_052_01	21-Jul-2023	34.8969	34.8885	34.8886	
PS137_052_01	21-Jul-2023	34.8988	34.8909	34.8917	
PS137_052_01	21-Jul-2023	34.8989	34.8909	34.8917	
PS137_058_01	25-Jul-2023	34.9331	34.9237	34.9237	
PS137_058_01	25-Jul-2023	34.9331	34.9237	34.9237	
PS137_058_01	25-Jul-2023	34.9316	34.9228	34.923	
PS137_058_01	25-Jul-2023	34.9318	34.9228	34.923	
PS137_058_01	25-Jul-2023	34.9295	34.9214	34.9217	
PS137_058_01	25-Jul-2023	34.9302	34.9214	34.9217	

### Preliminary (expected) results

Early results from data obtained during the connected expedition PS131 ATWAICE show spatial gradients of meltwater content in the upper ocean on Yermak Plateau, as well as temporally varying boundary layer mixing in the shallowest meters of the water column during an observational period of three weeks (Reifenberg et al., 2023). Reifenberg et al. also show that the vertical heat flux in the upper ocean is low (or even negative) during the observed time

period, obtained from nine different microstructure stations within the Marginal Ice Zone on Yermak Plateau, caused in part by strong stratification from meltwater, and weak temperature gradients. In consequence, given the background conditions present during PS131, heat provided by the Atlantic Water might only be carried to the ice by strong mixing events due to storms or lateral advection at the surface.

A first look on MicroCAT data from mooring Y1-1 shows high variability of temperature and temperature gradients in the upper ocean over the course of one year (see Fig. 10.5). Furthermore, the variability of the pressure record, indicative of tilt of the mooring due to ocean currents, exhibits time periods of more dynamic activity as well as calmer periods. This very early look at the data already shows that the mooring setup was suitable for observing the targeted processes at the temporal and spatial scales of interest.

Preliminary data from mooring Y3-1 suggests that the tube was ripped off on 7 February 2023 (see Fig. 10.6). At this point in time the pressure readings of the two uppermost MicroCATs suddenly and simultaneously increase, indicating a change of the depth of the instruments. Most likely, the line sank down while the benthos packages in the center of the mooring line now provided the buoyancy for the remaining instruments.

The data from the recovered moorings on the present cruise PS137 will allow an analysis of the seasonal variability of key oceanographic variables related to ice-ocean coupling such as heat fluxes and ocean currents (mainly related to Q2 above). These observations will complement the towed observations and extensive ice station work during PS131. The CTD stations close to the respective mooring locations will allow a quality assessment and correction of the moored instrument data.

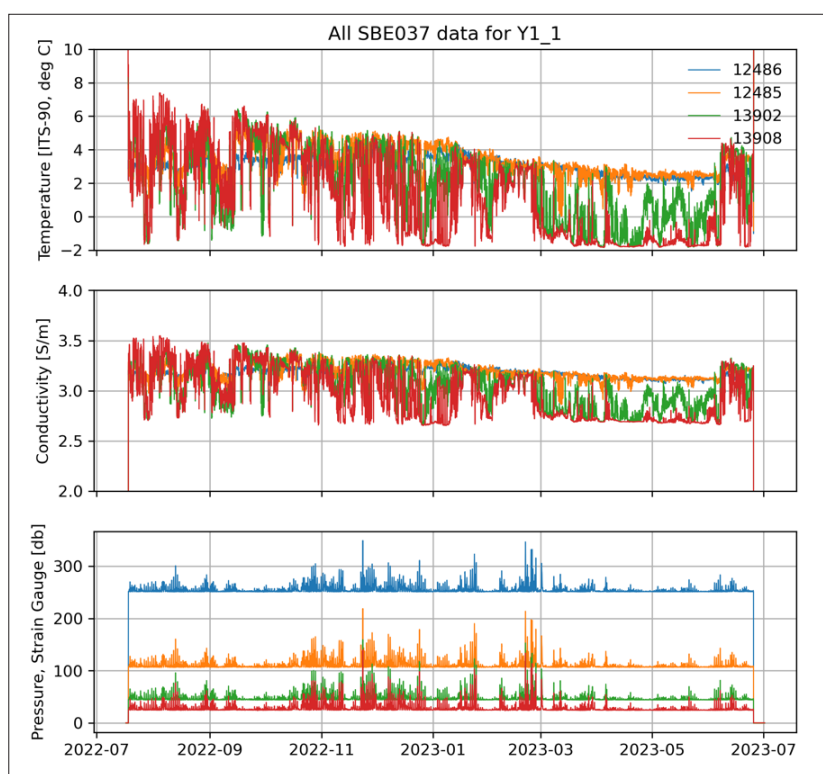


Fig. 10.5: Time series of temperature (top), conductivity (middle) and pressure (bottom) from four SBE037 MicroCATs on the recovered mooring Y1-1.

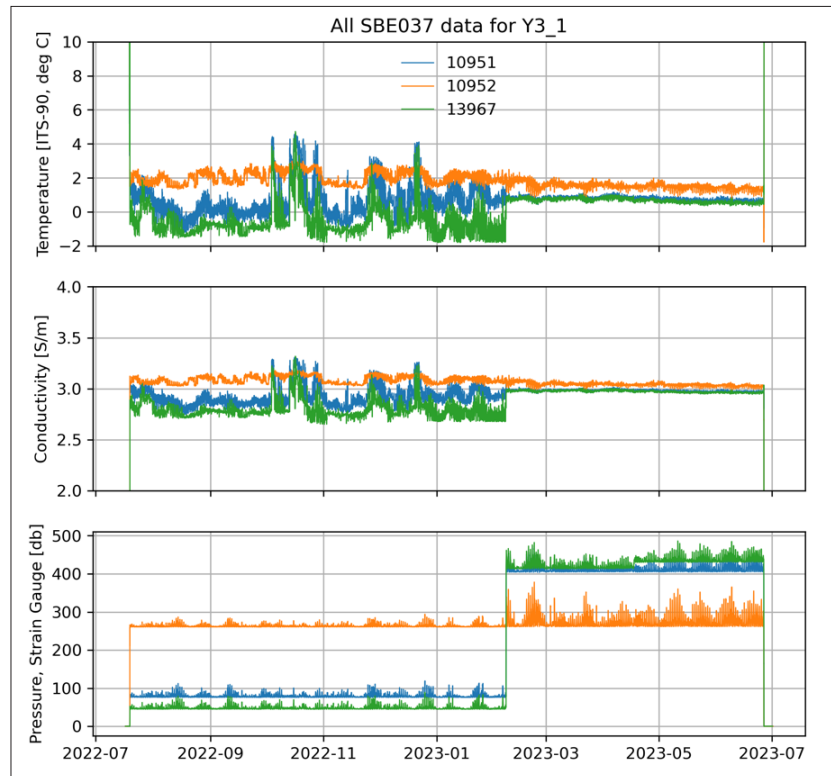


Fig. 10.6: Same as Figure 10.5, but for mooring Y3-1. The pressure record clearly shows the time when the top part of the mooring, which was attached to the tube, sank down until it was hanging upside-down from the next buoyancy in the line. This happened on 07 February 2023.

## Data management

Environmental data will be archived, published and disseminated according to international standards by the World Data Center PANGAEA Data Publisher for Earth & Environmental Science (<https://www.pangaea.de>) within two years after the end of the expedition at the latest. By default, the CC-BY license will be applied.

This expedition was supported by the Helmholtz Research Programme “Changing Earth – Sustaining our Future” Topic 2, Subtopic 2.1.

In all publications based on this expedition, the **Grant No. AWI\_PS137\_09** will be quoted and the following publication will be cited:

Alfred-Wegener-Institut Helmholtz-Zentrum für Polar- und Meeresforschung (2017) Polar Research and Supply Vessel POLARSTERN Operated by the Alfred-Wegener-Institute. Journal of large-scale research facilities, 3, A119. <http://dx.doi.org/10.17815/jlsrf-3-163>.

## References

- von Appen WJ, Strass VH, Bracher A, Xi H, Hörstmann C, Iversen M, & Waite A (2020) High-resolution physical–biogeochemical structure of a filament and an eddy of upwelled water off northwest Africa. *Ocean Science* 16:253–270
- Kanzow T (2023) The Expedition PS131 of the Research Vessel Polarstern to the Fram Strait in 2022/ H. Bornemann (editor), *Berichte zur Polar- und Meeresforschung = Reports on polar and marine research*, Bremerhaven, Alfred-Wegener-Institut Helmholtz-Zentrum für Polar- und Meeresforschung, 770. [https://doi.org/10.57738/BzPM\\_0770\\_2023](https://doi.org/10.57738/BzPM_0770_2023)
- Reifenberg SF, von Appen W-J, Fer I, Haas C, Hoppmann M & Kanzow T (2023) Observations of Sea Ice Melt and Ice-Ocean Boundary Layer Heat Fluxes in the Marginal Ice Zone North of Fram Strait, EGU General Assembly 2023, Vienna, Austria, 24–28 Apr 2023, EGU23-14268. <https://doi.org/10.5194/egusphere-egu23-14268>, 2023

**Tab. 10.1:** List of moorings to be recovered. All moorings were deployed during PS131 in 2022.

Name	Longitude		Latitude		Depth	Top	Depl. Station	Depl. Time	Rec. Station	Rec. Time	CTD Station	
	Degrees	Minutes	Degrees	Minutes								
Y1-1	10	3.66	E	80	24.08	N	691	23	PS131	UTC	PS137	
Y2-1	10	3.65	E	80	25.00	N	693	128	58-2	2022/07/18 07:25	02-1	2023/06/25 10:25
Y3-1	8	43.30	E	80	56.95	N	768	6	59-2	2022/07/18 09:53	03-1	2023/06/25 13:36
Y4-1	8	42.18	E	80	57.95	N	790	16	62-2	2022/07/19 09:28	08-1	2023/06/26 14:15
Y5-1	7	9.13	E	81	30.08	N	485	17	63-2	2022/07/19 12:51	07-1	2023/06/26 11:11
Y7-1	1	4.34	E	81	20.97	N	1548	22	66-2	2022/07/20 11:47	11-1	2023/06/27 12:00
Y8-1	3	10.27	E	81	18.82	N	800	16	83-2	2022/07/27 18:12	13-1	2023/06/28 14:07
AURORA-1	6	15.04	W	82	53.87	N	3906	96	77-2	2022/07/25 15:49	21-1	2023/07/03 23:08
									85-2	2022/07/29 05:34		<i>not recovered</i>

## 11. SEA ICE

Victor Lion<sup>2</sup>

not on board: Natascha Oppelt<sup>2</sup>

Not realized campaign by Gerit Birnbaum<sup>1</sup>, Lena Buth<sup>1</sup>, Gunnar Spreen<sup>3</sup>, Niklas Neckel<sup>1</sup>, Christian Haas<sup>1</sup>, Niels Fuchs<sup>4</sup>

<sup>1</sup>DE.AWI

<sup>2</sup>DE.CAU

<sup>3</sup>DE.UNI Bremen

<sup>4</sup>DE.UNI Hamburg

**Grant-No. AWI\_PS137\_11**

### Objectives

The main objective of the sea-ice group during the PS137 expedition is to study melt processes at the sea-ice surface, in particular properties of melt ponds. Melt ponds lead to a decrease in reflectivity of sea ice, which has consequences for the energy and mass balance of the ice and the primary productivity in the upper ocean. Additionally, the extent of melt ponds is a sign of the extent of surface melting and freshwater release to the ocean, both of which contribute to upper ocean stratification.

There have been studies on deriving the bathymetry of melt ponds using airborne hyperspectral or RGB imagery (König et al., 2020a; Fuchs, 2023) but so far the methods have mostly been used for individual ponds. One main focus of our intended sea-ice research activities is therefore to carry out helicopter and drone survey flights collecting data on 3-dimensional melt pond geometry and the distribution of melt ponds for entire floes. In particular floes featuring a composite of sea ice of different age and structure will be considered in order to further study the relationship between these parameters and melt ponds properties (Landy et al., 2015).

The combination of the RGB images from the DSLR cameras mounted on the helicopter and the multispectral sensor on the drone allow for a method comparison in deriving pond geometry, which constitutes a second main research focus of the sea-ice team aboard *Polarstern*.

Satellite remote sensing serves as a valuable supplement to *in-situ* measurements and allows for synoptic and multi-temporal data collection. Therefore, we will use remote sensing data (Sentinel-2) to enhance and verify algorithms for retrievals such as floe size, melt pond coverage, melt pond depth (König et al., 2019) and ice drift (König et al., 2020b; Wang et al., 2021). The satellite remote sensing retrieval of these parameters, including the spectral behaviour of sea ice and melt ponds, is dependent on spectral information, which requires a retrieval of their optical properties (e.g., König et al., 2019; Malinka et al., 2018).

During the cruise, especially drone survey will be conducted to bridge from field to satellite scale. The drone is equipped with a sensor with the same spectral setting as Sentinel-2 which allows for a direct comparison in the spectral domain.

The surveyed region will potentially be revisited during the IceBird Summer campaign in August 2023 when the melt ponds are expected to start refreezing. Therefore, the current expedition plays a role in strengthening the existing set of campaign data for statistical analysis of open ponds in summer. It will thereby expand the data set of optical imagery in the area surveyed during previous IceBird Summer and *Polarstern* campaigns.

## Work at sea

### Helicopter surveys

No helicopter surveys were carried out because this programme was cancelled before the cruise. Therefore, the campaign of AWI/University of Bremen could not be realized.

### Drone surveys

A total of thirteen drone surveys over the sea ice as well as of melt ponds were conducted. All flights were carried out either automatically or manually on the sea ice. Main information about the flights is summarized in Table 11.1. Since the hyperspectral AISAeagle sensor operated from the helicopter in previous expeditions was not available, we used a DJI Matrice 210 RTK V2 equipped with the MicaSense RedEdge-MX Dual Camera (see Fig. 11.1). This multispectral camera enables high spatial resolution imaging of snow and ice as well as water surfaces. The MicaSense RedEdge-MX Dual Camera offers ten spectral bands (from coastal blue at 444 nm to near infrared at 842 nm) with wavelength ranges corresponding to the bands of Sentinel-2.



Fig. 11.1: DJI Matrice 210 RTK V2 with attached MicaSense RedEdge-MX Dual Camera.  
Photo: Lilian Böhringer

Tab. 11.1: List of all drone flights performed during ALOIS

No.	Date	Start time	End time	Flight level [m]	Flight speed [m/s]	Recording interval [s]	Weather condition
1	25 June 2023	20:14:55	20:41:45	25	3	2	Overcast
2	26 June 2023	17:35:55	17:55:06	25	3	2	Overcast/ Fog
3	28 June 2023	10:59:12	11:06:19	150	4	4	Clear sky
4	28 June 2023	12:01:19	12:10:09	150	4	4	Clear sky
5	01 July 2023	15:04:52	15:36:45	25	2	2	Clear sky/ Cirrus
6	01 July 2023	15:43:28	15:57:25	150	5	4	Clear sky/ Cirrus

No.	Date	Start time	End time	Flight level [m]	Flight speed [m/s]	Recording interval [s]	Weather condition
7	04 July 2023	10:38:33	11:18:48	150	5	4	Clear sky
8	05 July 2023	13:34:27	13:53:04	50	6	2	Clear sky
9	13 July 2023	09:43:14	10:04:01	150	6	4	Cirrus
10	13 July 2023	10:07:11	10:19:41	25	2	2	Cirrus
11	20 July 2023	09:51:20	10:00:41	150	5	2	Cirrus
12	20 July 2023	10:01:32	10:03:59	25	2	1	Cirrus
13	25 July 2023	09:14:35	10:04:57	200	6	4	Clouds/ Clear sky



Fig. 11.2: Spectral measurement of the *Stickle* during melt pond transect in a small and shallow melt pond.  
Photo: Lilian Böhringer



Fig. 11.3: *Stickle* transect operation in a larger pond with additional water depth measurement.  
Photo: Timo Hecken

### The *Stickle*

Due to so-called “mummy chair” operations as well as helicopter flights it was possible to organize small ice stations lasting between two and five hours. As a result of this, previously prepared *in-situ* observations could be carried out. One of them is the *Stickle* which is a measuring unit equipped with three OceanOptics STS-VIS spectro-radiometers on a person-mounted and gimbal-stabilized monopod (see Fig. 11.2). Two of the spectro-radiometers measure down- and upwelling irradiance simultaneously. An additional spectro-radiometer for measuring upwelling radiance is also attached.

The *Stickle* was mainly used in melt ponds to obtain valuable spectro-radiometer measurements in combination with the drone survey data from the MicaSense RedEdge-MX Dual Camera. The *Stickle* was operated on a transect between two orange markers laid out before the drone flight with a melt pond region between them. Spectral measurements were taken every one to two meters (depending on the distance between the markers) as well as measurements to determine the water depth (see Fig. 11.3). The *Stickle* was used during six of eight ice stations (see Tab. 11.2 for an overview).

**Tab. 11.2:** List of all *Stickle* operations performed during ALOIS

No.	Date	Marker distance [m]	Distance between two measurement points [m]	Number of spectral measurements for each point	Type	Weather condition
1	28 June 2023	26	1	5	Two-sided	Clear sky
2	01 July 2023	30	1	4	One-sided	Clear sky/ Cirrus
3	04 July 2023	108	2	4	One-sided	Clear sky
4	05 July 2023	59	2	4	Two-sided (with offset)	Clear sky
5	13 July 2023	196	1.3 (length of <i>Stickle</i> )	4	One-sided	Cirrus
6	20 July 2023	175 (abort after 73 meter – too deep)	1.3 (length of <i>Stickle</i> )	4	One-sided	Cirrus/Clouds
7	25 July 2023	171 (abort after 13 meter – too deep)	1.3 (length of <i>Stickle</i> )	4	One-sided	Clear sky

### *Goniometer*

Also part of the *in situ* observations on the sea ice was the Goniometer. The Goniometer was used to study the backscattering behavior of snow and ice surfaces as well as frozen melt ponds and thus to collect information about the BRDF (Bidirectional Reflectance Distribution Function) of these surfaces. The sun's electromagnetic radiation is scattered in different directions on the underlying surface and is measured by a spectro-radiometer. This is mounted on a frame which can move fully automatically to in total 48 different angular positions on a hemisphere (see Fig. 11.4). A second spectro-radiometer was used to monitor the downwelling spectral irradiance. The cruise resulted in a dataset containing twelve different Goniometer positions and four various major underlying surface types. Table 11.3 shows an overview of the Goniometer measurements taken during PS137.



*Fig. 11.4: Goniometer position on 04 July 2023 with underlying thin ice layer on top of snow/ice surface*

**Tab. 11.3:** List of all Goniometer measurements performed during ALOIS

No.	Date	Start time	Latitude	Longitude	Underlying surface type	Weather condition
1	25 June 2023	20:01:59	80.4668088 N	10.1372557 E	Snow/ice	Overcast
2	26 June 2023	17:16:25	80.9375302 N	8.748497 E	Snow/ice	Overcast/ Fog
3	26 June 2023	18:17:18	80.9383715 N	8.744066 E	Frozen melt pond (large)	Overcast/ Fog
4	28 June 2023	08:40:28	81.5049888 N	1.2022802 E	Snow/ice	Clear sky
5	28 June 2023	09:33:46	81.5061323 N	1.2091415 E	Frozen melt pond (small)	Clear sky
6	28 June 2023	10:23:25	81.5067755 N	1.2158077 E	Snow/ice	Clear sky
7	01 July 2023	08:25:30	82.7152725 N	5.196823 W	Snow/ice	Clear sky
8	01 July 2023	08:54:30	82.7143773 N	5.1832827 W	Slush ice	Clear sky
9	01 July 2023	09:19:03	82.7136068 N	5.172586 W	Snow/ice	Clear sky
10	04 July 2023	08:31:04	82.656785 N	4.7474378 W	Thin ice layer on top of snow/ice	Clear sky
11	05 July 2023	11:20:09	82.4157767 N	4.9556642 W	Snow/ice	Clear sky
12	05 July 2023	11:51:11	82.4135702 N	4.9600171 W	Thin ice layer on top of snow/ice	Clear sky

## Preliminary results

### *Drone surveys*

Depending on the flight altitude and speed, the recording interval of the MicaSense RedEdge-MX Dual Camera was selected so that the overlap between two images was  $> 75\%$ . The individual images were then radiometrically and geometrically corrected by Agisoft Metashape Professional (Trial Version). Geo-located orthomosaics were also created in the software. Figure 11.5 shows an example of a truecolor orthomosaic subset from 13 July 2023.

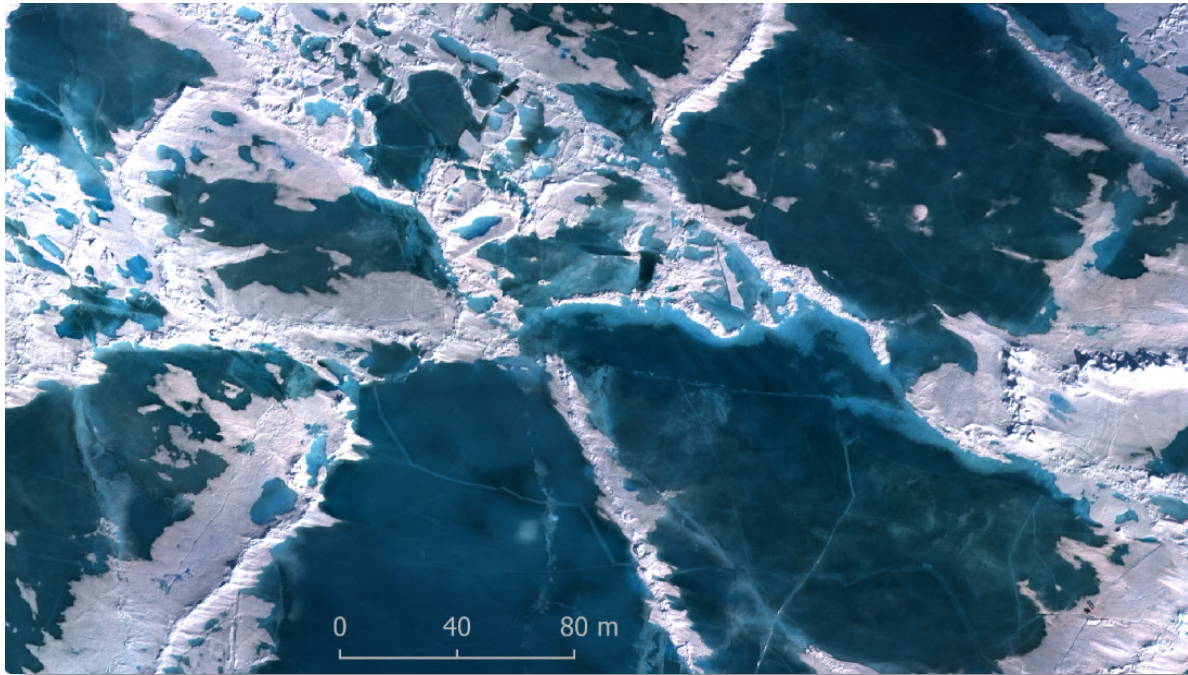
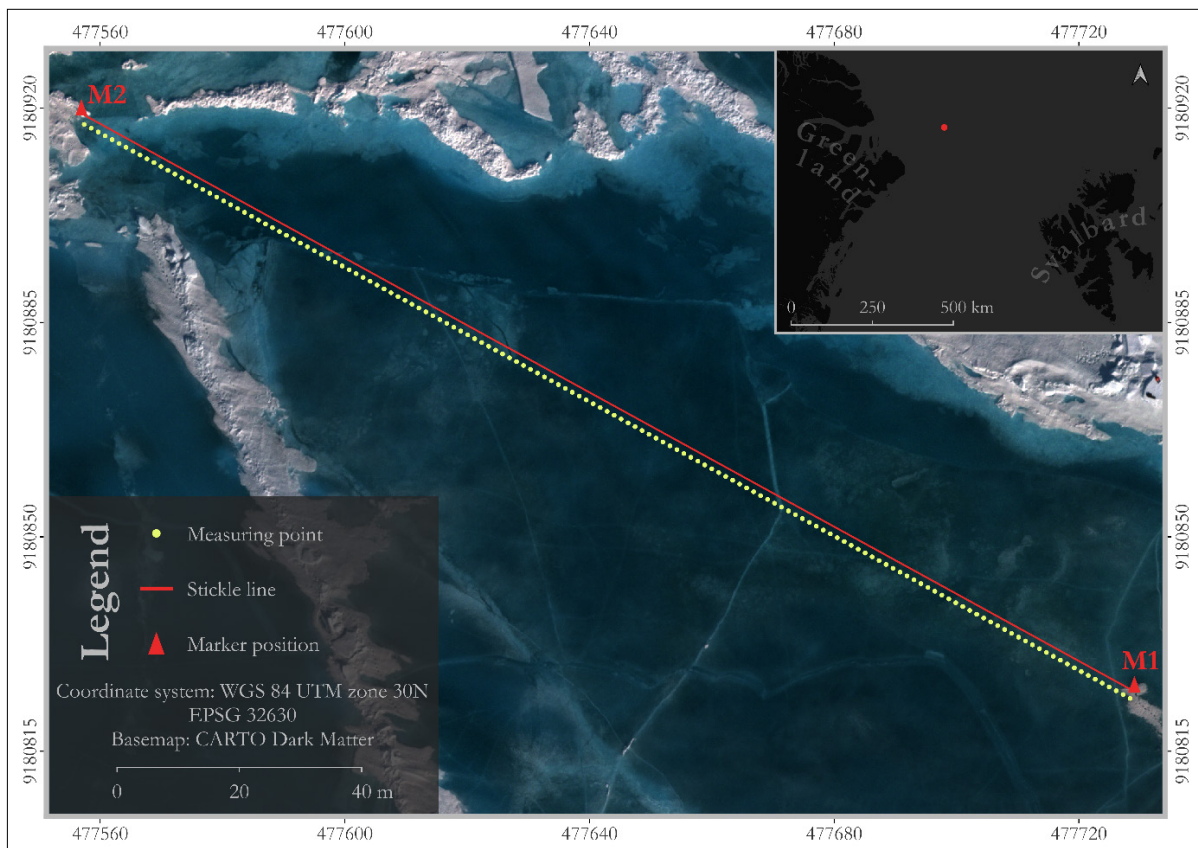


Fig. 11.5: Subset of drone orthomosaic from 13 July 2023

### *The Stickle*

On 13 July 2023 an extensive *Stickle* transect was carried out (see Fig. 11.6). The transect was 196 meters long and consisted of 151 measurement points between two markers (M1 & M2) placed on each side of the melt pond. The distance between each measurement point is the length of the *Stickle* monopod and gimbal (1.3 meters). At every measurement point each spectro-radiometer measured four spectra. Additionally, for each of these points the water depth was measured with a folding rule. Figure 11.7 shows the course of the melt pond depth. The measured points are not exactly on the red line between the markers but offset by 1.33 meters (distance of the spectro-radiometer to the user, who is on the transect line) to the southwest. The mean water depth is -46.9 centimeters. The maximum water depth of -67.9 centimeters is reached after 152 meters starting at marker M1.



*Fig. 11.6: Map of the Stickle transect through a large pond on 13 July 2023. The measuring points are not exactly on the line between the markers but offset by 1.33 meters (distance of the spectro-radiometer to the user, who is on the transect line) to the southwest.*

The 05 July 2023 serves as an example for a two-sided transect from marker M1 to marker M2 (see Fig. 11.8). The transect was 59 meters long and consisted of 58 measuring points. Points same side (north east or south west) are two meters from each other. The measuring points in the north east are offset by one meter compared to the points in the south west. Figure 11.9 shows the course of the melt pond depth. The measured points are not exactly on the red line between the markers but offset by 1.33 meters (distance of the spectro-radiometer to the user, who is on the transect line) to the southwest. The mean water depth is -14.6 centimeters. The maximum water depth of -26.2 centimeters is reached after 28 meters starting at marker M1.

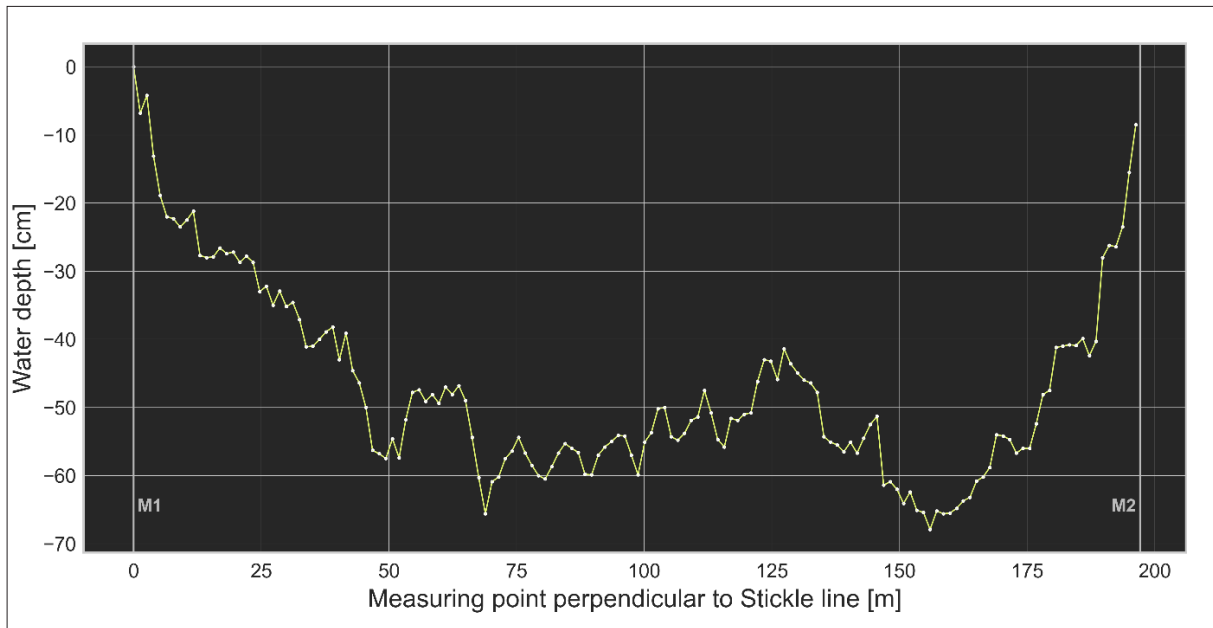


Fig. 11.7: Course of measured melt pond water depth on 13 July 2023 depending on the distance between the two markers M1 and M2

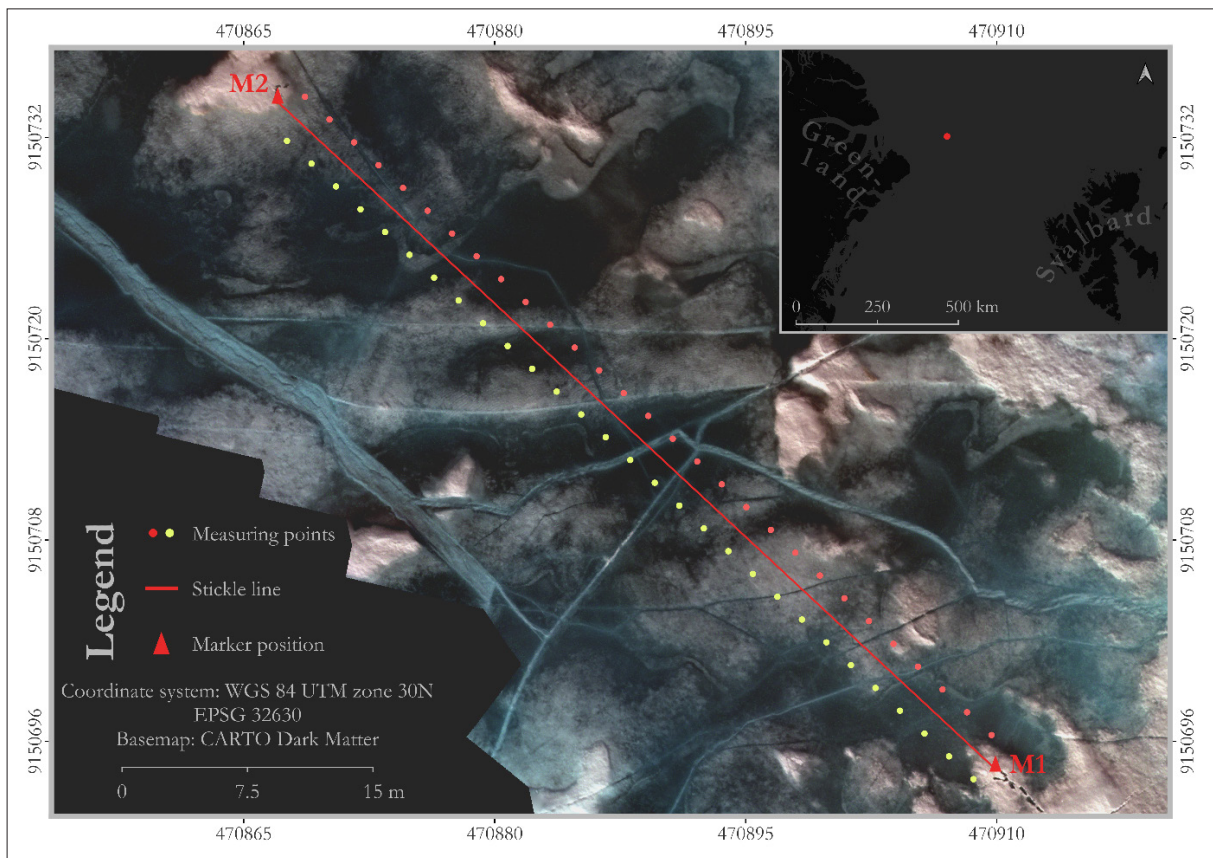


Fig. 11.8: Map of the Stickle transect through a melt pond system on 05 July 2023. The measuring points are not exactly on the line between the markers but offset by 1.33 meters (distance of the spectro-radiometer to the user, who is on the transect line) to the south west and north east.

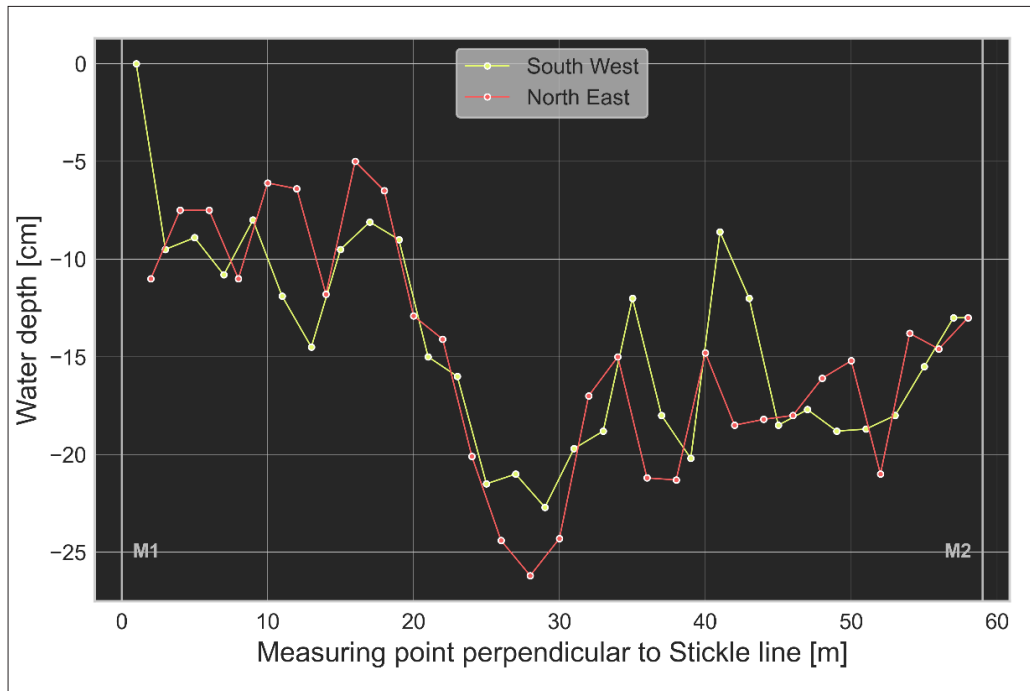


Fig. 11.9: Course of measured melt pond water depth on 05 July 2023 depending on the distance between the two markers M1 and M2

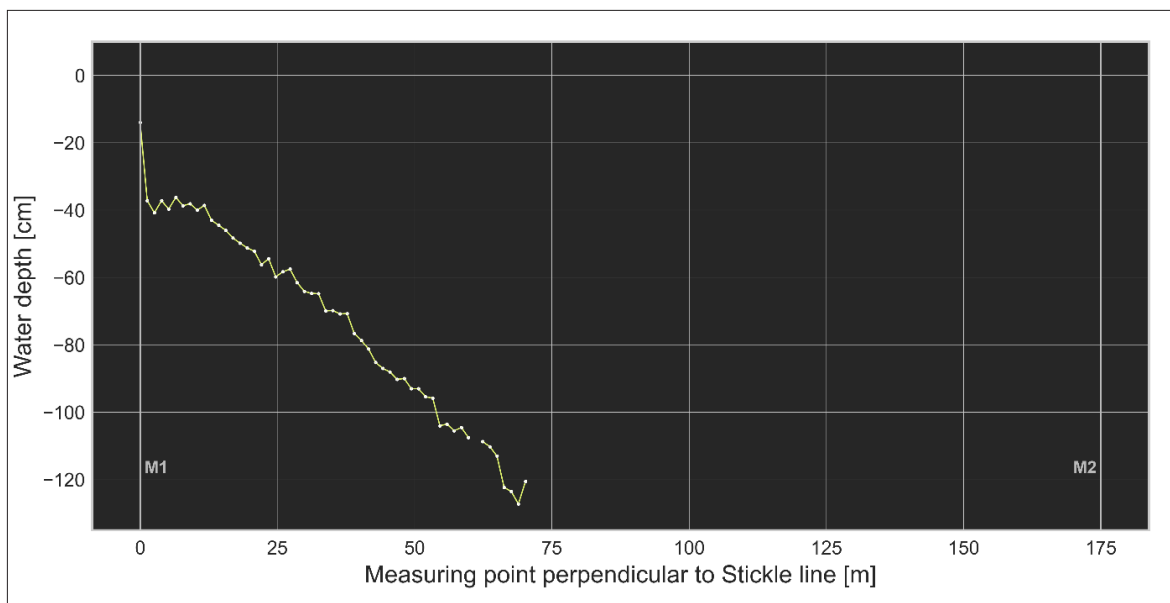
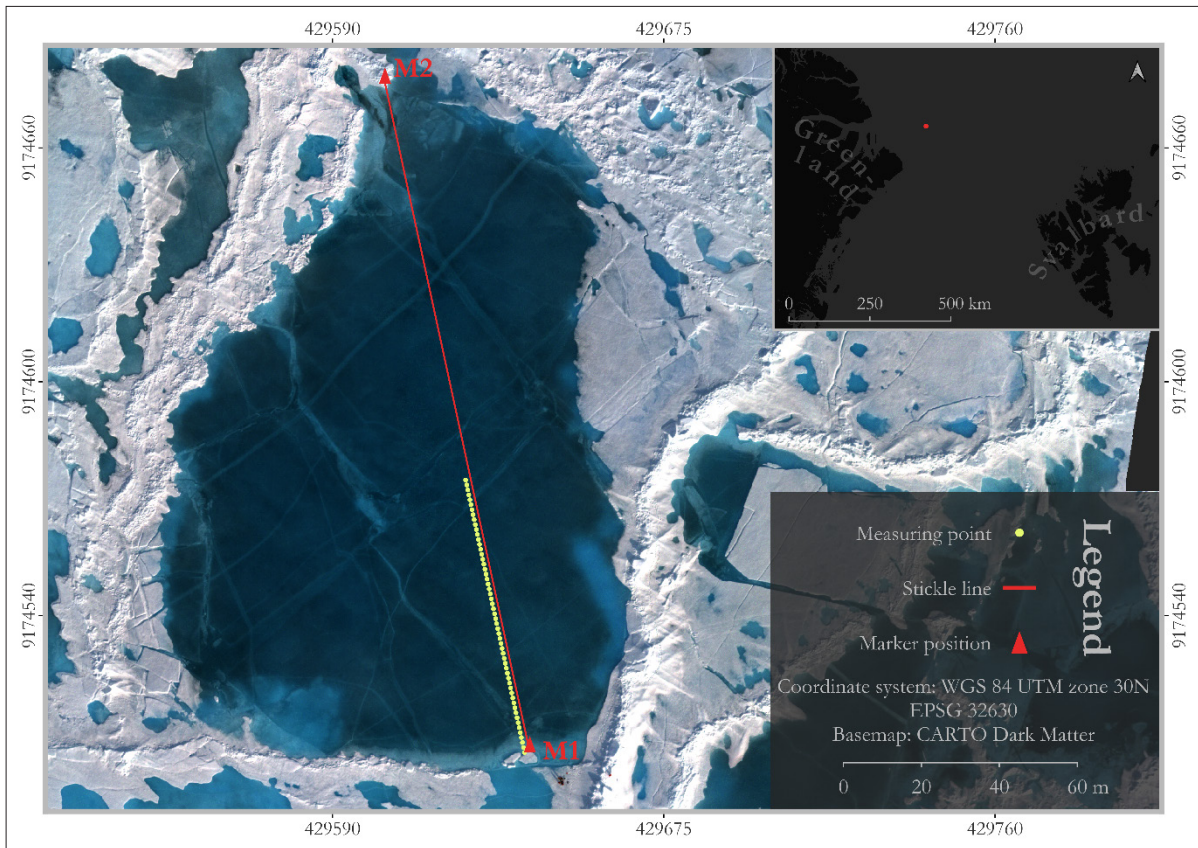


Fig. 11.10: Course of the measured melt pond water depth on 20 July 2023 depending on the distance between the two markers M1 and M2

It was also possible to take spectral measurements in water depths of more than one meter. On 20 July 2023 a 175 meter long *Stickle* transect was planned (see Fig. 11.11). During this transect, a maximum water depth of -127.2 centimeters was measured. The mean water depth was -72.64 centimeters. The pond became even deeper, so that the transect had to be abandoned after 73 meters as the *Stickle* was no longer operational for this great depth. This melt pond was the deepest examined during the cruise. Figure 11.10 shows the course of the measured water depths.



*Fig. 11.11: Map of the Stickle transect through a melt pond on 20 July 2023. The measuring points are not exactly on the line between the markers but offset by 1.33 meters (distance of the spectro-radiometer to the user, who is on the transect line)*

### Goniometer

The Goniometer measured the backscattered radiation of an underlying surface in a total of 48 different angular positions. The backscattering behavior can be visualized for a specific wavelength in the spectral range of the OceanOptics STS-VIS spectro-radiometers (337 nm and 823 nm) by a polar plot. Figure 11.12 shows the polar plot at 820 nm for an underlying snow/ice surface during clear sky conditions on 28 July 2023. The sun is located at azimuth angle  $180^\circ$  and a forward scattering can be detected. This is also visualized by plotting the spectra of two points at azimuth angle  $330^\circ$  – zenith angle  $60^\circ$  and azimuth angle  $150^\circ$  – zenith angle  $60^\circ$ , respectively (see Fig. 11.13). Over the spectrum, the point at azimuth angle  $330^\circ$  – zenith angle  $60^\circ$  has a fairly constant high measured values, whereas the spectrum of the other point flattens out with increasing wavelength starting in the blue wavelength range.

The other example in Figure 11.14 and Figure 11.15 shows an underlying snow/ice surface during overcast conditions. During that condition a diffuse backscattering can be expected. This can be confirmed by examining the measurements shown in Figure 11.14. The sun is located at azimuth angle  $180^\circ$ . Values of high backscattering are located at zenith angle  $60^\circ$  around the entire hemisphere with decreasing values in the direction of the zenith. A specific direction of backscattering as in the previous example cannot be detected. This phenomenon is also visualized by the spectra in Figure 11.15. Previously, a clear difference can be seen between the spectra of the two points. Now the spectra are similar in terms of shape and intensity of the scattering. Similarities to the lower spectrum of the Figure 11.13 are recognisable.

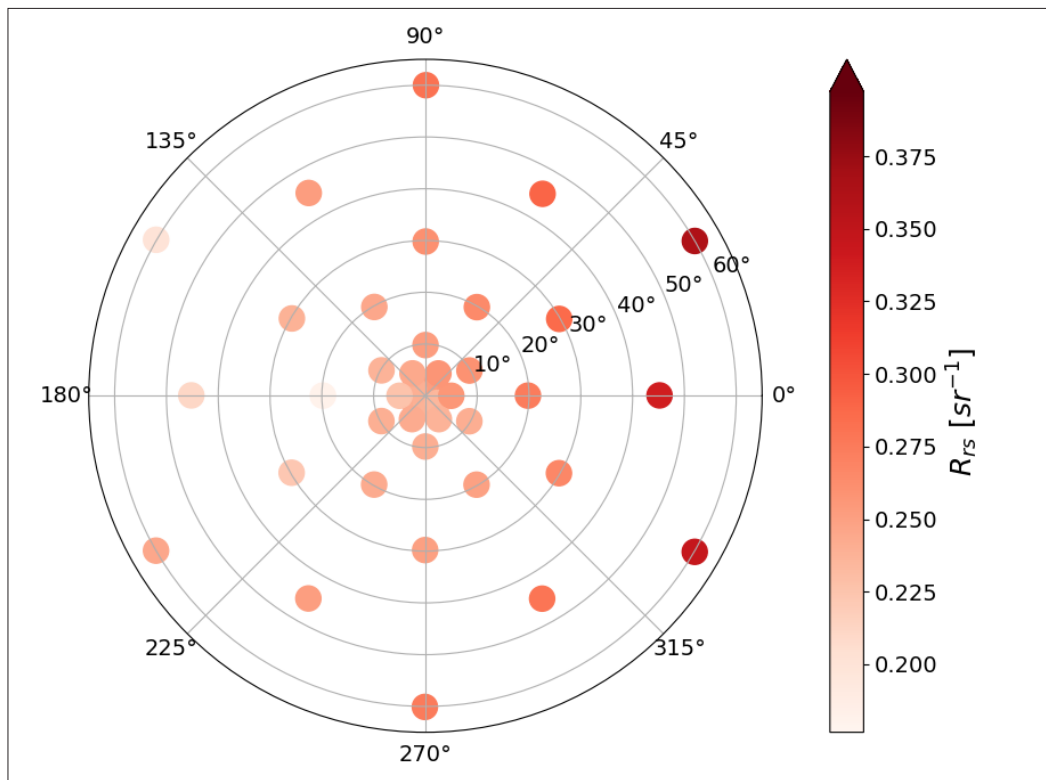


Fig. 11.12: Polar plot of an underlying snow/ice surface during clear sky conditions on 28 July 2023

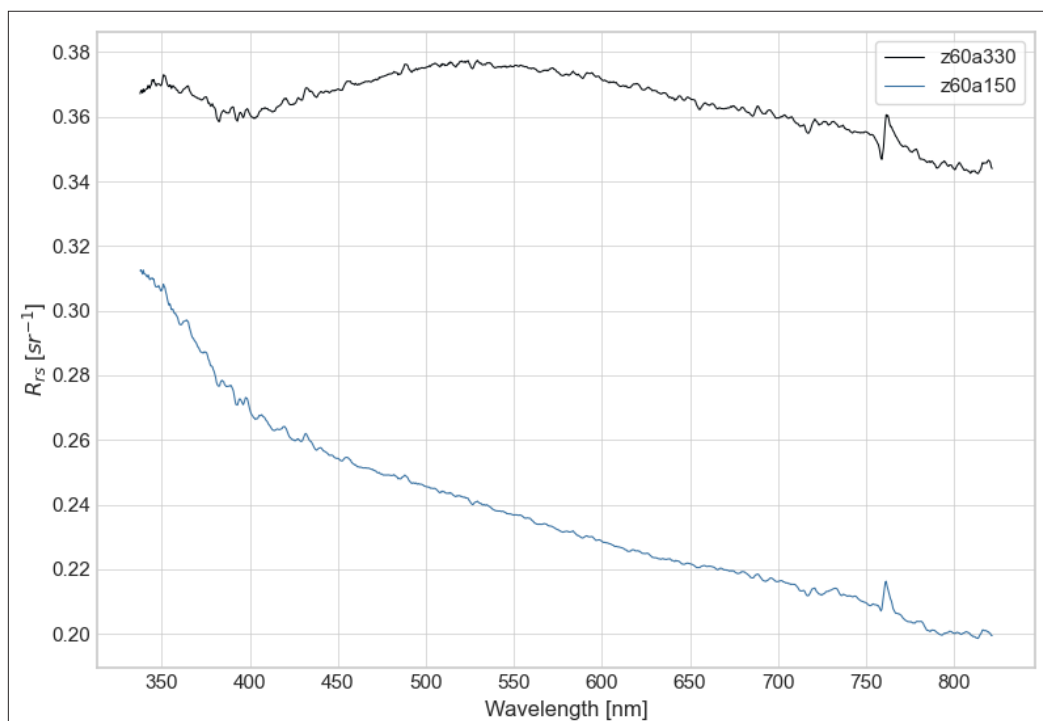


Fig. 11.13: Spectra of in Figure 11.12 marked angular positions. According to König & Oppelt 2020, the Goniometer spectra are smoothed with a running average filter with a width of 5 nm to minimize the amount of noise in the data.

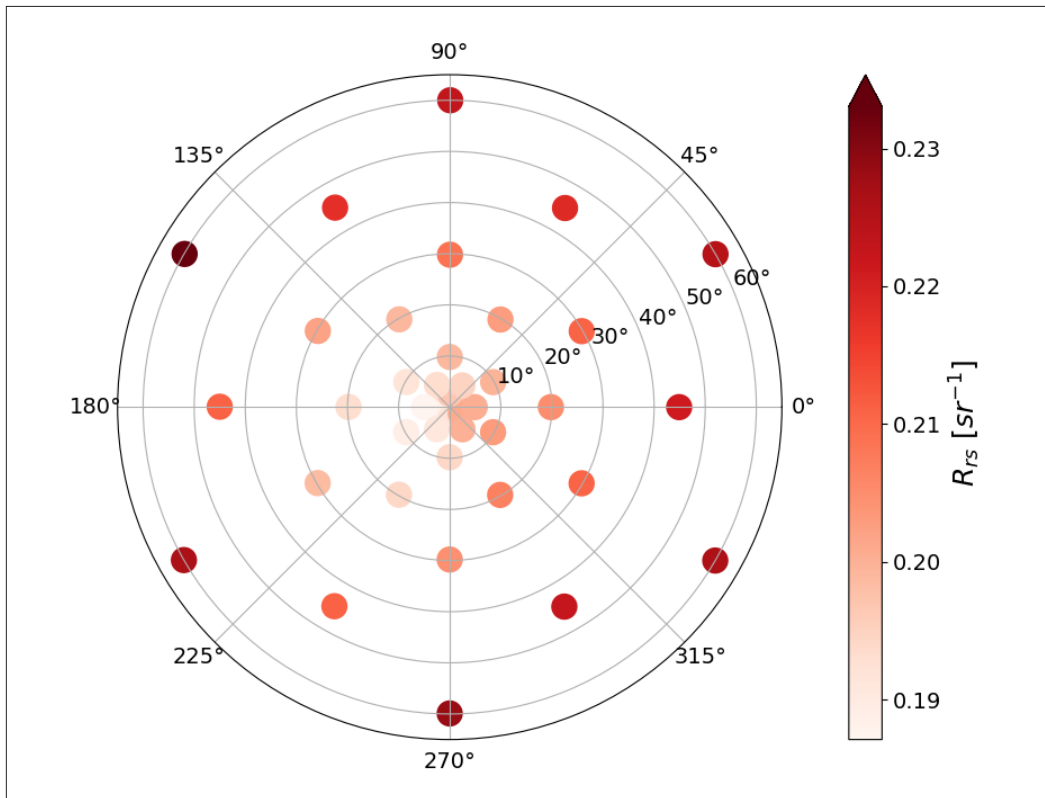


Fig.11.14: Polar plot of an underlying snow/ice surface during overcast conditions on 26 July 2023

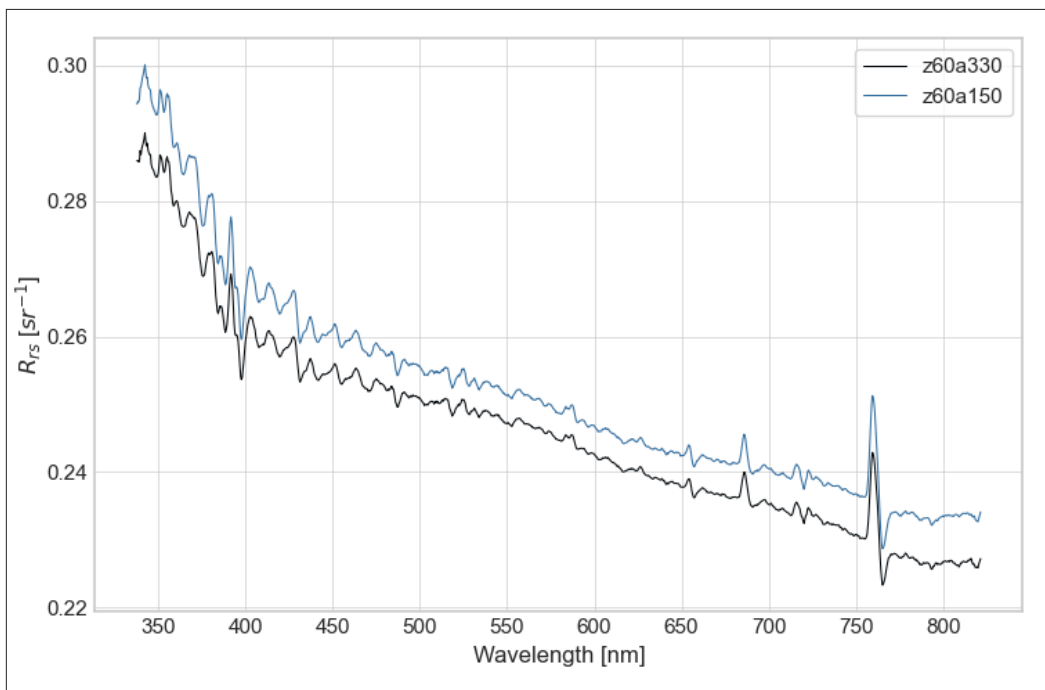


Fig.11.15: Spectra of in Figure 11.14 marked angular positions. According to König & Oppelt 2020, the Goniometer spectra are smoothed with a running average filter with a width of 5 nm to minimize the amount of noise in the data.

## Data management

Environmental data will be archived, published and disseminated according to international standards by the World Data Center PANGAEA Data Publisher for Earth & Environmental Science (<https://www.pangaea.de>) within two years after the end of the expedition at the latest. By default, the CC-BY license will be applied.

This expedition was supported by the Helmholtz Research Programme “Changing Earth – Sustaining our Future” Topic 2, Subtopic 2.1.

In all publications based on this expedition, the **Grant No. AWI\_PS137\_11** will be quoted and the following publication will be cited:

Alfred-Wegener-Institut Helmholtz-Zentrum für Polar- und Meeresforschung (2017) Polar Research and Supply Vessel POLARSTERN Operated by the Alfred-Wegener-Institute. Journal of large-scale research facilities, 3, A119. <http://dx.doi.org/10.17815/jlsrf-3-163>.

## References

- Fuchs N (2023) A multidimensional analysis of sea ice melt pond properties from aerial images. PhD Thesis, submitted to the University of Bremen, Germany.
- König M, Hieronymi M, and Oppelt N (2019) Application of Sentinel-2 MSI in Arctic Research: Evaluating the Performance of Atmospheric Correction Approaches Over Arctic Sea Ice. *Front. Earth Sci.* 7. <https://doi.org/10.3389/feart.2019.00022>
- König M, Birnbaum G, Oppelt N (2020) Mapping the Bathymetry of Melt Ponds on Arctic Sea Ice Using Hyperspectral Imagery Remote Sensing 12(16):2623. <https://doi.org/10.3390/rs12162623>.
- König M, Wagner M, and Oppelt N (2020) Ice floe tracking with Sentinel-2. *Proc. SPIE 11529, Remote Sensing of the Ocean, Sea Ice, Coastal Waters, and Large Water Regions 2020*, 1152908 (20 September 2020). <https://doi.org/10.1117/12.2573427>
- König M, Oppelt N (2020) A linear model to derive melt pond depth on arctic sea ice from hyperspectral data. *The Cryosphere* 14 (8): 2567-2579. <https://doi.org/10.5194/tc-14-2567-2020>
- Landy JC, Ehn JK & Barber DG (2015) Albedo feedback enhanced by smoother Arctic sea ice. *Geophys. Res. Lett.* 42:10714–10720. <https://doi.org/10.1002/2015GL066712>
- Malinka A, Zege E, Istomina L, Heygster G, Spreen G, Perovich D & Polashenski C (2018) Reflective properties of melt ponds on sea ice. *The Cryosphere* 12:1921–1937. <https://doi.org/10.5194/tc-12-1921-2018>
- Wang M, König M & Oppelt N (2021) Partial Shape Recognition for Sea Ice Motion Retrieval in the Marginal Ice Zone from Sentinel-1 and Sentinel-2. *Remote Sensing* 13(21). <https://doi.org/10.3390/rs13214473>

## **APPENDIX**

**A.1 TEILNEHMENDE INSTITUTE / PARTICIPATING INSTITUTES**

**A.2 FAHRTTEILNEHMER:INNEN / CRUISE PARTICIPANTS**

**A.3 SCHIFFSBESATZUNG / SHIP'S CREW**

**A.4. STATIONSLISTE / STATION LIST**

## A.1 TEILNEHMENDE INSTITUTE / PARTICIPATING INSTITUTES

Affiliation	Address
DE.AWI	Alfred-Wegener-Institut Helmholtz-Zentrum für Polar- und Meeresforschung Postfach 120161 27515 Bremerhaven Germany
DE.CAU	Christian-Albrechts-Universität zu Kiel Christian-Albrechts-Platz 4 24118 Kiel Germany
DE.DRF	DRF Luftrettung gAG Laval Avenue E312 77836 Rheinmünster Germany
DE.DRIFT NOISE	Stavendamm 17 28195 Bremen Germany
DE.DWD	Deutscher Wetterdienst Seewetteramt Bernhard Nocht Str. 76 20359 Hamburg Germany
DE.IUP	Institut für Umweltphysik Universität Bremen Otto-Hahn Allee 1 28359 Bremen Germany
DE.MARUM	MARUM – Center for Marine Environmental Sciences University of Bremen Leobener Str. 8 D-28359 Bremen Germany
DE.MPIMM	Max Planck Institute for Marine Microbiology Celsiusstraße 1 28359 Bremen Germany
DE.NHC	Northern Helicopter GmbH Gorch-Fock-Straße 103 26721 Emden Germany
DE.UNI Bremen	Universität Bremen Bibliothekstraße 1 28359 Bremen Germany

---

<b>Affiliation</b>	<b>Address</b>
DE.UNI Münster	Westfälische Wilhelms-Universität Münster Corrensstrasse 24 48149 Münster Germany
NO.UIB	University of Bergen P.O.Box 7800 5020 Bergen Norway
US.JPL	NASA Jet Propulsion Laboratory 4800 Oak Grove Drive Pasadena CA 91109 USA
US.UW	Applied Physics Laboratory University of Washington 1013 NE 40 <sup>th</sup> Street Seattle WA 98105 USA
US.WHOI	Woods Hole Oceanographic Institution Woods Hole Road Woods Hole MA 02543 USA
<b>Not on board</b>	
DE.UNI-Hamburg	Universität Hamburg Mittelweg 177 20148 Hamburg Germany

## A.2 FAHRTTEILNEHMER:INNEN / CRUISE PARTICIPANTS

<b>Name/ Last name</b>	<b>Vorname/ First name</b>	<b>Institut/ Institute</b>	<b>Beruf/ Profession</b>	<b>Fachrichtung/ Discipline</b>
Albers	Elmar	US.WHOI	Scientist	Geology
Böhringer	Lilian	DE.AWI	PhD candidate	Biology
Branch	Andrew	US.JPL	Engineer	Engineering Sciences
Bünger	Hans Jakob	DE.DRIFT NOISE	Scientist	Sea Ice Physics
Curran	Molly	US.WHOI	Engineer	Oceanography
Dalpe	Allisa	US.WHOI	Engineer	Oceanography
Dettling	Nicolas	DE.AWI	PhD candidate	Oceanography
Engicht	Carina	DE.AWI	Technician	Oceanography
Genske	Felix	DE.UNI-Münster	Scientist	Geology
German	Christopher	US.WHOI	Scientist	Geoscience
Gischler	Michael	DE.NHC	Pilot	Helikopter Service
Hecken	Timo	DE.DRF	Technician	Helikopter Service
Hellbrück	Annika	DE.AWI	Student	Geophysics
Höppner	Laura	DE.AWI	Student	Geophysics
Isler	Tea	DE.AWI	PhD candidate	Geophysics
Jakuba	Michael	US.WHOI	Engineer	Engineering Sciences
Kaul	Norbert	DE.UNI-Bremen	Scientist	Geophysics
Kirk	Henning	DE.AWI	Technician	Geophysics
Klaembt	Christopher	DE.MPIMM	Student	Geoscience
Klesh	Andrew	US.JPL	Scientist	Glaciology
Lensch	Norbert	DE.AWI	Technician	Geophysics
Lindzey	Laura	US.UW	Engineer	Engineering Sciences
Lion	Victor	DE.CAU	Student	Geoscience
Loer	Rosemary	US.WHOI	Student	Engineering Sciences
Mette	Jonathan	DE.UNI-Bremen	Student	Oceanography
Molari	Massimiliano	DE.MPIMM	Scientist	Biology
Naklicki	Victor	US.WHOI	Scientist	Engineering Sciences
Pilot	Matthias	DE.AWI	PhD candidate	Geophysics
Plötz	Hannah	DE.AWI	Student	Geophysics
Reifenberg	Simon	DE.AWI	PhD candidate	Oceanography
Ritter	Josefa Lotte	DE.CAU	Student	Geophysics
Rohleder	Christian	DE.DWD	Technician	Meteorology
Schaubensteiner	Stefan	DE.NHC	Pilot	Helikopter Service
Schlindwein	Vera	DE.AWI	Scientist	Geophysics
Schmidt-Aursch	Mechita	DE.AWI	Scientist	Geophysics

---

<b>Name/ Last name</b>	<b>Vorname/ First name</b>	<b>Institut/ Institute</b>	<b>Beruf/ Profession</b>	<b>Fachrichtung/ Discipline</b>
Seewald	Jeffrey	US.WHOI	Scientist	Oceanography
Seifert	Michael	DE.DRF	Technician	Helikopter Service
Silvia	Matthew	US.WHOI	Engineer	Engineering Sciences
Suter	Patrick	DE.DWD	Scientist	Meteorology
Thamm	Viktoria	DE.AWI	Student	Geophysics
Tobisch	Chiara	DE.AWI	Student	Geophysics
Unland	Ellen	DE.AWI	Student	Geophysics
Walter	Maren	DE.UNI-Bremen	Scientist	Oceanography
Warnke	Fynn	DE.AWI	Scientist	Geophysics
Wegener	Gunter	DE.UNI-Bremen	Scientist	Biology
Zhu	Qing Zeng	DE.UNI-Bremen	Scientist	Geoscience

### A.3 SCHIFFSBESATZUNG / SHIP'S CREW

No.	Name / Last Name	Vorname / First Name	Position / Rank
1	Langhinrichs	Moritz	Master
2	Langhinrichs	Jacob	Chiefmate
3	Eckenfels	Hannes	Chiefmate Cargo
4	Rusch	Torben	Chief
5	Weiß	Daniel	2nd Mate
6	Peine	Lutz	2nd Mate
7	Dr. Guba	Klaus	Ships Doc
8	Pliet	Johannes Oliver	ELO
9	Ehrke	Tom	2nd. Eng
10	Westphal	Henning	2nd. Eng
11	Farysch	Tim	2nd. Eng
12	Pommerencke	Bernd	SET
13	Frank	Gerhard	ELO
14	Schwedka	Thorsten	ELO
15	Winter	Andreas	ELO
16	Krüger	Lars	ELO
17	Brück	Sebastian	Bosun
18	Keller	Euge Jürgen	Carpen.
19	Möller	Falko	MP Rat.
20	Buchholz	Joscha	MP Rat.
21	Schade	Tom	MP Rat.
22	Decker	Jens	MP Rat.
23	Niebuhr	Tim	MP Rat.
24	Lutz	Johannes	MP Rat.
25	Luckhardt	Arne	MP Rat.
26	Jassmann	Marvin	MP Rat.
27	Probst	Lorenz	MP Rat.
28	Clasen	Nils	MP Rat.
29	Deutschbein	Felix Maximilian	MP Rat.
30	Schröder	Paul	MP Rat.
31	Fink	Anna-Maria	MP Rat.
32	Preußner	Jörg	Storek.
33	Schnieder	Sven	Cook

No.	Name / Last Name	Vorname / First Name	Position / Rank
34	Bogner	Christoph Friedemann	Cooksm.
35	Lang	Gerd Martin	Cooksm.
36	Witusch	Petra	Chief Stew.
37	Ilk	Romy	2nd Stew
38	Fehrenbach	Martina	2nd Stew
39	Golla	Gerald	2nd Stew
40	Winkler	Maria	2nd Stew
41	Shi	Wubo	2nd Stew
42	Chen	Quanlun	Laundrym
43	Chen	Jirong	2nd Stew

## A.4 STATIONSLISTE / STATION LIST PS137

Station list of expedition PS137 from Tromsø – Tromsø; the list details the action log for all stations along the cruise track.

See <https://www.pangaea.de/expeditions/events/PS137> to display the station (event) list for expedition PS137. This version contains Uniform Resource Identifiers for all sensors listed under <https://sensor.awi.de>. See <https://www.awi.de/en/about-us/service/computing-centre/data-flow-framework.html> for further information about AWI's data flow framework from sensor observations to

Event label	Optional label	Date/Time	Latitude	Longitude	Depth [m]	Gear	Action	Comment
PS137-track		2023-06-21T00:00:00	69.67800	18.98980		CT	Station start	Tromsø – Tromsø
PS137-track		2023-07-31T00:00:00	69.67800	18.98980		CT	Station end	Tromsø – Tromsø
PS137_0_Underway-3		2023-06-22T05:45:20	71.23431	19.50154	203	ADCP	Station start	
PS137_0_Underway-3		2023-07-30T14:04:34	71.58713	18.89144	255	ADCP	Station end	
PS137_0_Underway-7		2023-06-22T05:51:40	71.25220	19.48630	206	AUTOFIM	Station start	
PS137_0_Underway-7		2023-07-30T14:10:29	71.57182	18.90994		AUTOFIM	Station end	
PS137_0_Underway-11		2023-06-22T05:42:00	71.22488	19.50926	207	MYON	Station start	
PS137_0_Underway-11		2023-07-30T14:11:44	71.56854	18.91382		MYON	Station end	
PS137_0_Underway-13		2023-06-22T05:51:00	71.25032	19.48791	207	FBOX	Station start	
PS137_0_Underway-13		2023-07-30T14:09:50	71.57352	18.90802		FBOX	Station end	
PS137_0_Underway-20		2023-06-24T12:04:59	78.21453	9.46052	328	ICERAD	Station start	
PS137_0_Underway-20		2023-07-28T08:39:50	78.73985	5.09223	2344	ICERAD	Station end	
PS137_0_Underway-23		2023-06-22T05:48:45	71.24396	19.49333	208	MAG	Station start	
PS137_0_Underway-23		2023-07-30T14:09:16	71.57499	18.90631		MAG	Station end	
PS137_0_Underway-24		2023-06-22T05:49:00	71.24466	19.49273	207	GRAV	Station start	
PS137_0_Underway-24		2023-07-30T14:08:42	71.57645	18.90450	257	GRAV	Station end	
PS137_0_Underway-31		2023-06-22T05:40:00	71.21928	19.51410	203	NEUMON	Station start	
PS137_0_Underway-31		2023-07-30T14:12:06	71.56760	18.91497		NEUMON	Station end	

\* Comments are limited to 130 characters. See <https://www.pangaea.de/expeditions/events/PS137> to show full comments in conjunction with the station (event) list for expedition PS137

Event label	Optional label	Date/Time	Latitude	Longitude	Depth [m]	Gear	Action	Comment
PS137_0_Underway-34		2023-06-22T05:48:30	71.24325	19.49394	208	pCO2	Station start	
PS137_0_Underway-34		2023-07-30T14:07:01	71.58078	18.89916	257	pCO2	Station end	
PS137_0_Underway-35		2023-06-22T05:45:55	71.23595	19.50019	205	pCO2	Station start	
PS137_0_Underway-35		2023-07-30T14:07:48	71.57876	18.90161	257	pCO2	Station end	
PS137_0_Underway-39		2023-06-22T11:43:00	72.26188	18.58624	356	PS	Station start	
PS137_0_Underway-39		2023-07-30T14:00:10	71.59861	18.87795	253	PS	Station end	
PS137_0_Underway-43	TSK1	2023-06-22T05:45:30	71.23477	19.50116	204	TSG	Station start	
PS137_0_Underway-43	TSK1	2023-07-30T14:06:32	71.58204	18.89770	257	TSG	Station end	
PS137_0_Underway-44	TSK2	2023-06-22T05:45:00	71.23336	19.50231	204	TSG	Station start	
PS137_0_Underway-44	TSK2	2023-07-30T14:05:22	71.58507	18.89406	256	TSG	Station end	
PS137_0_Underway-53		2023-06-21T18:00:00	69.74731	19.14246		SWEAS	Station start	
PS137_0_Underway-53		2023-07-31T06:33:34	69.74741	19.14230		SWEAS	Station end	
PS137_0_Underway-54		2023-06-22T07:55:15	71.60569	19.18304	234	DS3	Station start	
PS137_0_Underway-54		2023-07-30T14:00:30	71.59774	18.87898	252	DS3	Station end	
PS137_0_Underway-55	Pacific Gyre Universal Tracker 2023P281	2023-07-01T09:00:00	82.64305	-5.86920	4552	ISVP	Station start	
PS137_0_Underway-55	Pacific Gyre Universal Tracker 2023P281	2023-07-13T10:20:15	82.90231	-6.24183	3899	ISVP	Station end	
PS137_0_Underway-56	Pacific Gyre Universal Tracker 2023P282	2023-07-01T10:00:00	82.64201	-5.83514	4507	ISVP	Station start	

Event label	Optional label	Date/Time	Latitude	Longitude	Depth [m]	Gear	Action	Comment
PS137_0_Underway-56	Pacific Gyre Universal Tracker 2023P282	2023-07-13T10:10:15	82.90269	-6.23919	3908	ISVP	Station end	
PS137_0_Underway-57	Pacific Gyre Universal Tracker 2023P283	2023-07-09T16:00:00	82.94303	-6.45509	4144	ISVP	Station start	
PS137_0_Underway-57	Pacific Gyre Universal Tracker 2023P283	2023-07-13T10:40:05	82.90055	-6.24669	3897	ISVP	Station end	
PS137_0_Underway-58	Pacific Gyre Universal Tracker 2023P281	2023-07-14T09:00:00	83.02938	-4.89389	1912	ISVP	Station start	
PS137_0_Underway-58	Pacific Gyre Universal Tracker 2023P281	2023-07-30T11:41:01	71.95604	18.44139	301	ISVP	Station end	
PS137_0_Underway-59	Pacific Gyre Universal Tracker 2023P282	2023-07-20T12:00:00	83.03306	-6.64927	3722	ISVP	Station start	

Event label	Optional label	Date/Time	Latitude	Longitude	Depth [m]	Gear	Action	Comment
PS137_0_Underway-59	Pacific Gyre Universal Tracker 2023P282	2023-07-30T11:40:29	71.95738	18.43970	303	ISVP	Station end	
PS137_1-1		2023-06-24T14:39:19	78.31612	8.10934	2329	CTD-RO	max depth	
PS137_1-2		2023-06-24T16:01:01	78.31660	8.10728	2364	DS3	Station start	
PS137_1-2		2023-06-24T19:40:00	78.41581	8.34722	1881	DS3	Station end	
PS137_2-1	Y1-1	2023-06-25T09:57:45	80.40010	10.06070	689	MOOR	Station start	recovery
PS137_2-1	Y1-1	2023-06-25T11:50:36	80.39524	10.10188	711	MOOR	Station end	recovery
PS137_3-1	Y2-1	2023-06-25T12:06:13	80.41563	10.12004	708	MOOR	Station start	recovery of lower part cancelled due to ice situation
PS137_3-1	Y2-1	2023-06-25T15:31:38	80.41662	10.05246	691	MOOR	Station end	recovery of lower part cancelled due to ice situation
PS137_4-1		2023-06-25T17:13:35	80.42267	10.17739	726	CTD-RO	max depth	
PS137_5-1		2023-06-25T18:57:44	80.46142	10.09258	713	ICE	Station start	
PS137_5-1		2023-06-25T21:09:54	80.47120	10.21876	742	ICE	Station end	
PS137_6-1		2023-06-26T09:25:06	80.96016	8.64656	778	CTD-RO	max depth	
PS137_7-1	Y4-1	2023-06-26T11:04:10	80.96682	8.70302	794	MOOR	Station start	recovery
PS137_7-1	Y4-1	2023-06-26T12:42:29	80.96430	8.71681	792	MOOR	Station end	recovery
PS137_8-1	Y3-1	2023-06-26T13:20:04	80.95189	8.71769	769	MOOR	Station start	recovery
PS137_8-1	Y3-1	2023-06-26T15:58:55	80.94665	8.73739	758	MOOR	Station end	recovery
PS137_9-1		2023-06-26T16:40:07	80.93933	8.74187	754	ICE	Station start	
PS137_9-1		2023-06-26T18:51:20	80.94048	8.73299	754	ICE	Station end	
PS137_10-1		2023-06-27T08:42:52	81.50245	7.09974	489	CTD-RO	max depth	
PS137_11-1	Y5-1	2023-06-27T12:00:00	81.50196	7.14954	482	MOOR	Station start	recovery
PS137_11-1	Y5-1	2023-06-27T13:33:48	81.49913	7.12672	479	MOOR	Station end	recovery
PS137_12-1		2023-06-28T04:57:11	81.31283	3.12662	806	CTD-RO	max depth	

Event label	Optional label	Date/Time	Latitude	Longitude	Depth [m]	Gear	Action	Comment
PS137_13-1	UIB_Mooring_Y7	2023-06-28T13:58:26	81.34884	1.07020	1539	MOOR	Station start	recovery
PS137_13-1	UIB_Mooring_Y7	2023-06-28T17:09:04	81.35494	1.10453	1498	MOOR	Station end	recovery
PS137_14-1		2023-06-28T18:32:02	81.36297	1.06694	1507	CTD-RO	max depth	
PS137_15-1		2023-06-29T08:51:09	81.86884	-0.45845	1930	NUI	Station start	
PS137_15-1		2023-06-29T14:22:55	81.86104	-0.45720	2753	NUI	Station end	
PS137_16-1		2023-06-30T09:58:48	82.51791	-5.53964	4514	DRG	Station start	
PS137_16-1		2023-06-30T18:50:08	82.48078	-5.55007	4522	DRG	Station end	
PS137_17-1		2023-06-30T18:52:36	82.48056	-5.54732	4507	OBS	Station start	
PS137_17-1		2023-06-30T21:09:39	82.47070	-5.44590	3886	OBS	Station end	
PS137_18-1		2023-07-01T01:50:10	82.60966	-5.88640	4544	CTD-RO	max depth	
PS137_19-1		2023-07-01T05:32:41	82.61464	-5.73483	4230	OBS	Station start	
PS137_19-1		2023-07-01T07:20:45	82.61287	-5.65684	4019	OBS	Station end	
PS137_20-1		2023-07-01T08:33:12	82.64354	-5.88550	4557	HF	Station start	
PS137_20-1		2023-07-01T15:49:59	82.63952	-5.62101	3890	HF	Station end	
PS137_21-1	AURORA1	2023-07-02T22:51:44	82.89800	-6.24955		MOOR	Station start	recovery
PS137_21-1	AURORA1	2023-07-03T01:45:58	82.89908	-6.23321	3897	MOOR	Station end	recovery
PS137_22-1		2023-07-03T03:56:32	82.89759	-6.23351	3912	CTD-RO	max depth	
PS137_23-1		2023-07-03T12:00:27	82.90896	-6.25270	4049	NUI	Station start	
PS137_23-1		2023-07-03T17:04:08	82.90596	-6.21461	3965	NUI	Station end	
PS137_24-1		2023-07-03T17:45:31	82.90332	-6.25297	3953	INSIPU	Station start	
PS137_24-1		2023-07-03T20:15:52	82.89692	-6.24438	3929	INSIPU	Station end	
PS137_25-1		2023-07-04T19:38:07	82.94910	-5.92880	4400	OBS	Station start	
PS137_25-1		2023-07-04T21:08:36	82.94699	-5.95145	4396	OBS	Station end	
PS137_26-1		2023-07-05T05:21:22	82.89249	-6.20160	4075	CTD-RO	max depth	
PS137_27-1		2023-07-05T14:18:45	82.91033	-6.20164	3987	OBS	Station start	

Event label	Optional label	Date/Time	Latitude	Longitude	Depth [m]	Gear	Action	Comment
PS137_27-1		2023-07-05T14:51:19	82.91049	-6.19745	3986	OBS	Station end	
PS137_28-1		2023-07-05T22:10:52	82.90699	-6.41576	4186	CTD-yoyo	Station start	
PS137_28-1		2023-07-06T03:30:42	82.90284	-6.38053	4160	CTD-yoyo	Station end	
PS137_29-1		2023-07-06T14:25:05	82.87218	-5.78236	3903	OBS	Station start	
PS137_29-1		2023-07-06T16:14:36	82.87232	-5.74854	3905	OBS	Station end	
PS137_30-1		2023-07-06T16:48:56	82.87249	-5.74985	3904	HF	Station start	
PS137_30-1		2023-07-06T23:25:33	82.87384	-5.68508	3808	HF	Station end	
PS137_31-1		2023-07-07T11:42:45	82.88919	-6.43698	4237	OBS	Station start	
PS137_31-1		2023-07-07T15:49:41	82.88433	-6.27982	4188	OBS	Station end	
PS137_32-1		2023-07-07T20:15:00	82.89738	-6.46816	4210	NUI	Station start	
PS137_32-1		2023-07-08T07:43:45	82.92000	-6.07775	4009	NUI	Station end	
PS137_33-1		2023-07-08T15:30:33	82.90552	-6.32411	4096	CTD-RO	max depth	
PS137_34-1		2023-07-09T01:42:37	82.84412	-6.66834	4395	OBS	Station start	
PS137_34-1		2023-07-09T09:40:57	82.79198	-6.59712	4574	OBS	Station end	
PS137_35-1		2023-07-09T20:00:30	82.93176	-6.36381	4199	OBS	Station start	
PS137_35-1		2023-07-10T04:20:12	82.88613	-6.34177	4177	OBS	Station end	
PS137_36-1		2023-07-10T10:18:58	82.90451	-6.28740	4046	CTD-yoyo	Station start	
PS137_36-1		2023-07-10T12:42:44	82.89278	-6.27255	4035	CTD-yoyo	Station end	
PS137_37-1		2023-07-10T19:38:47	82.90761	-6.36778	4117	NUI	Station start	
PS137_37-1		2023-07-11T06:39:42	82.86948	-6.31798	4338	NUI	Station end	
PS137_38-1	AUR005	2023-07-12T01:32:49	82.91986	-6.72413	3930	OBS	Station start	recovery
PS137_38-1	AUR005	2023-07-12T03:26:53	82.91281	-6.73785	3853	OBS	Station end	recovery
PS137_39-1		2023-07-12T05:58:50	82.87578	-7.57217	2823	OFOBS	max depth	
PS137_40-1		2023-07-12T18:13:45	82.90540	-6.29767	4071	CTD-RO	max depth	
PS137_41-1		2023-07-13T12:22:35	82.89631	-6.24263	3943	CTD-RO	max depth	
PS137_42-1		2023-07-13T20:42:06	82.97558	-5.02921	1665	OFOBS	max depth	
PS137_43-1		2023-07-15T09:47:57	83.81314	-6.00091	3076	HF	Station start	

Event label	Optional label	Date/Time	Latitude	Longitude	Depth [m]	Gear	Action	Comment
PS137_43-1		2023-07-15T15:02:54	83.79770	-5.97299	3174	HF	Station end	
PS137_44-1		2023-07-15T19:02:40	83.76278	-5.44084	2964	HF	Station start	
PS137_44-1		2023-07-15T23:52:18	83.74116	-5.42665	2778	HF	Station end	
PS137_45-1		2023-07-16T02:37:10	83.72490	-4.86479	2402	HF	Station start	
PS137_45-1		2023-07-16T07:11:50	83.70234	-4.86720	2180	HF	Station end	
PS137_46-1		2023-07-16T13:34:30	83.68184	-3.57587	4090	HF	Station start	
PS137_46-1		2023-07-16T18:37:08	83.67377	-3.71622	3974	HF	Station end	
PS137_47-1		2023-07-18T02:40:05	83.84610	-3.47198	2464	OFOBS	max depth	technical problem; station aborted due to technical problem
PS137_48-1		2023-07-18T05:50:10	83.83712	-3.44443	2798	HF	Station start	
PS137_48-1		2023-07-18T12:07:44	83.81065	-3.43308	3062	HF	Station end	
PS137_49-1		2023-07-18T13:19:22	83.80618	-3.41344	3099	CTD-RO	max depth	
PS137_50-1		2023-07-20T19:55:43	82.90113	-6.37345	4157	NUI	Station start	
PS137_50-1		2023-07-21T07:39:11	82.89752	-6.16080	4016	NUI	Station end	
PS137_51-1	AUR006	2023-07-21T14:43:08	82.96755	-6.46657	4229	OBS	Station start	recovery
PS137_51-1	AUR006	2023-07-21T16:56:06	82.96977	-6.44890	4241	OBS	Station end	recovery
PS137_52-1		2023-07-21T21:09:19	82.89811	-6.39847	4207	CTD-RO	max depth	
PS137_53-1		2023-07-22T05:43:04	82.89815	-6.29327	3992	CTD-RO	max depth	
PS137_54-1		2023-07-22T12:36:53	82.89073	-6.24919	4035	CTD-RO	max depth	
PS137_55-1		2023-07-22T16:56:13	82.89863	-6.24231	3859	CTD-RO	max depth	
PS137_56-1		2023-07-22T19:27:30	82.86065	-6.56012	4374	HF	Station start	
PS137_56-1		2023-07-23T09:55:20	82.83834	-6.29440	4828	HF	Station end	
PS137_57-1		2023-07-24T21:43:19	81.41572	-3.44845	2995	NUI	Station start	
PS137_57-1		2023-07-25T11:11:09	81.34216	-3.53984		NUI	Station end	
PS137_58-1		2023-07-25T16:48:37	81.36924	-3.39574	3265	CTD-RO	Station start	Yoyo-CTD
PS137_58-1		2023-07-25T19:14:53	81.35868	-3.40118	3238	CTD-RO	Station end	Yoyo-CTD
PS137_59-1		2023-07-25T22:26:08	81.37610	-3.08431	2435	OFOBS	max depth	
PS137_60-1		2023-07-26T06:30:19	81.38005	-3.41709	3301	DRG	Station start	
PS137_60-1		2023-07-26T10:05:12	81.36529	-3.35849	3098	DRG	Station end	

Event label	Optional label	Date/Time	Latitude	Longitude	Depth [m]	Gear	Action	Comment
PS137_61-1		2023-07-26T11:52:37	81.38658	-3.42014	3155	CTD-RO	max depth	Yoyo-CTD
PS137_62-1		2023-07-26T16:35:00	81.38159	-3.41156	3253	OFOBS	max depth	
PS137_63-1		2023-07-28T16:00:15	77.55215	7.54070	3478	OBS	Station start	JOT01
PS137_63-1		2023-07-28T16:05:35	77.54989	7.54416	3476	OBS	Station end	JOT01
PS137_64-1		2023-07-28T16:50:33	77.50426	7.85046	3057	OBS	Station start	JOT02
PS137_64-1		2023-07-28T16:54:09	77.50346	7.84971	3064	OBS	Station end	JOT02
PS137_65-1		2023-07-28T17:35:27	77.43036	8.05873	2312	OBS	Station start	JOT03
PS137_65-1		2023-07-28T17:37:38	77.43012	8.05897	2313	OBS	Station end	JOT03
PS137_66-1		2023-07-28T18:04:48	77.37196	7.87745	2612	OBS	Station start	JOT04
PS137_66-1		2023-07-28T18:16:52	77.36039	7.84128	2663	OBS	Station end	JOT04
PS137_67-1		2023-07-28T18:52:46	77.38814	7.56247	3622	OBS	Station start	JOT05
PS137_67-1		2023-07-28T18:55:19	77.38746	7.56115	3620	OBS	Station end	JOT05
PS137_68-1		2023-07-28T19:40:36	77.47207	7.20769	2740	OBS	Station start	JOT06
PS137_68-1		2023-07-28T19:51:48	77.47249	7.16941	2758	OBS	Station end	JOT06
PS137_69-1		2023-07-28T20:23:24	77.39046	7.00368	2683	OBS	Station start	JOT07
PS137_69-1		2023-07-28T20:33:09	77.38311	6.98855	2661	OBS	Station end	JOT07

\* Comments are limited to 130 characters. See <https://www.pangaea.de/expeditions/events/PS137> to show full comments in conjunction with the station (event) list for expedition PS137

<b>Abbreviation</b>	<b>Method/Device</b>
ADCP	Acoustic Doppler Current Profiler
AUTOFIM	Automated Filtration for Marine Microbes
CT	Underway cruise track measurements
CTD-RO	CTD/Rosette
CTD-yoyo	Yoyo-CTD
DRG	Dredge
DS3	Swath-mapping system Atlas Hydrosweep DS-3
FBOX	FerryBox
GRAV	Gravimetry
HF	Heat-Flow probe
ICE	Ice station
ICERAD	Ice radar
INSIPU	<i>In-situ</i> pump
ISVP	Surface velocity profiler
MAG	Magnetometer
MOOR	Mooring
MYON	DESY Myon Detector
NEUMON	Neutron monitor
NUI	Hybrid ROV/AUV Nereid Under Ice
OBS	Ocean bottom seismometer
OFOBS	Ocean Floor Observation and Bathymetry System
PS	ParaSound
SWEAS	Ship Weather Station
TSG	Thermosalinograph
pCO2	pCO2 sensor

Die **Berichte zur Polar- und Meeresforschung** (ISSN 1866-3192) werden beginnend mit dem Band 569 (2008) als Open-Access-Publikation herausgegeben. Ein Verzeichnis aller Bände einschließlich der Druckausgaben (ISSN 1618-3193, Band 377-568, von 2000 bis 2008) sowie der früheren **Berichte zur Polarforschung** (ISSN 0176-5027, Band 1–376, von 1981 bis 2000) befindet sich im electronic Publication Information Center (**ePIC**) des Alfred-Wegener-Instituts, Helmholtz-Zentrum für Polar- und Meeresforschung (AWI); see <https://epic.awi.de>. Durch Auswahl "Reports on Polar- and Marine Research" (via "browse"/"type") wird eine Liste der Publikationen, sortiert nach Bandnummer, innerhalb der absteigenden chronologischen Reihenfolge der Jahrgänge mit Verweis auf das jeweilige pdf-Symbol zum Herunterladen angezeigt.

The **Reports on Polar and Marine Research** (ISSN 1866-3192) are available as open access publications since 2008. A table of all volumes including the printed issues (ISSN 1618-3193, Vol. 377-568, from 2000 until 2008), as well as the earlier **Reports on Polar Research** (ISSN 0176-5027, Vol. 1–376, from 1981 until 2000) is provided by the electronic Publication Information Center (**ePIC**) of the Alfred Wegener Institute, Helmholtz Centre for Polar and Marine Research (AWI); see URL <https://epic.awi.de>. To generate a list of all Reports, use the URL <http://epic.awi.de> and select "browse"/"type" to browse "Reports on Polar and Marine Research". A chronological list in declining order will be presented, and pdf-icons displayed for downloading.

#### **Zuletzt erschienene Ausgaben:**

**781 (2023)** The Expedition PS137 of the Research Vessel POLARSTERN to the Arctic Ocean in 2023 edited by Vera Schlindwein with contributions of the participants

**780 (2023)** The Expedition PS136 of the Research Vessel POLARSTERN to the Fram Strait in 2023, edited by Thomas Soltwedel with contributions of the participants

**779 (2023)** The Expedition PS135/1 and PS135/2 of the Research Vessel POLARSTERN to the Atlantic Ocean in 2023, edited by Yvonne Schulze Tenberge and Björn Fiedler with contributions of the participants

**778 (2023)** The MOSES Sternfahrt Expeditions of the Research Vessels ALBIS, LITTORINA, LUDWIG PRANDTL, MYA II and UTHÖRN to the Elbe River, Elbe Estuary and German Bight in 2022, edited by Ingeborg Bussmann, Norbert Anselm, Holger Brix, Norbert Kamjunke, Matthias Koschorreck, Björn Raupers, Tina Sanders with contributions of the participants

**777 (2023)** The Expedition PS134 of the Research Vessel POLARSTERN to the Bellingshausen Sea in 2022/2023, edited by Karsten Gohl with contributions of the participants

**776 (2023)** The Expedition PS129 of the Research Vessel POLARSTERN to the Weddell Sea in 2022, edited by Mario Hoppema with contributions of the participants

**775 (2023)** The Expedition PS133/2 of the Research Vessel POLARSTERN to the Scotia Sea in 2022, edited by Sabine Kasten with contributions of the participants

**774 (2023)** The Expedition PS133/1 of the Research Vessel POLARSTERN to the Atlantic Ocean in 2022, edited by Christine Klaas with contributions of the participants

**773 (2023)** A computational approach of locomotion, energy demand and dispersal of the common comatulid crinoid *Promachocrinus kerguelensis* (Echinodermata) and its circum-Antarctic success, by Nils Owsianowski

#### **Recently published issues:**



**ALFRED-WEGENER-INSTITUT**  
HELMHOLTZ-ZENTRUM FÜR POLAR-  
UND MEERESFORSCHUNG

**BREMERHAVEN**

Am Handelshafen 12  
27570 Bremerhaven  
Telefon 0471 4831-0  
Telefax 0471 4831-1149  
[www.awi.de](http://www.awi.de)

**HELMHOLTZ**